

Dissertation

submitted to the
Combined Faculties for the Natural Sciences and for Mathematics
of the Ruperto-Carola University of Heidelberg, Germany
for the degree of
Doctor of Natural Sciences

Presented by
Lic. Fernanda M. Rodriguez
from Rosario, Argentina

oral examination: 04.05.07

Study of the interaction between the DnaK chaperone and its substrates

Referees: Prof. Dr. Bernd Bukau
Prof. Dr. Felix Wieland

A Pablo, a mi mamá, a mi papá y a Julia

Table of contents

Zusammenfassung	1
Abstract	3
Overview	5
1. Hsp70 chaperone machinery	9
DnaK interaction with substrates.....	14
DnaJ interaction with substrates.....	14
Natively folded substrates of DnaK.....	16
Heat-shock transcription factor σ^{32}	16
RepE replication initiator protein.....	18
2. Amide hydrogen exchange	23
Exchange mechanism in peptides.....	24
Exchange mechanism in proteins.....	25
Mass spectrometry for monitoring hydrogen exchange.....	27
Mass spectrometer.....	29
3. A quenched-flow setup	31
Quench-flow system setup.....	32
The quench-flow system setup is accurate and reproducible.....	34
The quench-flow system setup time interval is limited by k_{ch}	36
The three-helix bundle of σ^{32} has protected amide hydrogens.....	38
Conclusions.....	41
4. Crystallization of the σ^{32}-DnaK complex	43
Cloning of σ^{32} and DnaK.....	44
Purification of the complex.....	45
Initial crystal screenings.....	47
Trypsin partial proteolysis.....	48
Deletion mutants form complex with DnaK.....	49
Conclusions.....	50
5. Regulation of σ^{32} by the DnaK chaperone system	51
σ^{32} binds specifically to DnaK immobilized in poros material.....	52
DnaK protects at least two amide hydrogens in the DnaK binding site of σ^{32}	54
DnaK destabilizes the N-terminus of σ^{32}	57
DnaJ binds in the N-terminus of σ^{32}	59
σ^{32} - Δ N and σ^{32} - Δ C bind DnaK like σ^{32} wild-type.....	61

DnaJ destabilizes σ^{32}	61
DnaJ opens σ^{32} next to the DnaK binding site.....	62
Conclusions.....	64
6. Study of σ^{32} stable mutants.....	67
Comparison of σ^{32} I54N and σ^{32} wt	68
σ^{32} L47Q-L55Q is more stable than σ^{32} wt in vitro	70
DnaJ destabilizes σ^{32} I54N and σ^{32} L47Q-L55Q	72
DnaJ affinity for these mutants is reduced.....	72
Conclusions.....	73
7. The replication initiator protein RepE.....	75
Monomeric RepE is more stable than dimeric RepE.....	76
The dimer interface locates in region 97-128.....	77
Monomerization of RepE requires marked conformational changes.....	79
Monomeric and dimeric RepE bind to DnaK.....	81
DnaK binds in the C-terminus of RepE.....	81
Conclusions.....	84
Discussion.....	85
Materials and methods.....	95
References.....	129
Publications.....	139
Abbreviations.....	141
Acknowledgment.....	143

Zusammenfassung

Chaperone der Hsp70-Familie sind an einer Vielzahl zellulärer Proteinfaltungsvorgänge beteiligt, indem sie über ATP verbrauchende Reaktionszyklen Substrate binden und freisetzen. Diese Reaktionszyklen werden durch J-Proteine sowie Nukleotidaustausch-faktoren reguliert. Hsp70 Chaperone binden überwiegend ungefaltete Polypeptide, interagieren jedoch im allgemeinen nicht mit deren nativ gefalteten Formen. Hsp70 erkennt aber auch hochspezifisch bestimmte nativ gefaltete Proteine, insbesondere regulatorische Proteine, als Substrate und moduliert deren Aktivität. Obwohl die Bindung an Substrate bereits extensiv untersucht wurde, wobei hauptsächlich Modellpeptide zum Einsatz kamen, ist es immer noch weitgehend unverstanden, wie die Bindung an nativ gefaltete Substrate erfolgt. Außerdem ist unklar, ob Hsp70 Proteine ihre Substrate nur in einem ungefalteten Zustand halten können oder eine aktive Rolle übernehmen, indem sie Konformationsänderungen im Substrat auslösen. Das Ziel dieser Arbeit war, zum Verständnis der Interaktion zwischen Hsp70 und nativ gefalteten Substraten beizutragen, indem deren Konformation und durch Hsp70 verursachte Konformationsänderungen untersucht wurden. Ich analysierte dafür die Interaktion zwischen dem Hsp70-Homologen aus *E. coli* DnaK sowie dessen Co-Chaperon DnaJ mit zwei Proteinsubstraten, deren Aktivität über DnaK und DnaJ reguliert wird: den Hitzeschocktranskriptionsfaktor σ^{32} und das Replikationsinitiatorprotein RepE.

Die Bindestellen von DnaK und DnaJ in σ^{32} wurden mittels Amidprotonenaustausch und Massenspektrometrie sowie über Deletions- und Punktmutationskonstrukte identifiziert. Ich konnte zeigen, dass beide Chaperone die Konformation von σ^{32} beeinflussen, indem sie bestimmte Regionen destabilisieren, welche erstaunlicherweise entfernt von der jeweiligen Bindestelle liegen. Die Bindung von DnaJ an σ^{32} destabilisiert einen Bereich nahe der Bindestelle von DnaK, wodurch die katalytische Aktivität von DnaJ erklärt wird, welche darin besteht, das Substrat auf DnaK zu laden und die ATPase-Aktivität von DnaK synergistisch zu stimulieren. DnaK destabilisiert eine Region in der N-terminalen Domäne, dem Hauptangriffspunkt der Protease FtsH, die σ^{32} *in vivo* abbaut.

RepE führt abhängig vom Oligomierzustand verschiedene Funktionen aus: Als Dimer verhindert es seine eigene Synthese, als Monomer begünstigt es die Initiation der Replikation. DnaK reguliert die Monomerisierung von RepE. Ich konnte den molekularen Mechanismus der Monomerisierung aufklären, indem ich die Konformation des dimeren RepE und einer konstitutiv monomeren Varianten, RepE54, mittels Amidprotonenaustausch-Experimenten verglich. Dadurch konnte ich die Dimerisierungsgrenzfläche kartieren und außerdem die Bindestelle von DnaK identifizieren, welche überraschenderweise nicht in der räumlichen Nähe der Dimerisierungsregion liegt.

Abstract

Hsp70 chaperones assist a large variety of protein folding processes in the cell by ATP-controlled cycles of substrate binding and release that are regulated by J-proteins and nucleotide exchange factors. Hsp70 chaperones bind to almost all unfolded proteins but generally do not interact with their native counterparts. However, Hsp70 also recognize certain folded proteins as substrates, like natively folded regulatory proteins, and modulates their activities. Even though the binding to peptide substrates has been extensively studied, it is still unclear how the binding to natively folded substrates occurs. It is also unknown whether Hsp70 proteins keep their substrates in an unfolded conformation in solution or play a more active role by inducing conformational changes on them. The aim of this Thesis was to contribute to a deeper understanding of the Hsp70 interaction with natively folded substrates, studying their conformation and probing possible conformational changes due to the action of Hsp70. I have analyzed the interaction of the *E. coli* Hsp70 homologue DnaK and its co-chaperone DnaJ with two protein substrates whose activity is regulated by DnaK and DnaJ: the heat-shock transcription factor σ^{32} and the replication initiator protein RepE.

Using amide hydrogen exchange experiments combined with mass spectrometry, and deletion and point-mutation constructs, I have identified the DnaK and DnaJ binding sites in σ^{32} . I have been able to show that both chaperones influence the conformation of σ^{32} by destabilizing specific regions distant to their binding sites. DnaJ binding to σ^{32} destabilizes a region in close spatial vicinity to the DnaK binding site, thereby explaining the catalytic action of DnaJ in loading σ^{32} onto DnaK and the synergistic stimulation of DnaK's ATPase activity by the simultaneous interaction of DnaJ and σ^{32} . DnaK destabilizes a region in the N-terminal domain, the primary target for the FtsH protease, which degrades σ^{32} *in vivo*.

RepE, on the other hand, performs different functions depending on its oligomeric state: as a dimer it represses its own synthesis while as a monomer it promotes replication initiation. Monomerization of RepE is regulated by DnaK. I have characterized the molecular mechanism of this regulation by investigating the conformation of dimeric RepE wild type and the constitutively monomeric variant RepE54 by amide hydrogen exchange experiments. I have been able to map the dimer interface in RepE and to identify the DnaK binding site which, interestingly, is not close to the dimer interface.

Overview

Protein folding is the process by which a protein assumes its characteristic functional tertiary structure or native state. The information for the proper folding of a protein is encoded in its amino acid sequence (Anfinsen, 1973). At low protein concentration and low temperatures many purified proteins can fold spontaneously *in vitro*. However, the situation inside the cell is more complex. The cellular environment is crowded with high protein concentrations (300 to 400 mg/ml), and *in vivo* proteins have to fold at physiological temperature (Zimmerman & Trach 1991, Ellis 2001). In addition, protein stability depends on factors such as pH, temperature and salt concentrations that can be affected by environmental changes inducing misfolding of many proteins. To antagonize these risks, cells have evolved a system of molecular chaperones that assist the folding of other proteins.

Most proteins can only fulfill their biological function when they are properly folded. The importance of protein folding and its regulation by molecular chaperones is

evidenced by cellular abnormalities observed when proteins misfold. Despite the ability of molecular chaperones to efficiently hinder protein aggregation, misfolding of some proteins cannot be prevented. This is the case, for example, for Alzheimer's, Huntington's, and prion diseases. In other situations, like cystic fibrosis, even though a protein carrying a mutation is sufficiently active to prevent the disease state, the product is captured by the quality control system in the endoplasmic reticulum (ER) and never reaches its site of function.

Many of the molecular chaperones were first identified by exposing cells to elevated temperatures, and are for this reason called heat-shock proteins (Hsp). Hsp are divided in different families according to their molecular weight: Hsp100, Hsp90, Hsp70, Hsp60, Hsp40, and the small Hsp. The Hsp70 family is one of the best-studied families of molecular chaperones. Hsp70 activity requires ATP and the cooperation of co-factors (co-chaperones) that control the Hsp70 ATPase cycle and target the chaperone to specific substrates. Hsp70 proteins and its co-chaperones assist a large variety of protein folding processes in the cell under both normal and stress conditions. Under stress conditions they prevent aggregation and assist refolding of misfolded proteins, whereas under normal conditions they: (a) assist folding of some newly synthesized proteins, (b) guide translocation of protein across organelle membranes, (c) disassemble oligomeric protein structures, (d) facilitate proteolytic degradation of unstable proteins, and (e) control the activity of regulatory proteins (Bukau and Horwich, 1998). Figure O.1 shows an overview of the cellular functions of the *E. coli* Hsp70 chaperone DnaK. Hsp70 chaperones bind to almost all unfolded proteins but generally do not interact with their native counterparts. This property could be explained through the elucidation of the binding motif of Hsp70: it was found that Hsp70 recognize hydrophobic peptide stretches, which are exposed in unfolded proteins but buried inside the folded ones. However, Hsp70 proteins also recognize certain folded proteins as substrates. For example, DnaK binds to natively folded heat-shock transcription factor σ^{32} , replication factors RepA and RepE, and the DNA replication initiation complex of bacteriophage λ , namely λ O and λ P proteins (Straus *et al.*, 1990; Ishiai *et al.*, 1994; Alfano and McMacken, 1989; Wawrzynow and Zylicz, 1995; Wawrzynow *et al.*, 1995). In the case of native substrates, it is unclear which properties of the proteins make them a substrate for Hsp70.

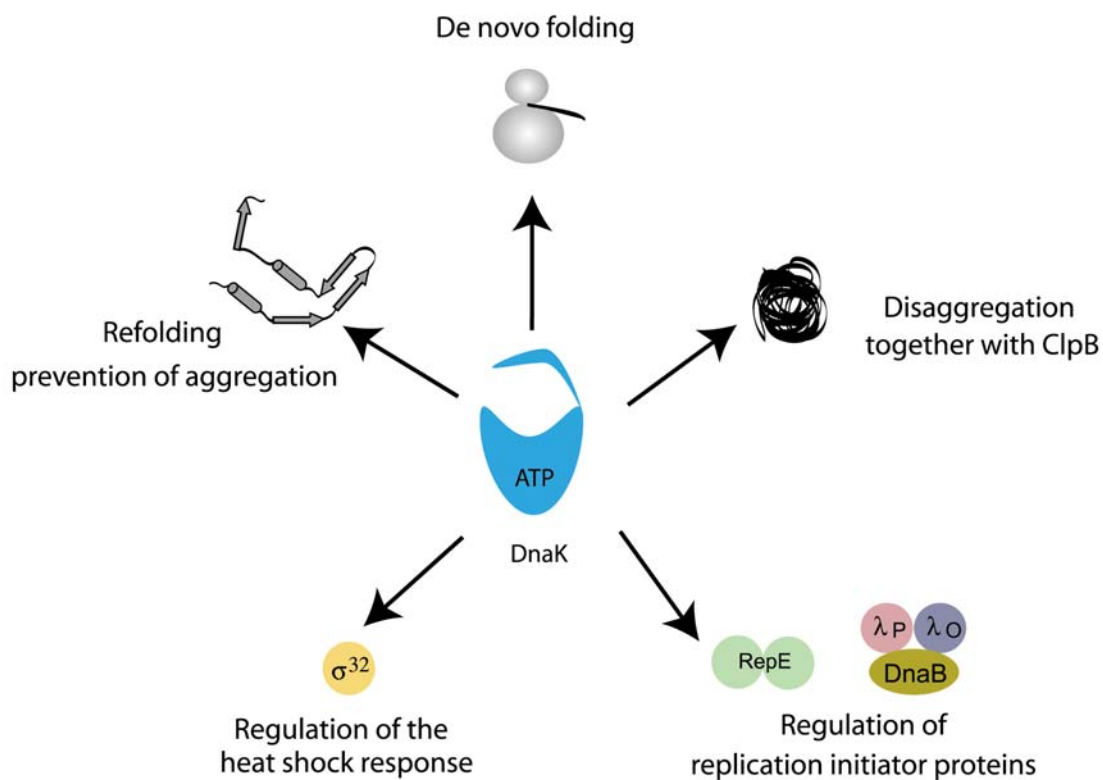


Figure O.1. Cellular functions of the Hsp70 chaperone DnaK.

Even though Hsp70 proteins have been extensively studied, it is not completely clear how they interact with their substrates and whether they merely keep the substrate in an unfolded conformation in solution or they play a more active role inducing conformational changes in the substrate. These are fundamental questions that have not been solved in the chaperone field.

The aim of this thesis is to obtain a deeper understanding of Hsp70-substrate interactions, studying the conformation of substrates and probing possible conformational changes due to the action of Hsp70. We have studied the *E. coli* DnaK chaperone, a member of the well-conserved Hsp70 family, and two native protein substrates whose activities are regulated by DnaK: the heat-shock transcription factor σ^{32} and the replication initiator protein RepE. We have examined the molecular mechanism of DnaK by identifying binding sites and possible DnaK-induced conformational changes in these two substrate proteins. These issues have been addressed using mainly hydrogen

exchange (HX) experiments but also traditional biochemistry techniques, as will be described in more detail in the course of the following chapters.

The structure of this thesis is the following:

- In Chapter 1 we review fundamental aspects of the Hsp70 chaperone machinery. We focus on the structural properties of the *E. coli* Hsp70 and its co-chaperone DnaJ, and the interaction of both with their substrates.
- In Chapter 2 we review fundamental aspects relating to hydrogen exchange experiments that are later applied in Chapters 3, 5, 6 and 7.
- In Chapter 3 we present a quenched-flow setup system that allows HX experiments with exchange times as short as 100 msec, and evaluate its performance and reproducibility. We then investigate the conformational properties of *E. coli* heat-shock transcription factor σ^{32} free in solution. These results were published in the journal Protein Science (Rist W., Rodriguez F., Jorgensen T., Mayer M.P., Protein Sci. 2005 14: 626-632).
- In Chapter 4 we present a crystallization approach that we have performed for the DnaK- σ^{32} complex. We show the purification strategy and the results of the crystallization trials.
- In Chapter 5 we study the interaction of DnaK and DnaJ with σ^{32} . We confirm that the previously identified DnaK binding site in σ^{32} is the binding site in the native protein and we identify the segment involved in DnaJ binding. Using HX exchange experiments, we find that DnaK and DnaJ induce conformational changes upon binding to σ^{32} . A manuscript describing these studies has been submitted for publication.
- In Chapter 6 we consider two mutants of σ^{32} that have a longer half-life *in vivo*. The purpose of this study was to elucidate why these mutants are more stable and to understand the molecular mechanism of σ^{32} regulation.
- Finally, in Chapter 7 we study RepE as another model substrate for DnaK. First, we characterize the RepE monomer and dimer, and then we identify the DnaK binding site in RepE. The results described in this chapter constitute a manuscript currently in preparation.

Chapter 1

Hsp70 chaperone machinery

The Hsp70 chaperone machinery is composed of Hsp70 proteins and co-chaperones that regulate their activities. Hsp70 proteins consist of an actin-like N-terminal ATPase domain of 45 kDa (Flaherty *et al.*, 1990; Flaherty *et al.*, 1991), a substrate-binding domain (SBD) of approx. 15 kDa, and a C-terminal domain of approx. 10 kDa whose function is not completely clear (Zhu *et al.*, 1996) (Figure 1.1). The three-dimensional structure of the bovine Hsp70 ATPase domain has been solved. It consists of two lobes with a deep cleft between them; ATP binds at the base of this cleft (Flaherty *et al.*, 1990). The crystal structure of the substrate-binding domain of *E. coli* DnaK, in complex with a peptide substrate, has also been determined: it consists of a β -subdomain and a C-terminal α -helical subdomain (helical lid). The peptide substrate is bound in a cavity

formed by two pairs of inner and outer loops protruding upwards from the β -sandwich. Two elements are crucial for peptide binding: a hydrophobic pocket that accommodates a single hydrophobic side chain and an arch that encloses the peptide backbone (Zhu *et al.*, 1996). The peptide substrate is tightly packed into the binding cavity. But how can a substrate find its way into such a tight spot? Clearly, the substrate-binding site must undergo conformational changes to allow substrate binding.

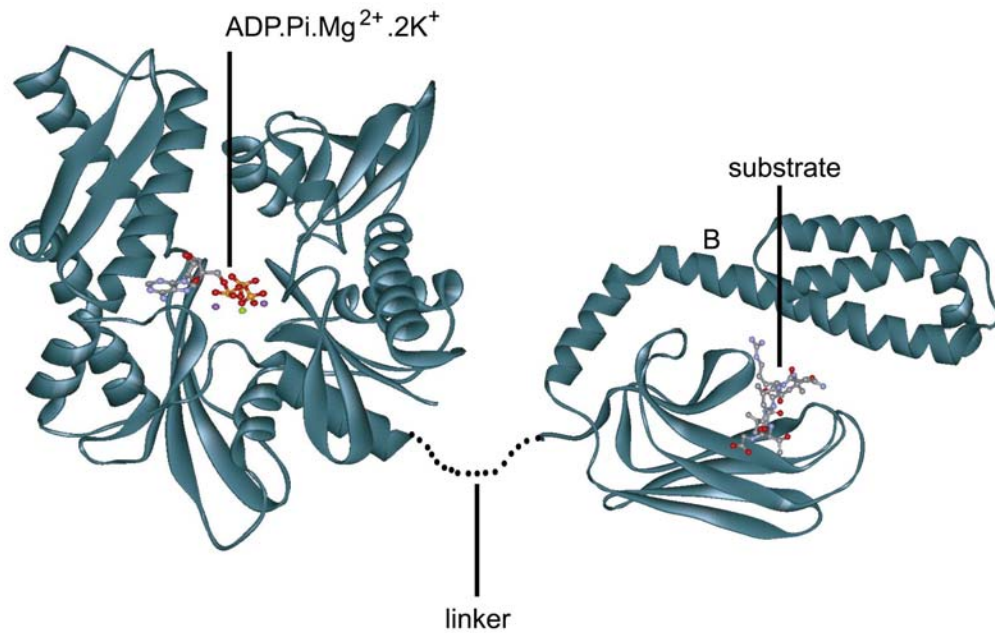


Figure 1.1. Structure of ATPase domain and substrate-binding domain of Hsp70. Left, ribbon representation of the bovine Hsc70 ATPase domain in complex with Mg^{2+} .ADP.Pi and two K^{2+} ions (1BUP) (Flaherty *et al.*, 1990). Right, *E. coli* DnaK substrate domain in complex with peptide substrate (1DKX) (Zhu *et al.*, 1996), connected with a dotted line representing the linker.

Structural data suggest that the helical lid and the β -sheet may move to allow substrate binding. Two distinct conformations in the lid were observed in the crystal structure of the DnaK substrate-binding domain (Zhu *et al.*, 1996). In one structure, the long α -helix (α -helix B) that lies over the substrate-binding site was kinked in the middle

and slightly bent upwards. NMR studies of truncated substrate-binding domain showed that α -helix B is capable of unwinding at almost the same region where the kink was observed (Wang *et al.*, 1998). Therefore, the opening of the substrate-binding domain can be achieved in part by bending of the α -helix B or pivoting of the complete α -helical domain away from the substrate-binding site. A lidless mutant of DnaK retains the capacity of allosteric stimulation of peptide release by ATP but to a lesser extent (Mayer *et al.*, 2000a; Misselwitz *et al.*, 1998; Pellicchia *et al.*, 2000; Buczynski *et al.*, 2001). This data indicates that the β -sheet domain also undergoes conformational changes upon substrate binding. In addition, HX experiments with DnaK in the presence of ATP have shown that ATP induces opening of the substrate-binding pocket mainly in the β -sheet sub-domain (Rist *et al.*, 2006).

Hsp70 interaction with substrates is regulated by ATP and co-chaperones that modulate the ATPase cycle (Mayer *et al.*, 2000b). ATP binding to the ATPase domain of Hsp70 decreases the affinity of the substrate-binding domain for substrates by increasing both the association and the dissociation rates for substrates. In contrast, in the ADP-bound state the affinity for substrate is high but the association and dissociation rates are low (Schmid *et al.*, 1994; Mayer *et al.*, 2000a; Gisler *et al.*, 1998). Hsp70 proteins alternate between the ATP- and ADP-bound states (Figure 1.1). For most Hsp70 proteins, the rate-limiting step of the cycle is the ATP hydrolysis (McCarty *et al.*, 1995; Theyssen, 1996). ATP hydrolysis is strongly accelerated by Hsp40 or DnaJ proteins in the presence of substrates (Liberek *et al.*, 1991; Karzai *et al.*, 1996; Barouch *et al.*, 1997; Misselwitz *et al.*, 1998; Laufen, 1999). In addition, DnaJ proteins also can target Hsp70 partner proteins to pre-selected substrates (Mayer and Bukau 1998). The release of ADP and Pi from some Hsp70 is regulated by nucleotide exchange factors.

The Hsp70 chaperone system in *E. coli* is composed of DnaK, DnaJ, and GrpE. DnaK is the Hsp70 protein, DnaJ stimulates nucleotide hydrolysis and targets substrates to DnaK, and GrpE promotes the exchange of ADP for ATP. DnaJ and GrpE act in concert to control the flux of unfolded polypeptides into and out of the substrate-binding domain of DnaK by regulating its nucleotide bound state.

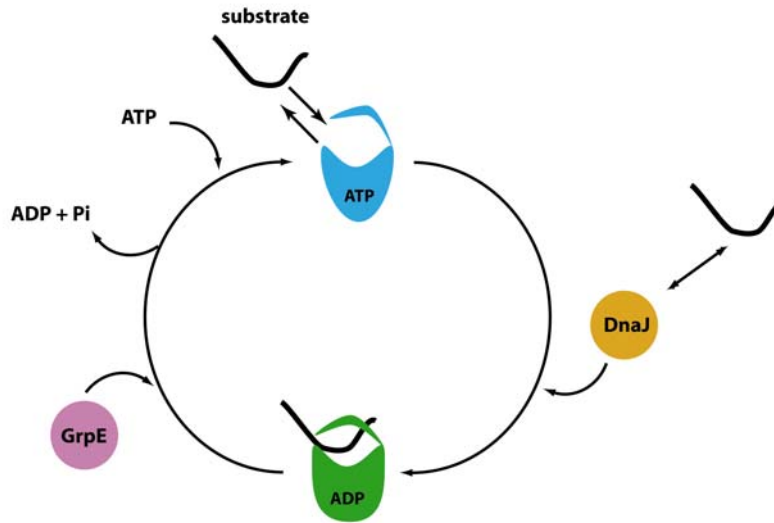


Figure 1.2. Functional cycle of DnaK.

The DnaJ-proteins (or Hsp40) family comprises multi-domain proteins that are defined by the presence of the highly conserved J domain. DnaJ is the prototype of this family. It has four domains: the J domain, the Gly/Phe-rich region, the zinc finger region and the C-terminal domain. The DnaJ-proteins family is divided in three subfamilies according to the degree of homology to DnaJ: (a) type I share significant homology to all four domains of DnaJ, (b) type II lack the zinc binding domain, and (c) type III only have the J domain in common with DnaJ. The type III subfamily can have a large variety of additional domains and protein motifs. The J domain is essential for the ATP stimulation of Hsp70 proteins (McCarty *et al.*, 1995; Liberek *et al.*, 1991; Laufen *et al.*, 1999; Misselwitz *et al.*, 1998; Russell *et al.*, 1999; Wall *et al.*, 1994). DnaJ can bind denatured substrates through its C-terminal domain (Langer, *et al.* 1992; Szabo *et al.*, 1996; Szabo *et al.*, 1994; Li *et al.*, 2003). It has therefore been suggested that DnaJ is a chaperone itself. In addition, DnaJ can bind to nascent ribosome-bound polypeptides suggesting that DnaJ may protect polypeptide chains from aggregation and, in cooperation with Hsp70, promotes their correct folding (Hendrick *et al.*, 1993).

High resolution structures have been solved for isolated J domains (Figure 1.3): three helices pack together into a compact structure, with the highly conserved tripeptide histidine–proline–aspartate (HPD) exposed in a loop between helices II and III (Szyperski *et al.*, 1994; Pellicchia *et al.*, 1996; Berjanskii *et al.*, 2000; Qian *et al.*, 1996).

Mutations of this tripeptide reduce or abolish stimulation of the Hsp70 ATPase reaction, suggesting that the J domain plays an important part in the interaction of an Hsp40 protein with its Hsp70 partner. NMR studies have suggested that the interacting surface on the J domain might be as small as residues 2–35, including helix II and the HPD tripeptide segment. In DnaK, the site of J domain interaction might be in a small cleft between subdomains IA and IIA of the ATPase domain. Alanine substitution of residues lining both sides of this cleft dramatically altered binding to DnaJ (Gässler *et al.*, 1998).

The co-chaperone GrpE functions as a nucleotide exchange factor to promote dissociation of ADP from the nucleotide-binding cleft of DnaK. GrpE was identified in a genetic screen for mutants that failed to propagate the bacteriophage λ in *E. coli* (Saito and Uchida, 1977). GrpE has been crystallized in complex with the ATPase domain of DnaK, showing that the former is an asymmetric dimer that is bent towards the latter as a result of the break in the long α -helix in the GrpE monomer proximal to DnaK. GrpE binding to DnaK opens the ATPase domain resulting in nucleotide dissociation.

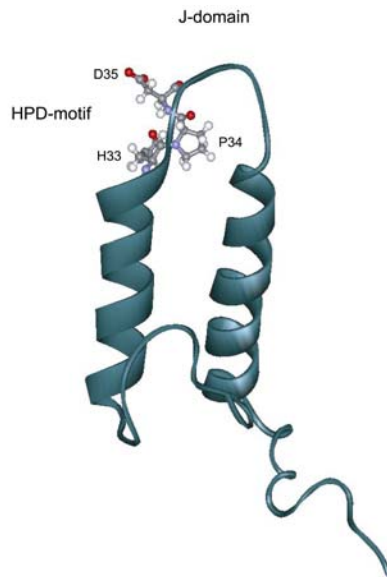


Figure 1.3. NMR structure of *E. coli* J-domain. The conserved HPD motif is marked as ball-and-stick model (1XBL, Pellicchia *et al.*, 1996).

DnaK interaction with substrates

In the crystal structure of the DnaK substrate-binding domain in complex with a peptide substrate, the peptide is bound over a stretch of five residues through two types of interactions. First, hydrogen bonds which are formed between the backbones of both the cavity-forming loops and the peptide. Secondly, van der Waals interactions which are formed between hydrophobic side chains of the binding cavity and the substrate peptide. At a central position within the binding cavity, two residues of DnaK form an arch that reaches over the bound substrate, and a hydrophobic pocket facing downwards accommodates a single hydrophobic side chain of the substrate. These latter interactions make the most important contributions to substrate binding (*Zhu et al.*, 1996).

DnaK interacts promiscuously with almost all unfolded proteins. Its substrate specificity was analyzed using a library of cellulose-bound 13-mer peptides scanning the sequences of natural proteins with an overlap of ten amino acids (*Rüdiger et al.*, 1997). With this approach a consensus motif for DnaK binding sites was identified. It is composed of a core of up to 5 hydrophobic residues flanked by sequences rich in positively charged amino acids. The DnaK binding motif is frequent in protein sequences. On average, this site occurs in proteins every 36 residues. In the native state, these sites are buried in the hydrophobic core of the protein, explaining why most native proteins are not substrate of DnaK.

All DnaK potential binding sites of a substrate can be determined using peptide libraries. However, a different approach is required to identify the DnaK binding site in a native folded protein. For example, the DnaK and DnaJ binding sites in RepA have been identified using deletion mutants and point mutants: DnaK binds in the N-terminus of RepA and DnaJ binds in the C-terminus (*Kim et al.*, 2002).

DnaJ interaction with substrates

The binding motif of DnaJ has also been determined by screening of peptide libraries. It consists of a hydrophobic core of approximately eight residues enriched with aromatic and large aliphatic residues and arginine (*Rüdiger et al.*, 2001). Most DnaK-binding peptides are recognized by DnaJ, and only a minority of peptides with affinity for

DnaK are not substrate for DnaJ. However, differences between the two chaperones arised when the affinity for D-amino acids was evaluated. DnaK's affinity for peptides is lost in the D-stereoisomers even when the side chain conformation is conserved, demonstrating that backbones are essential for DnaK-substrate interactions (Feifel *et al.*, 1998; Rüdiger *et al.*, 2001). This fact is consistent with the crystal structure of DnaK substrate-binding domain in complex with a peptide substrate, which shows hydrogen bonds between DnaK and the substrate backbone (Zhu *et al.*, 1996). DnaJ, unlike DnaK, can bind to polypeptides consisting of D-amino acids. In the case of DnaJ, only the side chains are important for the interaction with substrates (Rüdiger *et al.*, 2001; Feifel *et al.*, 1998). The zinc-binding domain is also important for substrate binding (Banecki *et al.*, 1996; Szabo *et al.*, 1996; Linke *et al.*, 2003). The yeast DnaJ homologue Ydj1 has been crystallized in complex with a peptide substrate. In that structure, interactions with the substrate backbone and Ydj1 were important and aromatic residues did not make any contact. This structure is not in agreement with DnaJ substrate specificity, suggesting that DnaJ substrate recognition may not be similar in different DnaJ-proteins. Substrate binding to DnaJ is not an essential function since mutants that cannot bind substrate still support DnaK-DnaJ dependent replication of bacteriophage λ and refolding of denatured proteins. However, higher concentrations of the DnaJ mutants are needed in this case (Wall *et al.*, 1994 JBC; Linke *et al.*, 2003 JBC).

Two mechanisms have been proposed for the substrate targeting action of DnaJ to DnaK. In the first model, DnaJ and DnaK bind to the same hydrophobic patch. DnaJ binds first, and then the binding site is handed over to DnaK while DnaJ is dissociating. Alternatively, DnaK and DnaJ associate with different hydrophobic patches, followed by a DnaJ- and substrate-dependent ATP hydrolysis by DnaK, which locks the substrate in DnaK. The direct transfer mechanism is not operative in the case of RepA since DnaK and DnaJ have distinct binding sites in the RepA sequence (Kim *et al.*, 2002). It is important to determine whether this mode of action of the DnaK-DnaJ team is generally applicable for other substrates and for Hsp70 homologues.

Natively folded substrates of DnaK

Heat-shock transcription factor σ^{32}

The heat-shock response is a protective mechanism of cells against stress-induced damage of proteins (Morimoto *et al.*, 1990). In *E. coli* this response is mediated by the alternative σ transcription factor σ^{32} that activates the transcription of the heat-shock genes (Bukau, 1993; Connolly *et al.*, 1999; Gross *et al.*, 1996; Yura and Nakahigashi, 1999). σ factors bind to the catalytic core RNA polymerase (RNAP) to form the RNAP holoenzyme and recruit the RNAP to the promoter through sequence-specific binding of conserved, hexameric promoter elements located at positions -35 and -10 bp relative to the transcription start site (Gross *et al.*, 1998). With the exception of σ^{54} , all σ -factors comprise a homologous family (the σ^{70} family) with four flexibly linked domains: $\sigma_{1.1}$, σ_2 , σ_3 and σ_4 (Gruber and Bryant, 1997). The structures of the σ domains have been determined individually (Campbell *et al.*, 2002b; Li *et al.*, 2002; Malhotra *et al.*, 1996), in complex with anti- σ factors (Campbell *et al.*, 2002a, 2003) and in complex with the core RNAP (Murakami *et al.*, 2002; Vassylyev *et al.*, 2002). The structures of the corresponding σ -domains are nearly identical in the different cases but with a different relative positioning. It is also known that binding to core RNAP induces large relative movements of the σ -domains of σ^{70} (Callaci *et al.*, 1999). To date, no structure has been reported for σ^{32} . However, it was shown using amide hydrogen experiments that σ^{32} has a high degree of flexibility (Rist *et al.*, 2003).

Stress-dependent changes in heat-shock gene expression are mediated by changes in synthesis, activity and stability of σ^{32} . The levels of σ^{32} are regulated at the initiation of translation. Translational regulation is mediated by a secondary structure of the 5' region of the mRNA encoding for σ^{32} , which inhibits translation at low temperatures but is unstructured at high ones, enhancing ribosome loading and initiation of the translation (Morita *et al.*, 1999a; Morita *et al.*, 1999b; Yura and Nakahigashi, 1999).

Under normal growth conditions, σ^{32} is rapidly degraded with a half-life of approximately 1 minute (Connolly *et al.*, 1999; Gross *et al.*, 1996; Herman *et al.*, 1995; Kanemori *et al.*, 1997; Kanemori *et al.*, 1999; Tomoyasu *et al.*, 1995). The DnaK and GroELS chaperone systems act as negative modulators of the heat-shock response by

regulating the stability and activity of σ^{32} (Straus *et al.*, 1989; Tomoyasu *et al.*, 1998; Guisbert *et al.*, 2004). The DnaK system plays an important role in the regulation of the heat-shock response because its association with σ^{32} at optimal growth temperatures prevents the formation of the RNA polymerase- σ^{32} complex (Gamer *et al.*, 1992; Liberek *et al.*, 1992) and targets it to degradation. At high temperatures, the DnaK chaperone system binds to unfolded or aggregated proteins, liberating σ^{32} . Shutoff of the heat-shock response starts after 4 to 6 min at a heat stress temperature. When enough chaperones are synthesized, the heat-shock sigma factor is again bound to available DnaK molecules and redirected to degradation, thus decreasing the amount of σ^{32} to normal levels (Straus *et al.*, 1990; Straus *et al.*, 1987). In Figure 1.4 we show a model of the heat-shock regulation.

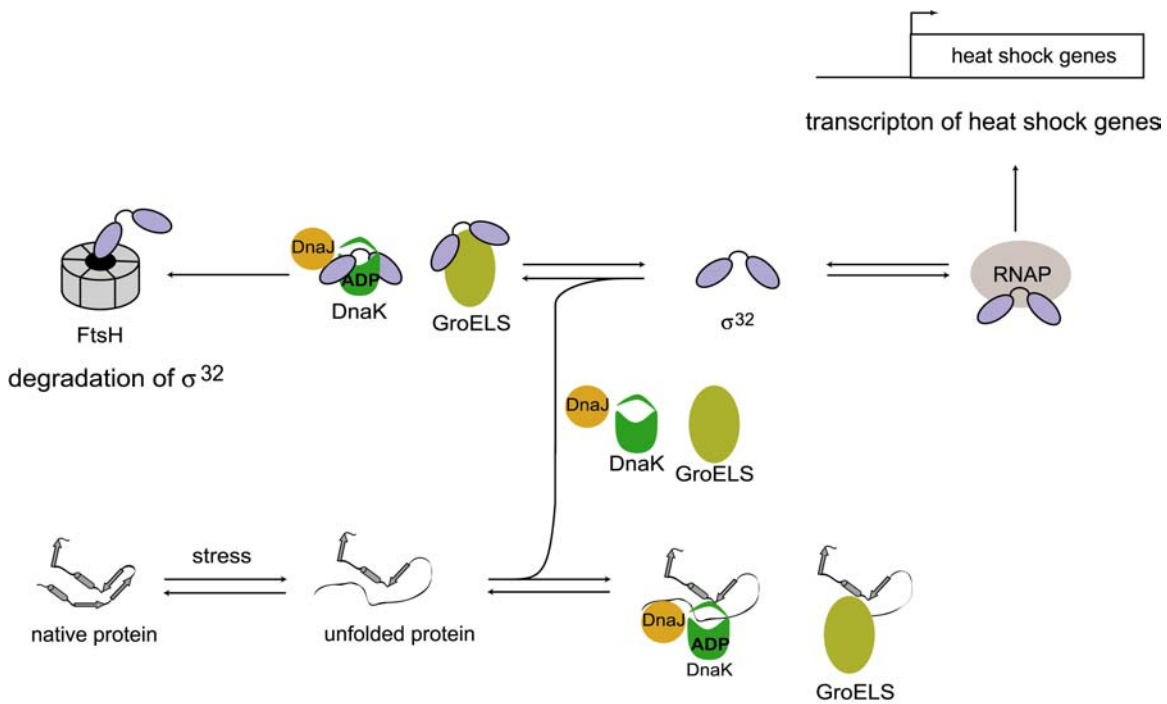


Figure 1.4. Homeostatic model of heat-shock regulation in *E.coli*. σ^{32} is in equilibrium between an active form that can bind to RNAP and an inactive form that is bound to DnaK/DnaJ or GroEL. These chaperones target σ^{32} for degradation by FtsH.

σ^{32} is degraded *in vivo* by the protease FtsH and perhaps by other cytosolic proteases including HslUV (ClpYQ). FtsH, a member of the AAA⁺ family of proteins, is a membrane-bound ATP-dependent metalloprotease with an active site facing the cytoplasm. It degrades membrane and cytoplasmic proteins. Unfortunately, it has been so far impossible to fully reconstitute *in vitro* the degradation of σ^{32} by FtsH; only slow degradation at 42°C is observed and this degradation is not facilitated by chaperones (Blaszczak *et al.*, 1999; Herman *et al.*, 2003). It also remains unclear how FtsH, a membrane protease, is able to rapidly degrade cytosolic σ^{32} . Early studies suggested that σ^{32} was degraded from the C-terminus. However, it was later shown using fluorescence polarization that the degradation of Cy3- σ^{32} proceeds from the N-terminus to the C-terminus (Okuno *et al.*, 2004).

In Chapters 4, 5 and 6 we have studied the heat-shock transcription factor σ^{32} as a model substrate for DnaK and DnaJ. The elucidation of the molecular mechanism of DnaK-DnaJ regulation of σ^{32} is essential to understand the heat-shock response.

RepE replication initiator protein

The replication of many bacterial plasmids depends on replication initiator (Rep) proteins. Cellular concentrations of Rep proteins determine the plasmid copy number by regulating the replication initiation. One such Rep protein is RepE, which regulates the replication initiation of the mini-F plasmid from the origin of replication *ori2* (Tolun *et al.*, 1982; Watson *et al.*, 1982; Maki *et al.*, 1984). The mini-F plasmid is a derivative of the F (fertility) factor, which is involved in sexual conjugation in *E. coli* (Lovett & Helinski, 1976). It is maintained at 1-2 copies per host chromosome by stringent control of replication initiation.

RepE has different functions depending on its oligomeric state. As a monomer, it functions as a replication initiation factor that binds to four directed repeats (iterons) at the replication origin to initiate plasmid replication. However, as a dimer, RepE represses its own transcription by binding to the operator of the *repE* gene consisting of an inverted repeat sequence.

The RepE oligomeric state is regulated by the DnaK system (Kawasaki *et al.*, 1990) (Figure 1.5). The first evidence that the DnaK system is involved in RepE regulation

arose from genetic studies. F plasmids cannot replicate in *E. coli* strains expressing *rpoH* mutants and cannot transform *E. coli* cells lacking σ^{32} (Kawasaki *et al.*, 1990). It was originally thought that σ^{32} controlled the transcription of RepE. However, *repE* mutants that can replicate in $\Delta rpoH$ mapped in the coding sequence, not in the promoter region of RepE (Kawasaki *et al.*, 1991). These mutants have reduced autogenous repressor activity and increased initiator activity. A second set of RepE mutants was isolated in a *dnaJ259* background (Ishiai *et al.*, 1992). These mutant plasmids were also able to replicate in *dnaK* and *grpE* mutants. The majority of these mutants carried a unique amino acid alteration in the coding region between residues 92 and 134. These RepE initiator variants bind *ori2* repeat sequences with higher affinities as compared to wild-type protein, but their affinity for the operator is reduced (Kawasaki *et al.*, 1992). Using purified proteins, Ishiai *et al.* demonstrated that the hyperactive initiator mutants are monomers and that RepE wild-type are dimers (Ishiai *et al.*, 1992). DnaK, DnaJ and ATP enhance the binding of RepE to *ori2* by promoting the conversion of dimeric RepE into monomeric RepE (Figure 1.5).

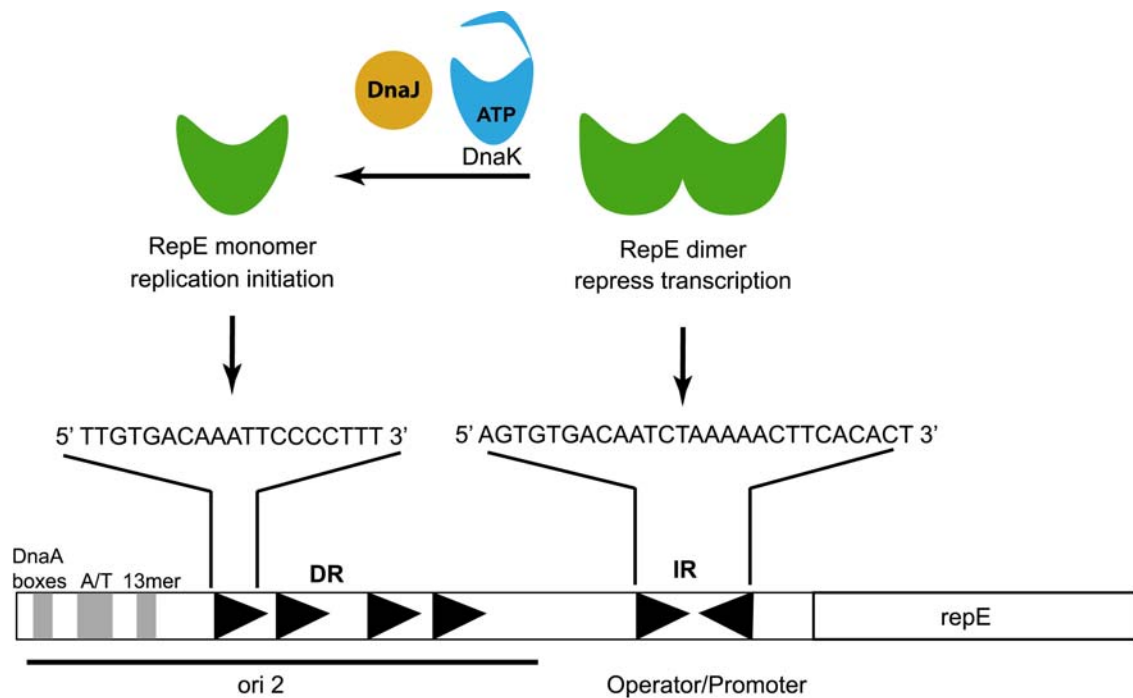


Figure 1.5. Schematic representation of RepE functions. RepE monomers bind to four iterons (direct repeats) of *ori2* to initiate replication. RepE dimers bind to the operator (inverted repeats) to repress *repE* transcription. The repeat sequences are also shown in the figure. DnaK and DnaJ regulate the monomerization of RepE.

A constitutively monomeric variant of RepE (RepE54) has been crystallized in complex with the iteron DNA (Komori *et al.*, 1999). It is a pseudo-symmetric protein with two winged-helice domains (WH): winged-helice domain 1 (WH1) and winged-helice domain 2 (WH2). WH consists of a helice-turn-helice DNA binding motif with one or two β -hair-pin wings (Figure 1.6). Recently, the structure of a dimeric N-terminal fragment of RepA was solved (Giraldo *et al.*, 2003). RepA is a replication initiator protein related to RepE that exhibits some structural rearrangements to form the dimer. The pseudo-symmetry of the two domains is broken, and the RepA dimer interface is formed by hydrogen bonds between β -sheets. In the dimers, the C-terminal WH (WH2) domain binds to each operator DNA repeat. In the monomers, WH2 binds to the end of each iteron that includes the core of the repeat sequence, while WH1 binds to the opposite iteron end. When RepE is monomerized, the N-terminal dimerization domain is converted to a second origin-binding module. Even though the structures of monomeric RepE and dimeric RepA have been solved, there is no available structure for the dimer RepE.



Figure 1.6. Ribbon representation of RepE54 (R118P) in complex with the iteron DNA (1REP). (Komori *et al.*, 1999)

In Chapter 7 we study RepE as a native substrate for DnaK. First, we characterize the RepE monomer and dimer by using hydrogen exchange experiments. We next map the DnaK binding site in RepE.

Chapter 2

Amide Hydrogen exchange

Hydrogen exchange (HX) experiments, first introduced by Linderstøm-Lang in the 1950s, are a powerful technique that can be used to study protein structure and dynamics. Hydrogen atoms in proteins can exchange with hydrogen atoms from the solvent molecules surrounding the protein. Protein hydrogens can be divided in three types according to their exchange rate under the conditions generally employed in HX experiments: (a) hydrogens covalently bound to carbon that essentially do not exchange, (b) hydrogens attached to functional groups on the side chains that exchange very fast, and (c) backbone amide hydrogens that exchange at rates that can be measured (Figure 2.1). Since backbone amide hydrogens are involved in the formation of hydrogen bonds in secondary structural elements their exchange rates are a reflection of the protein

structure. Hydrogen bonding and solvent inaccessibility protect hydrogens against exchange.

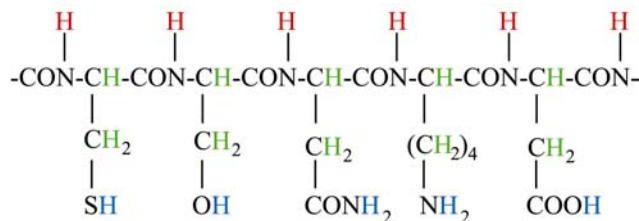


Figure 2.1. Different kinds of hydrogens in proteins. Hydrogens covalently bound to carbon are shown in green, those attached to functional groups on the side chains are depicted in blue, and the ones at the backbone amide positions in red.

Hydrogen exchange reactions can be quantified by measuring the exchange of protium (^1H) for deuterium (^2H) or tritium (^3H), deuterium being the isotope most commonly used. The kinetics of amide HX can be measured by nuclear magnetic resonance (NMR) spectroscopy and mass spectrometry (MS).

Exchange mechanism in peptides

In water-based solutions, amide hydrogen exchange is catalysed by OH^- (down to pH 3) and by H_3O^+ (below pH 3). The exchange rate for a freely exposed peptide amide hydrogen k_{ex} , also known as intrinsic chemical exchange rate, can be approximated as

$$k_{\text{ex}} = k_{\text{OH}} [\text{OH}^-] + k_{\text{H}} [\text{H}_3\text{O}^+] + k_0$$

where k_{OH} , k_{H} and k_0 are the rate constants for base-catalysed, acid-catalyzed and direct exchange with water. The latter exchange is insignificant in most studies.

The exchange rate depends on the pH of the solution. For each unit change in the pH there is a 10-fold increase in the exchange rate. The minimum exchange rate is at pH 2.5 to 3 (Figure 2.2). Hydrogen exchange rate is also temperature-dependent. The rate constants follow the Arrhenius equation, $\ln k = \ln A - E_a/(RT)$, where A is a constant, E_a is the activation energy, R is the gas constant and T is temperature. Thus, there is a 3-fold

increase in the exchange rate for every 10°C increase in temperature. At pH 7 and 25°C, the half-lives of exposed amide hydrogens are in the range of 0.05-0.01 s, whereas at 0°C

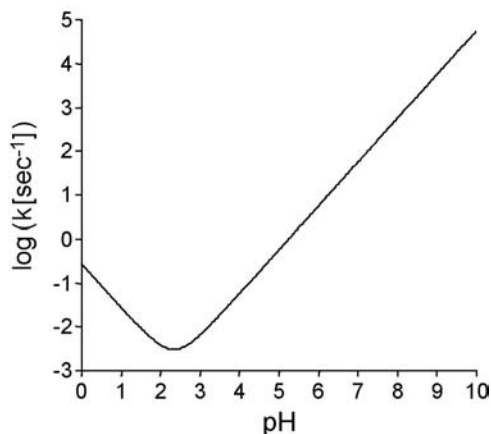
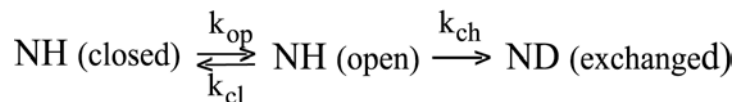


Figure 2.2. Rate constants for amide hydrogen exchange in an unstructured peptide as a function of pH (Bai *et al.*, 1993).

and pH 2.7 the half-lives are between 30 to 90 minutes. The latter conditions are used for quenching exchange reactions to preserve the isotope labels during analysis. Solvent composition also has an effect on the exchange rate—for example, miscible organic solvents generally slow it down. In addition, the neighbour residue side-chains influence the exchange constant. Bai *et al.* have assessed these neighbouring side-chain effects using model peptides (Bai *et al.*, 1993). With the parameters obtained in that study it is possible to predict the intrinsic chemical exchange rate of peptide amide hydrogens for all conditions.

Exchange mechanism in proteins

In unstructured peptides, amide hydrogen exchange occurs under physiological conditions within milliseconds. However, rates are much slower for hydrogens that are protected by hydrogen-bonds or that are buried inside the protein. Linderstrøm-Lang *et al.* proposed the following two-step model for structurally protected hydrogens,



where k_{op} and k_{cl} are the opening (unfolding) and closing (refolding) rates and k_{ch} is the chemical exchange rate of freely available, unprotected amide hydrogen (Linderstrøm-Lang, 1958). In this model, hydrogens are non-exchangeable in the closed state but can be exchanged in the open one.

According to this model, the exchange rate k_{ex} can be defined as

$$k_{ex} = \frac{k_{op} \cdot k_{ch}}{k_{op} + k_{cl} + k_{ch}}$$

For native proteins, one can usually assume that refolding is much faster than opening ($k_{cl} \gg k_{op}$), so k_{op} in the denominator can be neglected and the equation above simplifies as follows:

$$k_{ex} = \frac{k_{op} \cdot k_{ch}}{k_{cl} + k_{ch}}$$

Two limiting cases are possible. If the closing rate is small compared to the chemical exchange rate, the observed exchange rate is directly related to the opening rate $k_{ex} = k_{op}$. This regime is known as type 1 mechanism (EX1) or correlated exchange: all amide hydrogens exchange upon a single opening event. EX1 is observed under destabilizing buffer conditions like in the presence of chemical denaturants or extreme pH. In HX experiments where protons are exchanged for deuterons, EX1 mechanism yields peptides that contain either no deuterium or are fully deuterated, and thus two distinct mass peaks will be observed. In the type 2 mechanism (EX2), protein refolding is faster than the intrinsic exchange and folding-refolding occurs many times before hydrogen deuterium exchange is completed. The observed exchange rate is then

$$k_{ex} = \frac{k_{op}}{k_{cl}} \cdot k_{ch} = K_{op} \cdot k_{ch}$$

where K_{op} is the equilibrium constant for the opening (unfolding) reaction. Measuring k_{ex} and calculating k_{ch} leads to direct determination of the equilibrium constant K_{op} and the apparent free energy G_{HX} for the unfolding process (Bai *et al.*, 1994)

$$\Delta G_{HX} = -RT \cdot \ln(K_{op})$$

In EX2 refolding is more likely than exchange reactions, and the exchange is random or uncorrelated. The mass spectrum shows a single mass peak that gradually shifts to higher masses.

Experimental conditions like pH, temperature and chemical denaturants will determine which of the two exchange mechanisms dominates. It is also possible that both mechanisms, namely EX1 and EX2, are observed within the same protein.

Mass spectrometry for monitoring hydrogen exchange

The mass difference between hydrogen and deuterium is 1 Da; therefore, the changes in deuterium incorporation can be detected by changes in masses with a mass spectrometer. In native state HX, the exchange reaction is performed at physiological conditions for a certain amount of time and subsequently quenched by lowering the pH to 2.5 and temperature to 0°C, which decreases hydrogen exchange rates for amide hydrogens. Under these conditions, the half-life of amide hydrogen exchange is 30 to 120 minutes. This is enough time to analyze the sample by reverse-phase HPLC coupled to electrospray ionization mass spectrometry without a substantial loss of incorporated deuterium. The incorporated deuterium can be analyzed in a global manner (full-length proteins) or in a local one (peptides generated by proteolytic degradation), in which case more detailed information can be obtained. Peptides are produced by digesting the deuterium-labeled protein with pepsin under conditions of slow exchange (pH 2.5 and 0°C). Figure 2.3 shows a schematic representation of a typical HX experiment. Of the many exchangeable hydrogens present in proteins, only backbone amide hydrogens are measured with this method. Since the rate of exchange of amide hydrogens in a folded protein depends on the presence of hydrogen bonds and the solvent accessibility, this technique can be used to monitor dynamical and conformational changes. HX experiments

can also be used to map binding interfaces when amide hydrogens are involved in the interaction with a ligand. Figure 2.4 shows a schematic representation of these two applications of HX experiments.

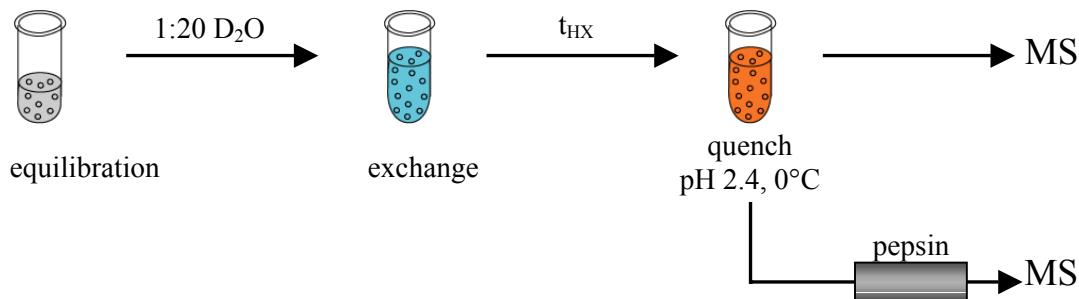


Figure 2.3. Schematic representation of a typical HX experiment. First, the protein sample is equilibrated in a water buffer. Then, the protein is diluted 1:20 in D₂O buffer and incubated for a certain time. The reaction is quenched with ice-cold low-pH buffer and injected into the mass spectrometer.

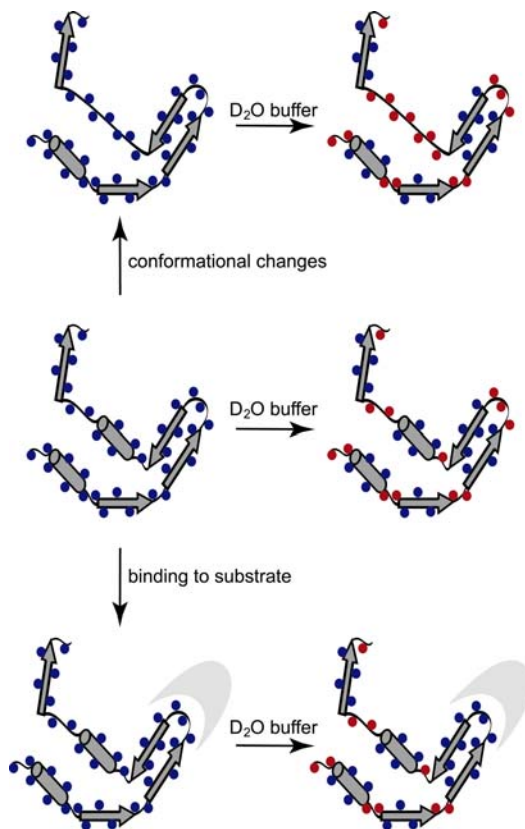


Figure 2.4. Schematic representation of D₂O experiments. ¹H are indicated in blue and ²H are indicated in red.

Mass spectrometer

A mass spectrometer consists of three main parts: (a) an ion source where gaseous ions are formed, (b) a mass analyser that separates the ions regarding the mass-charge-ratio (m/z), and (c) a detector. There are different ways of ionising analytes (Figure 2.4). For example, in electrospray ionisation (ESI) the sample is sprayed into an electrical field, while in MALDI (matrix assisted laser desorption ionisation) the sample is embedded in a crystal matrix and ions are produced after excitation of the matrix with a high intensity laser pulse of short duration. The ions can be separated by combining a magnetic and an electric field (sector field instruments), inside the RF field of a quadrupole, by a magnetic ion trap, or after a flight time in an ion flight tube combined with a pulsed ion formation (Time-Of-Flight instruments, TOF).

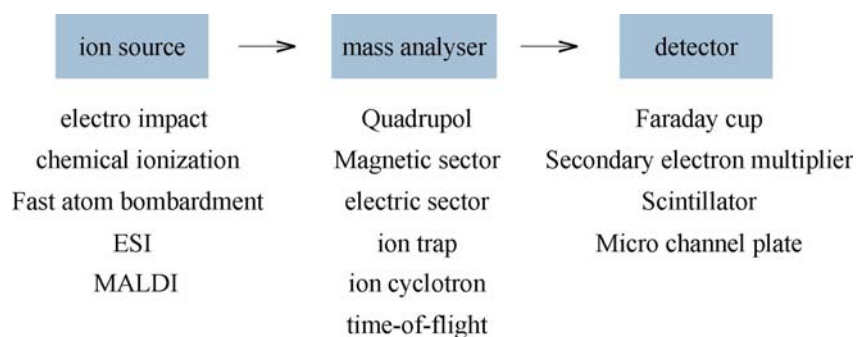


Figure 2.5. Components of a mass spectrometer.

Both ESI-MS and MALDI-MS can be used in amide hydrogen exchange experiments. However, ESI-MS is the most commonly used ionization method because the quenched sample can be introduced directly via HPLC into the electrospray source, thereby reducing the deuterium loss during the analysis. This loss of labeled deuterium is known as back-exchange.

Chapter 3

A quenched-flow setup

As mentioned in the previous chapter, amide hydrogen exchange (HX) combined with mass spectrometry (MS) is a powerful tool to analyze the folding and dynamics of proteins. In recent years this approach has become increasingly popular because of its high sensitivity, the accessibility of flexible structures, the greatly extended size range compared with NMR, and the possibility to detect coexisting conformations. The resolution of this method depends on the size (on average 10–15 residues) of peptides generated after the exchange reaction by proteolytic cleavage under quench conditions. The conformational properties of proteins in their native state are typically investigated by HX by incubating the proteins in deuterated buffer at neutral pH for different time intervals with subsequent acidification, desalting, and MS analysis (Engen and Smith 2001). In the traditional methodology the exchange time is controlled by manual pipeting,

therefore limiting the time resolution to several seconds. However, some conformational changes in proteins occur in the sub-second time scale. It is then necessary to perform HX at shorter time intervals. In our laboratory a completely on-line quenched-flow setup was developed that allows the performance of HX experiments in the 100 ms to 30 s time scale, on-line proteolytic digestion using immobilized proteases, rapid desalting, and MS analysis (Rist *et al.*, 2005). The purpose of this chapter is to evaluate the performance and reproducibility obtained with this setup. We have also used it to investigate the conformational properties of *E. coli* heat-shock transcription factor σ^{32} free in solution. Homology modeling of the σ^{32} sequence onto the structure of the σ -factor σ^A in complex with the RNA-polymerase indicated a helical structure in the C-terminus. Previous HX experiments had shown that the amide hydrogens of the C-terminus of σ^{32} exchange almost completely after 10 s, indicating that this region is very flexible. Using the quenched-flow setup we have detected amide protons in the C-terminal region of σ^{32} that are protected. Our results indicate that the C-terminal domain of σ^{32} , which is responsible for the recognition of the -35 region of heat-shock promoters, contains amide hydrogens involved in secondary structure.

Quenched-flow setup

Our setup consists of five HPLC pumps, two 10-port valves, an injection valve, a trap column for rapid desalting, an optional column with immobilized pepsin for on-line proteolytic digestion, and an optional analytical column for peptide separation before analysis by ESI-MS as shown in Figure 3.1. The sample is introduced in the injection valve and delivered by pump 1. It is next diluted 1:25 in a mixing tee with D₂O-buffer, delivered by pump 2, thereby starting the exchange reaction, which continues in the delay line. This exchange reaction is quenched by addition of quench buffer, delivered by pump 3, in a second mixing tee. The protein is subsequently trapped on a reversed-phase micro-trap column and, after switching the first 10-port valve, desalted with 0.05% trifluoroacetic acid in water, delivered by pump A. After switching the second 10-port valve, the sample is eluted with an acetonitrile gradient, generated by binary pump B, over an analytical microbore reversed-phase column directly into the electrospray ion source of the mass spectrometer. For localization of the exchanging regions within the

protein, a column with an immobilized protease, e.g., pepsin, is inserted into the system before the trap column. The duration of the exchange reaction can be adjusted to the desired times by choosing the delay line length and inner diameter. To limit back-exchange during proteolytic cleavage and desalting, the entire setup downstream of the delay line is submerged in an ice bath. When all pumps have reached the desired flow rates the exchange experiment is started by switching the injection valve to the inject position. This triggers a program that automatically switches the two 10-port valves at the preset time points. This full automation of the setup guarantees a high degree of reproducibility.

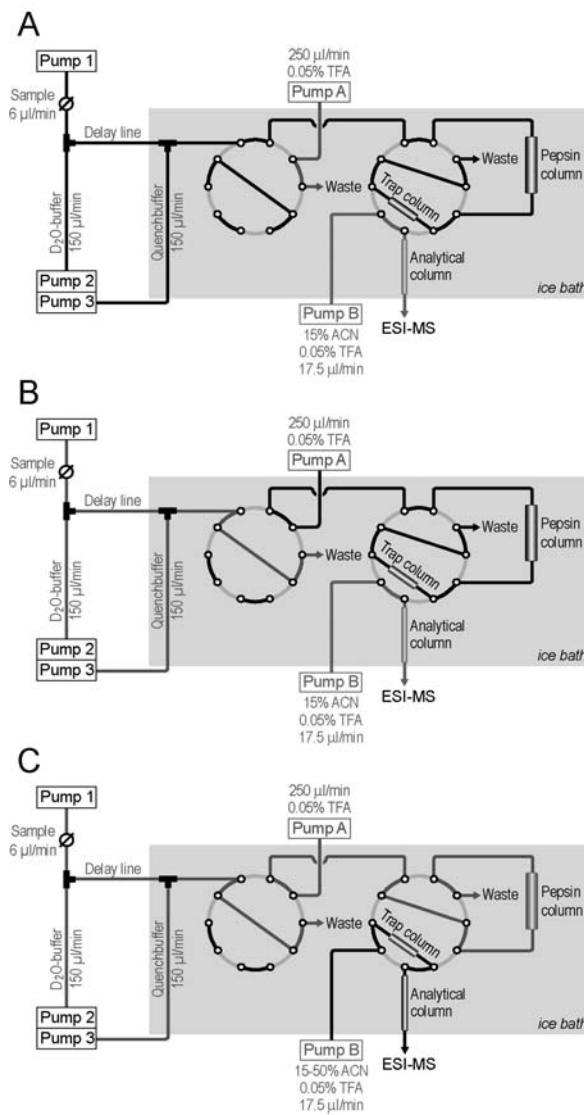


Figure 3.1. Schematic representation of the HPLC-MS quenched-flow setup (A) HX position, (B) desalting position and (C) MS analysis position.

The quench-flow setup is accurate and reproducible

Apo-myoglobin is a model protein generally used in Biophysics because it is well characterized and commercially available. In order to test our setup we have analyzed deuterium incorporation into native apo-myoglobin at different time intervals and compared them with manually-performed HX reactions. As shown in Table 3.1, between 30 s and 5 s both procedures have yielded identical results. Although gradual deuterium incorporation was observed with the quenched-flow setup in the millisecond-to-second time scale, reproducible manual sample handling was very difficult below 5 seconds and not possible below 2 seconds. For this reason we could not determine the deuterium incorporation with manual handling below 5 seconds. The total deuterium incorporated in the case of the quenched-flow setup was 1-2 Daltons smaller than in the case of manual handling. There are two possible explanations for this observation, one is that in the case of the quenched-flow setup the sample is in contact with the deuterium buffer for a shorter time than in the case of manual pipeting. The second possibility is that there is more back-exchange in the case of the quenched-flow setup. The first possibility can be excluded since the exchange time is determined by the length of the delay line. Then, the lower deuterium incorporation can be explained by increased back-exchange in the quenched-flow setup due to a prolonged exposure to protonated solvent. The sample is loaded into the quenched-flow system for a period of about 50 s (5 μ L at 6 μ L/min flow-rate at pump 1). Part of the sample remains slightly longer on the trap column compared with the sample obtained from the manually-performed initiation and quenching of isotopic exchange. Figure 3.2 shows some representative mass spectra of full-length apo-myoglobin. The quality of the spectra is good—all isotopic peaks are well defined. To determine the loss by back-exchange in both methods, the incorporation of deuterium was tested with a peptide that exchanged 100% of the hydrogens after 30 seconds. The percentage of incorporation was calculated assuming that all amide hydrogens with exception of the first one exchanged after 30 s. In both procedures the overall retention of incorporated deuterons was close to 90%. The small loss by back-exchange is due to the short time interval between the quench of the exchange reaction and the transition of the sample into the vacuum. Thus, the quench-flow setup is accurate and reproducible.

Table 3.1. Reproducibility of manual and quenched-flow amide hydrogen exchange.

Exchange time (seconds)	Off-line	On-line
1	-	16,992.4 ± 0.7
2	-	16,997.8 ± 0.9
5	17,006.3 ± 0.5	17,005.4 ± 0.7
10	17,013.0 ± 0.7	17,011.0 ± 0.7
30	17,023.9 ± 0.7	17,022.2 ± 0.1

Apo-myoglobin was diluted 1:25 in D₂O buffer by manual mixing or using the quenched-flow setup and deuterium incorporation determined after different time intervals. Desalting and analysis was identical for both methods.

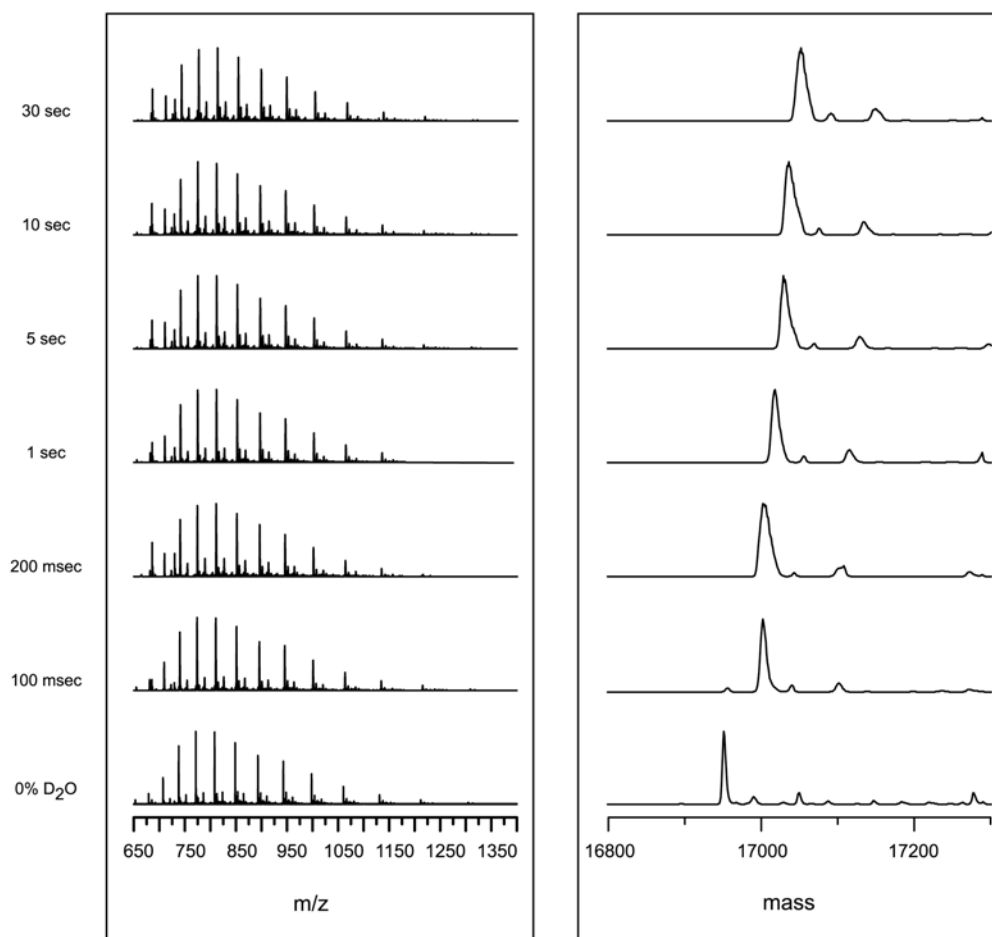


Figure 3.2. Quenched-flow amide hydrogen exchange of full-length apo-myoglobin. Protein mass spectra (left) and deconvoluted mass spectra (right) of apo-myoglobin after exposure to D₂O for different times.

The quench-flow system setup time interval is limited by k_{ch}

Our next step was to evaluate the performance of the quench-flow setup at time points between 100 ms and 30 s. To this aim we performed HX experiments with apo-myoglobin at two different pH values (7.6 and 8.5) and compared the conformational information obtained against previously published results. HX experiments were performed with full-length protein and the time course of deuterium incorporation for both pH was fitted. The curves of incorporated deuterium versus time can be fitted with a triple exponential. The amide hydrogens of the protein can be divided in three, depending on their exchange rate: solvent-exposed ones which exchange very fast, the ones involved in the flexible structure which have an intermediate exchange rate, and the ones participating in the stable structure which have the longest time constant. The smallest time constant for the measured deuterium incorporation could not be fitted and was set to the intrinsic chemical exchange time constant (dashed lines, Figure 3.3) as calculated for each amide hydrogen of the entire protein using the HXPep program (courtesy Z. Zhang, Bai *et al.*, 1993) with a triple exponential rate equation fit.

The fitted parameters indicated that 31 deuterons were incorporated into apo-myoglobin at pH 7.6 with a time constant shorter than 0.1 s. This is the number of completely exposed amide hydrogens. Seventeen deuterons were incorporated with a time constant of 1.7 s, revealing relatively fast fluctuations in amide hydrogen accessibility —most likely, in the form of opening and closing H-bonds. Additional 29 deuterons were incorporated with a time constant of 22 s. The total number of exchanging amide hydrogens at pH 7.6 as calculated from the fitting parameters was 77. Since apo-myoglobin has 147 exchangeable amide hydrogens, about 50% of the amide hydrogens are completely protected at the investigated time scale. Our results for the longest incubation times are similar to published data (Johnson and Walsh, 1994).

To show that the shortest exchange time that we can measure is determined by the intrinsic exchange rate, we evaluated the apo-myoglobin deuterium incorporation at pH 8.5. The intrinsic exchange rate is pH-dependent and is faster at pH 8.5 compared with pH 7.6. At pH 8.5, the intrinsic chemical exchange exceeds 98% already after 250 ms; any measured slower exchange therefore indicates protection by structural elements. As indicated by the fitting parameter, 47 deuterons were incorporated with a time constant <

0.1 s, 28 amide hydrogens exchanged with a time constant of 0.8 s, and additional 75 protons with a time constant < 70 s. The total number of exchanging amide hydrogens at pH 8.5 as calculated from the fitting parameters was 150, which is very similar to the total number of exchangeable amide hydrogens in apo-myoglobin. At pH 8.5, deuterium incorporation was therefore faster and more extensive than at pH 7.6, indicating pH-dependent structural fluctuations in apo-myoglobin. The increased rate of deuterium incorporation at higher pH values is caused by two effects. First, the accelerated intrinsic chemical exchange rate at higher pH increases the probability of exchange in any transient structural opening event. Second, the flexibility of apo-myoglobin increases at higher pH, in agreement with published data (Haouz *et al.*, 1998). These results demonstrate that our quenched-flow setup can accurately measure the deuterium incorporation into full-length proteins within the time interval limited by k_{ch} and the manual pipeting speed.

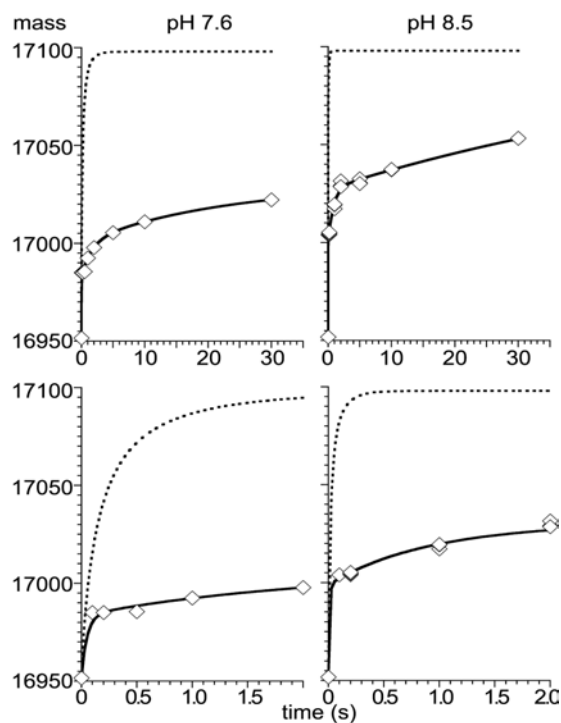


Figure 3.3. Quenched-flow amide hydrogen exchange of full-length apo-myoglobin (100 pmol). It was measured at pH 7.6 (*left*) and 8.5 (*right*) for 0.1 s to 30 s and compared to the overall intrinsic chemical exchange (dashed curves) as determined for each amide using the HXPep program (courtesy Z. Zhang). The solid line represents the fit of a triple exponential rate equation ($y = A_{\infty} - A_1 \cdot \exp(-k_1 \cdot t) - A_2 \cdot \exp(-k_2 \cdot t) - A_3 \cdot \exp(-k_3 \cdot t)$) to the data whereby for the fastest rate k_1 the value derived from a fit to the intrinsic chemical exchange data was used. The *lower* panels show a zoom of the first 2 s of the exchange reaction.

The three-helix bundle of σ^{32} has protected amide hydrogens

In a previous work at our laboratory, the temperature-dependent conformational changes of σ^{32} were studied using HX experiments. It was shown that there is a good overall consistency between a structural model of σ^{32} and the HX data, with the only exception of the C-terminus of σ^{32} showing disagreement. Even though the model predicted α -helices in the C-terminus, no protection was observed in HX (Rist *et al.*, 2003). This inconsistency could be explained either by the incorrectness of the model or by a highly dynamic nature of the α -helices in this region with opening and closing kinetics in the second time range. The shortest exchange time used in the reported experiments was 10 s, and therefore a dynamic structure of the α -helices would have remained undetected. Since this region is involved in the recognition of the -35 region of heat-shock promoters, its structural properties are important for the biological function of σ^{32} . To ascertain whether the α -helices are highly dynamical we performed HX experiments with the quenched-flow setup. A pepsin column was included before the trap column and a gradient was run to separate the peptides. We tested first whether the elution time of the peptides is reproducible. σ^{32} was diluted in quench buffer, injected into the system, and the retention times were determined—they ranged between 8 and 12 min. σ^{32} was then incubated in deuterated buffer, and the sample was quenched and injected into the HPLC system. The retention times for all the peptides were identical (some of them are shown in Table 3.2) for both conditions. This facilitates the assignment of peptides after deuteration since the same peptide would elute after the same time. We determined the back-exchange by using fully deuterated peptides and running the gradient. Deuterium loss during desalting and analytical chromatography was between 13% and 18%. Some representative mass spectra of peptic fragments of σ^{32} are shown in Figure 3.4.

When HX of σ^{32} was analyzed in our setup and the measured deuterium incorporation compared with the k_{ch} of the individual peptide segments, we found that a total of at least 30 amide protons in the C-terminal region are still protected after 1 s and at least 25 after 5 s. Figure 3.5 shows the kinetics of amide hydrogen exchange of individual peptide segments under native state conditions in comparison with the intrinsic chemical exchange kinetics of the corresponding unstructured peptides. While in some

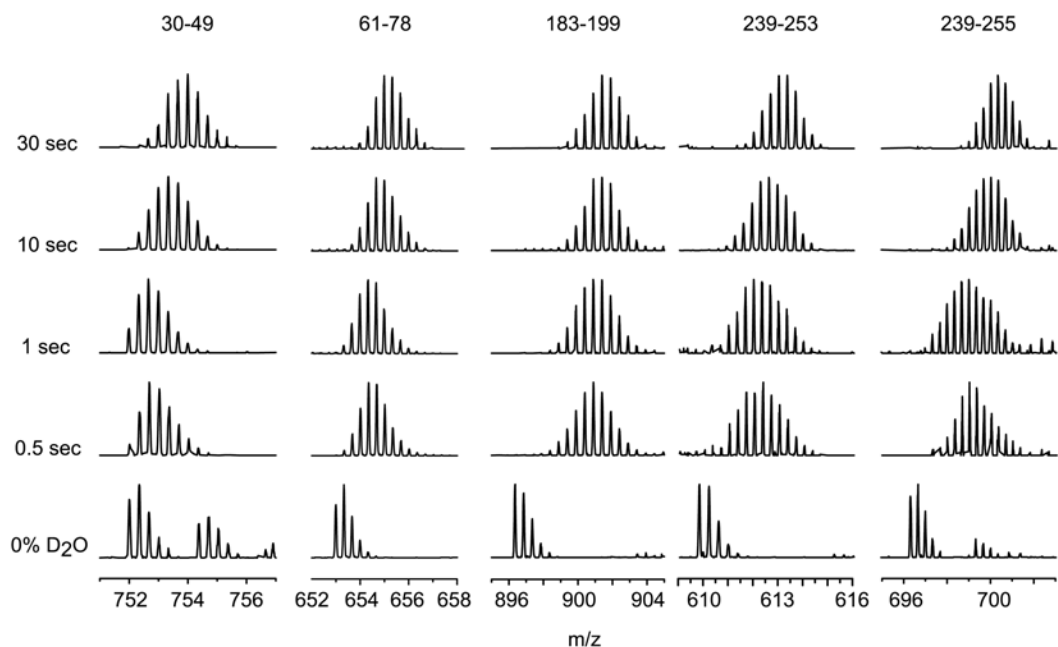


Figure 3.4. Amide hydrogen exchange of peptide segments within *E. coli* heat shock transcription factor σ^{32} . Mass spectra of 5 different peptides after exposure to D₂O for different times. The residue numbers for each peptide are indicated at the top.

peptide segments (amino acids 209–244, 240–253, 255–263, 259–272, and 258–294) (Figures 3.5 and 3.6, upper panel) significant protection was observed over a time interval of 1–5 s, other peptide segments (amino acids 184–199 and 201–208) exchanged almost all amide protons for deuterons within 0.5 s. The determined protection factors of the intermediately exchanging amide hydrogens were 10.0, 14.4, 33.9, 9.3, and 35.9 for peptides 209–244, 240–253, 255–263, 259–272 and 258–294, respectively. Repetitive determination of the m/z values for the different peptides at the individual time points of HX was within 0.1 m/z units, demonstrating high reproducibility. σ^{32} was modelled by homology onto the structure of *Thermus thermophilus* σ^A bound to RNA polymerase. Using this model the number of possible hydrogen bonds involving backbone amides was determined by measuring the distances between amide nitrogens and their corresponding carbonyl oxygens using the Insight II program (Accelrys). The number of potential hydrogen bonds are shown in the lower panel of Figure 3.6 (nitrogen–oxygen distance < 3.0 Å and < 3.2 Å, respectively) and compared with the number of protected amide

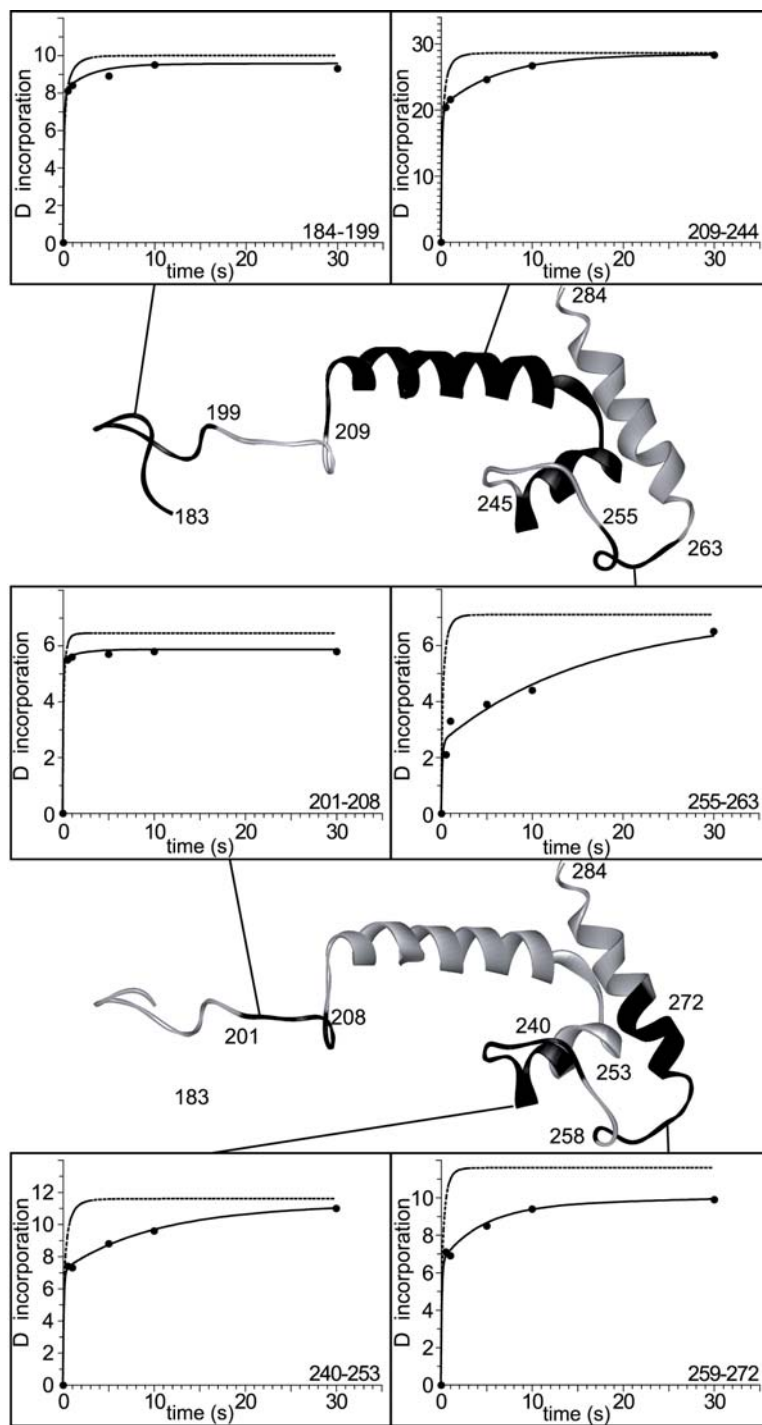


Figure 3.5. Amide hydrogen exchange kinetics of peptide segments within the *E. coli* heat-shock transcription factor σ^{32} . Incorporation of deuterium into σ^{32} was measured using quenched-flow with on-line peptic digestion. The exchange kinetics is shown for six different peptides [indicated in the structural model of σ^{32} (183–284) in black] and compared to their individual intrinsic chemical exchange kinetics (dashed line). The solid line represents the fit of a triple exponential rate equation ($y = A_{\infty} - A_1 \cdot \exp(-k_1 \cdot t) - A_2 \cdot \exp(-k_2 \cdot t) - A_3 \cdot \exp(-k_3 \cdot t)$) to the data whereby the values for the fastest rate, k_1 , and for the total number of exchangeable amides, A_{∞} , were derived from a fit to the intrinsic chemical exchange data.

hydrogens after different exchange times (Figure 3.5, upper panel). In most peptides originating from the C-terminal part of σ^{32} we observed a higher degree of protection of amide hydrogens than expected from the structural model using 3 Å or 3.2 Å as cutoff criterion for a stable hydrogen bond, indicating a more extensive secondary structure. In one peptide the opposite was observed: less amide hydrogens were protected than expected from the model. This discrepancy could be due to the fact that σ^{32} was modeled onto the RNA polymerase bound form of σ^A . Free in solution, this region may exhibit a more extensive secondary structure. Therefore, the C-terminal part of σ^{32} has protected amide hydrogens involved in secondary structure.

Table 3.2. Retention time of different σ^{32} peptides.

segment	Retention time in normal buffer (min)	Retention time in D ₂ O buffer (min)
184-199	8.5	8.5
240-253	9.5	9.5
255-263	10.5	10.5
259-272	9.5	9.5
258-294	10.5	10.5

The retention time with and without incubation with deuterium buffer was identical. The retention time was determined as the time where the maximum intensity for each peak was observed.

Conclusions

In this chapter we have presented a quenched-flow setup that allows HX experiments with as short as 100 ms exchange times. We have demonstrated that these experiments can be performed with our setup in a reproducible manner. All steps are performed automatically, thereby reducing the error due to sample handling. We have also shown that back-exchange is reduced since all steps are performed on-line.

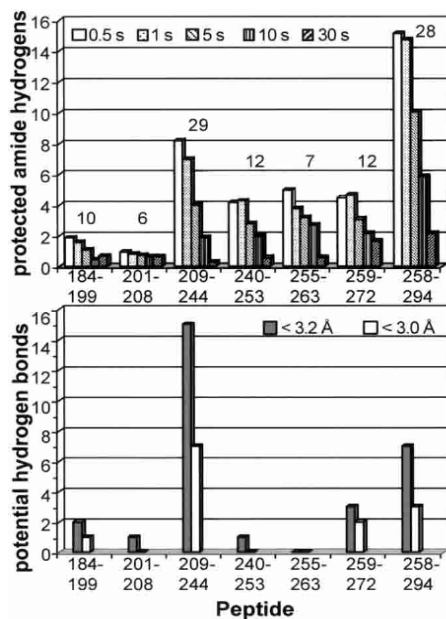


Figure 3.6. Comparison between expected and observed amide hydrogen exchange in the C-terminal region of σ^{32} . In the upper panel we show the number of protected amide hydrogens for different time points (0.5, 1, 5, 10 and 30 seconds). The number of potential hydrogen bonds are shown in the lower panel.

Using this setup we have then investigated the conformational properties of *E. coli* heat-shock transcription factor σ^{32} free in solution. We have shown that the amide hydrogens of the C-terminus of σ^{32} exchange almost completely after 10 s, indicating that this region is very flexible. Using the quenched-flow setup we have detected at least 30 amide protons in the C-terminal region of σ^{32} that are protected after 1 sec, and at least 25 after 5 s. Even though the number of hydrogens protected did not completely agree with the homology modeling of σ^{32} onto the RNA polymerase bound form of σ^A , we have shown that the C-terminal part of σ^{32} has protected amide hydrogens involved in secondary structure. Therefore, this setup is suitable for mapping short-term conformational changes and it will be useful for mapping ligand binding, enzyme catalysis or dimer interfaces with high dissociation rates.

Chapter 4

Crystallization of the σ^{32} -DnaK complex

With the exception of σ^{54} , all σ -factors comprise a homologous family (the σ^{70} family) with four flexibly linked domains, $\sigma_{1.1}$, σ_2 , σ_3 and σ_4 (Gruber and Bryant, 1997). The structures of σ_2 , σ_3 and σ_4 have been observed in complex with core RNAP (Murakami *et al.*, 2002a; Vassylyev *et al.*, 2002), in complex with anti- σ -factors (Campbell *et al.*, 2002a, 2003), and individually (Campbell *et al.*, 2002b; Li *et al.*, 2002; Malhotra *et al.*, 1996). In all cases, the structures of the corresponding σ -domains are nearly identical, suggesting that the relative positioning of the domains is responsible for the regulation of σ activity. It is also known that binding to core RNAP induces large relative movements of the σ -domains of σ^{70} (Callaci *et al.*, 1999). We would like to gain insight into the structure of σ^{32} -bound to DnaK. This is the reason why during this thesis we attempted to crystallize σ^{32} in complex with DnaK.

As described in Chapter 1, the structures of the two DnaK domains (ATPase domain and substrate-binding domain) have been determined separately by X-ray

crystallography. However, the structure of the full-length DnaK in complex with a substrate has not yet been determined. It is still unclear how the two DnaK domains interact with each other and which structure the linker region assumes. In addition, the substrate-binding domain was crystallized in complex with a heptamer substrate peptide and it is not known how a substrate protein is bound. Does the helical lid close when a protein is bound? Are there additional contact sites important for substrate specificity?

The aim of the studies reported in this chapter was to elucidate the molecular details of the σ^{32} -DnaK interaction by solving the structure of the complex using X-ray crystallography. σ^{32} forms a stable complex with DnaK. The apparent K_D for this complex is between 1 to 5 μ M. This indicated that the isolation of the complex was possible and encouraged us to try to crystallize it. This would help understanding the mechanism of Hsp70 chaperones. With this purpose we established a collaboration with the research group of Prof. Seth Darst (Rockefeller University). This group has solved the X-ray crystal structure of the flagellar σ -factor, σ^{28} , in complex with its anti- σ -factor, FlgM (Sorenson *et al.*, 2004), the crystal structure of the *E. coli* factor σ^E in an inhibitory complex with the cytoplasmic domain of its anti- σ , RseA (Campbell *et al.*, 2003), the structure of σ^{70} in complex with core RNAP (Murakami *et al.*, 2002a), the structure of individual σ domains (Campbell *et al.*, 2002b), the crystal structure of the initiating form of *Thermus aquaticus* RNA polymerase, containing core RNA polymerase and the promoter specificity σ sub-unit (Murakami *et al.*, 2002b), and the crystal structure of *Thermus aquaticus* core RNAP complexed with Rif (Campbell *et al.*, 2001). This project was initiated with my research visit to the laboratory of Prof. Seth Darst, where the purification of the complex and initial crystal screening were performed.

Cloning of σ^{32} and DnaK

The original idea was to co-express σ^{32} and DnaK (without the flexible C-terminal tail, up to amino acid 607, DnaK (1-607)), in order to purify *in vivo* pre-assembled complexes. We cloned the σ^{32} and DnaK (1-607) encoding genes into an IPTG inducible expression vector and overexpressed the proteins in a Δ dnaK52-host strain (BB1553, Bukau and Walker, 1990). We used a Δ dnaK strain given that we formed the complex

with a C-terminal deletion version of DnaK and we did not want to have wild-type contaminants in our complexes. However, in this background we found that the expression level of the complex was too low. This could be due to the fact that, *in vivo*, σ^{32} is degraded by the AAA+ protein FtsH, which is a membrane-anchored ATP-dependent metalloprotease (Tomoyasu *et al.*, 1998, Tatsuta *et al.*, 2000), and DnaK is necessary for this degradation. We transformed the vector expressing the complex into a Δ dnaK- Δ ftsH strain. This strain grew very slowly and was not suitable for the expression of the complex, so we decided to follow an alternative protocol: to express both proteins in separate strains and then to form the complex *in vitro*.

The *rpoH* gene, encoding σ^{32} , was cloned into a plasmid with an L-arabinose inducible promoter. At the N-terminus of σ^{32} we placed a hexahistidine-tag (His₆-tag) followed by a Ppx cleavage site. We changed the thrombin for the Ppx cleavage site because members of the Darst laboratory had found that the latter protease has a higher efficiency in cleaving. DnaK (1-607) was cloned in an IPTG inducible expression vector. Overexpression was performed in the Δ dnaK52-host strain. The substrate-binding domain of DnaK without the C-terminal tail (aa 389-607) was also cloned in an IPTG inducible expression vector and overexpressed in a Δ dnaK52-host strain. DnaK, substrate-binding domain of DnaK, and DnaJ do not contain a His-tag.

Purification of the complex

We purified σ^{32} using Ni²⁺-affinity chromatography, and then added DnaK (1-607) to σ^{32} bound to the Ni²⁺-column. The complex was formed in the Ni²⁺-column and the unbound DnaK (1-607) could be washed away. After elution and cleavage, we ran a gel filtration column to separate free σ^{32} from the complex. We also purified the DnaJ/ σ^{32} and the DnaK/DnaJ/ σ^{32} complexes.

DnaK/ σ^{32} complex. After gel filtration, the complex containing fractions were pooled and concentrated to a final concentration of 10 mg/ml. Figure 4.1 illustrates the sodium dodecyl sulfate polyacrylamide gel electrophoresis (SDS-PAGE) of the purified complex. Lanes 1 and 2 show the complex eluted from the Ni column, showing that it was indeed formed. Lanes 3 and 4 show the purified complex after gel filtration, which

not only removed contaminating protein but also separated DnaK/ σ^{32} complex from free σ^{32} . Lanes 5 and 6 show σ^{32} alone, before and after concentration of the sample. As we can see, the gel filtration column was unable to separate Ppx from the complex. Since Ppx protease has a GST tag, we finally ran a GST sepharose column to remove it.

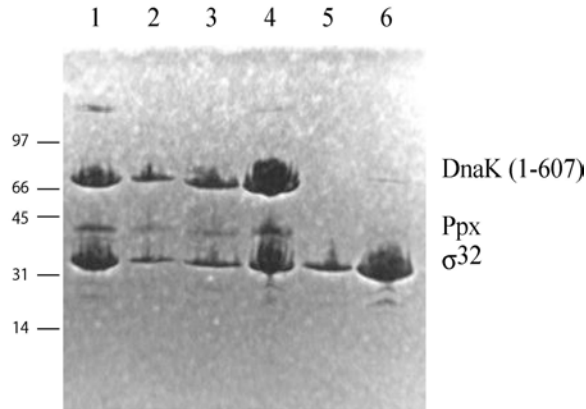


Figure 4.1. The purification of the DnaK/ σ^{32} complex was analyzed by SDS-PAGE using 8-25% PhastGels (Pharmacia). Lanes 1 and 2 show the complex eluted from the Ni-column at two different concentrations. Lanes 3 and 4 show the purified complex after gel filtration, before and after concentration of the sample. Lanes 5 and 6 show σ^{32} alone, also before and after concentration of the sample.

DnaJ/ σ^{32} complex. The DnaJ/ σ^{32} complex was purified in a similar way as described above for the DnaK/ σ^{32} complex. After elution, the protein was loaded onto a Superdex 200 column and the DnaJ/ σ^{32} complex containing fractions were pooled. Also in this case the gel filtration column was useful for the separation of the complex from free σ^{32} . In lanes 1 and 2 of Figure 4.2 we show the purified DnaJ/ σ^{32} complex, after gel filtration, purified on different days. As we can see, it was possible to purify it and was stable after gel filtration.

DnaK/DnaJ/ σ^{32} complex. DnaJ wild type was added to σ^{32} bound to the Ni²⁺-column. The two proteins were incubated during 20 min and then DnaK (1-607) was added with ATP during 30 min (concentration of ATP: 2 times the concentration of DnaK). The Ni²⁺-agarose was then washed to remove unbound DnaK and DnaJ. Ppx protease was added and incubated during 4 hours at 4°C. The purification of the ternary

complex was repeated one more time (purifications 1 and 2), and its eluted form was loaded onto a gel filtration column. We observed that it was also stable after gel filtration. Some contaminants remained in purification 1 (see Figure 4.2, lane 3), but not in number 2 (lane 4).

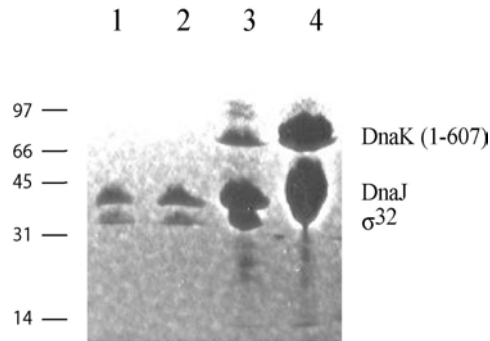


Figure 4.2. The purifications of the DnaJ/ σ^{32} and DnaK/DnaJ/ σ^{32} complexes were analyzed by SDS-PAGE using 8-25% PhastGels (Pharmacia). Lanes 1 and 2 show the purified DnaJ/ σ^{32} complex after gel filtration, purified at different days. Lanes 3 and 4 show the DnaK/DnaJ/ σ^{32} complex, also purified on different days.

Initial crystal screenings

The structure determination of the DnaK/ σ^{32} , DnaJ/ σ^{32} and DnaK/DnaJ/ σ^{32} complexes and σ^{32} alone is of utmost importance to understand the mechanism of action of the DnaK/DnaJ chaperone system. In this way, one can observe the interactions that are involved in the binding of these proteins and the effect of binding on the protein structure. For this reason we screened the three complexes and σ^{32} alone, in order to identify potential crystallization conditions. For the initial trial we used the classic buffers from Nextal. This commercial kit is composed of 96 unique conditions with high concentration of various precipitants. We used the DropGuard Crystallization Tool (Nextal) that allows for the screening of six complexes in the same well. With the first screening we found that some conditions could lead to crystal formation —e.g., ammonium sulfate precipitation. Therefore, we screened different ammonium sulfate concentrations and different values of pH. Ammonium sulfate had also been used

successfully in the Darst laboratory for the crystallization of other σ -factors. All screens were performed at 22°C and 4°C. For some of the conditions screened we observed the presence of microcrystals. However, none of them grew further, so they were not useful for diffraction.

Trypsin partial proteolysis

σ factors are loosely folded proteins. To succeed in the crystallization of a protein it is important to remove the flexible parts that avoid crystal formation. We used limited proteolysis of σ^{32} in the absence and presence of DnaK to map which regions of σ^{32} are flexible. σ^{32} or σ^{32} -DnaK complex was mixed with increasing amounts of trypsin and the fragments produced were separated by SDS-PAGE. In the σ^{32} -DnaK complex, at highest concentration of trypsin stable fragments appeared. These fragments were analyzed by mass spectrometry. It was possible to identify some fragments by their mass (see Table 4.1).

Table 4.1. Identification of σ^{32} fragments produced after trypsin proteolysis.

Observed mass	Calculated fragment	Theoretical mass	wt number
29820	2-263	29818.7	1-241
29106	2-257	29105.9	1-235
27875	2-246	27875.5	1-224
26267	24-254 (a)	26267.9	2-232
25496	2-225 (b)	25497.1	1-203

(a) cut after L, (b) cut after D

The fragments were identified by their mass.

As shown in Table 4.1, the fragments identified are deletions from the C-terminus. Rist *et al.* (Rist *et al.*, 2003) have shown, using HD experiments, that the C-terminus of σ^{32} is very accessible to the solvent. In Chapter 3 we have also demonstrated that the exchange times in HX experiments have to be short (less than 10 s) in order to see protection of the hydrogens involved in secondary structure. As initial step we decided to clone three different mutants lacking the C-terminus domain. We cloned up to residues

210, 218 and 224. In our structure model, there is an α -helix between residues 218-235. Therefore, we decided to construct two deletion mutants before that α -helix and the third one was the same as the fragment produced by trypsin (Figure 4.3).

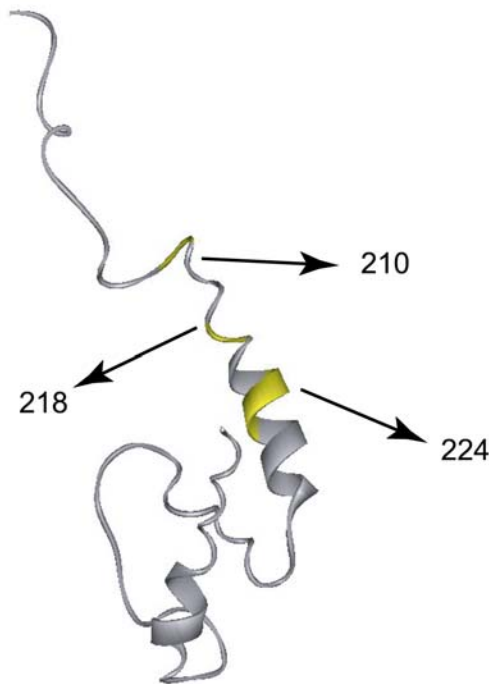


Figure 4.3. Zoom of the C-terminal region of σ^{32} . The positions of the deletion mutants are indicated in yellow. The DnaK binding domain is indicated in red.

Deletion mutants form complex with DnaK

To check that the deletion mutants can still form complex with DnaK (1-607), the three mutants were over-expressed and the mutants purified through a NiNTA column. Before elution from the NiNTA column, purified DnaK(1-607) was added and incubated for two hours. The free and bound σ^{32} were separated by gel filtration and analyzed by SDS-PAGE. The three deletion mutants still form complex with DnaK (1-607) (Figure 4.4). Unfortunately, these deletion mutants in complex with DnaK have not produced diffracting crystals.

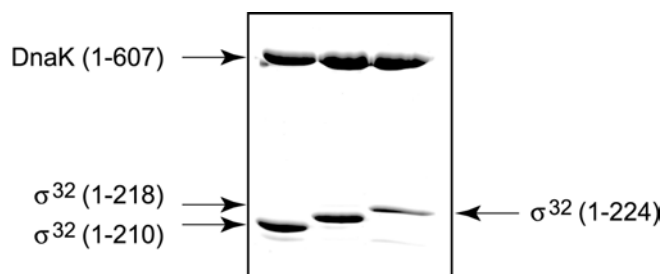


Figure 4.4. The purifications of the DnaK/ σ^{32} deletion variants complexes were analysed by SDS-PAGE using 12% gel.

Conclusions

In this chapter we have shown that it is possible to purify DnaK/ σ^{32} , DnaJ/ σ^{32} and DnaK/DnaJ/ σ^{32} complexes in the high concentrations required for crystallization trials. We have also found the regions of σ^{32} that are flexible when it is in complex with DnaK. It is important to remove these flexible regions to obtain crystals. We created deletion mutants and tested them for DnaK binding. We found that the three deletion mutants bound DnaK and they were suitable for crystal trials.

Even though we have not been successful yet in obtaining crystals for neither of the complexes, this project is a still ongoing collaboration. We are currently trying to purify the different complexes formed *in vivo*. For this we have created new plasmids and we are still searching for the right conditions for this purification.

Chapter 5

Regulation of σ^{32} by the DnaK chaperone system

In *E. coli* the heat-shock response is mediated by the alternative σ transcription factor σ^{32} that activates the transcription of the heat-shock genes (Bukau, 1993; Connolly *et al.*, 1999; Gross *et al.*, 1996; Yura and Nakahigashi, 1999). σ^{32} is regulated by the DnaK, DnaJ and GrpE chaperone system. The precise mechanism of the DnaK and DnaJ interaction with σ^{32} is still unclear. In order to obtain a complete picture of the heat-shock regulation, it is important to characterize the regions of σ^{32} directly involved in the DnaK and DnaJ-mediated control. Given that common substrates of DnaK and DnaJ are non-native polypeptides, it is important to determine which are the structural features that turn σ^{32} into a native protein substrate of DnaK and DnaJ. The interaction of DnaK and DnaJ with σ^{32} is considered to be a paradigm for the interaction of Hsp70 chaperones with regulatory native substrates. The DnaK binding site within the native σ^{32} protein has

been previously mapped employing a protease foot-printing approach in our laboratory. This approach assumes that DnaK binding prevents proteolytic cleavage of σ^{32} in the neighbourhood of its binding site. As a negative control, a DnaK mutant protein (DnaK-V436F) that had a 17-fold lower affinity for σ^{32} (Mayer *et al.*, 2000a) was included in the experiments. In the presence of a 5-fold molar excess of DnaK, the pattern of the σ^{32} bands changed. Three σ^{32} bands were less prominent in the presence of DnaK indicating a protected cleavage site. DnaK-V436F did not protect σ^{32} to the same extent. These bands were identified by MALDI-TOF mass spectrometry and N-terminal sequencing. The protected cleavage sites are at positions 204 and 201 of the σ^{32} polypeptide chain for trypsin and proteinase K, respectively. This region comprises a potential DnaK binding site with a core of 4 large hydrophobic amino acids (198Val-Leu-Tyr-Leu201). This site has also been experimentally identified by scanning of a σ^{32} peptide library (McCarty *et al.*, 1996; Rüdiger *et al.*, 1997)). A peptide that contains both cleavage sites (σ^{32} -M195-N207) also binds with high affinity to DnaK in solution (McCarty *et al.*, 1996). This peptide is the only segment within the entire region that experimentally shows high affinity for DnaK at the peptide level (Rüdiger *et al.*, 1997). The potential binding site was mutated and the affinity evaluated, showing a lower affinity for DnaK.

In this chapter we study the interaction of DnaK and DnaJ with σ^{32} . We confirm that the previously identified DnaK binding site in σ^{32} is the binding site in the native protein and we identify the segment where DnaJ binds. Using amide hydrogen exchange experiments, we find that DnaK and DnaJ induce conformational changes upon binding to σ^{32} . Our results provide mechanistic insights into the regulation of the heat shock response.

σ^{32} binds specifically to DnaK immobilized in porous material

Our purpose was to study the σ^{32} -DnaK interaction using HX-MS experiments. First, we performed the experiments with σ^{32} and σ^{32} -DnaK in solution. The resolution we obtained was insufficient to resolve all σ^{32} peptides because some of them overlapped with some DnaK peptides. To have all σ^{32} bound to DnaK, we needed to incubate with a large excess of DnaK and, since DnaK is larger than σ^{32} , DnaK peptides dominated the

spectra. For this reason we decided to follow a different approach. DnaK was immobilized on Poros AL material and packed onto a column. To evaluate if the binding of σ^{32} to immobilized DnaK was specific we incubated σ^{32} with immobilized DnaK and eluted it with ATP. The eluted protein was analyzed by SDS-PAGE. We tested whether immobilized DnaK could be reused after elution with low pH quench buffer by performing the binding experiments followed by ATP elution, then washed with quench buffer and regenerated the immobilized DnaK with ATP-containing buffer at physiological pH. This procedure was repeated 3 times. In all repetitions σ^{32} could be bound to the column and eluted with ATP, indicating that DnaK was still functional (Figure 4.1).

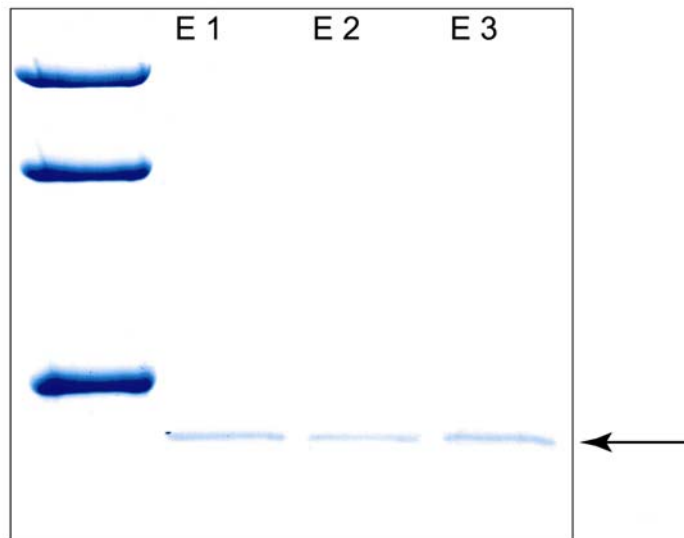


Figure 5.1. Eluted σ^{32} from the DnaK immobilized in poros material was analyzed by SDS-PAGE using a 12 % gel. σ^{32} was eluted with ATP. After each elution the immobilized DnaK was washed with quench buffer and re-equilibrated with HMK buffer.

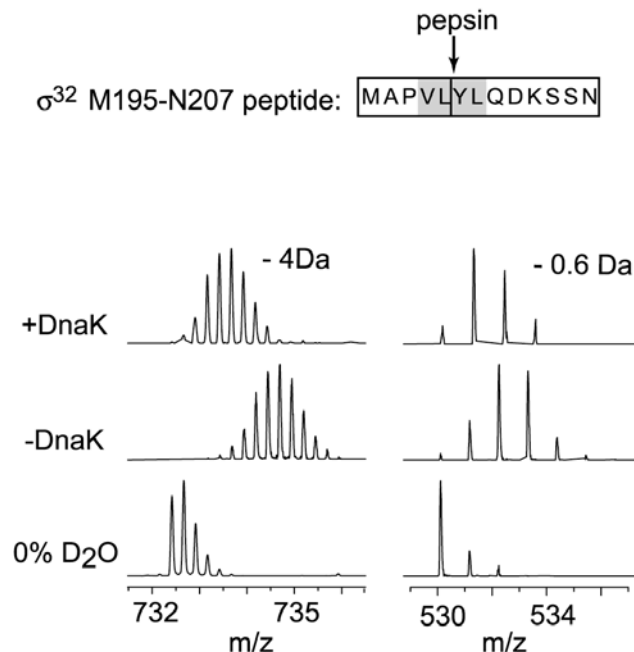


Figure 5.2. HX foot-printing of σ^{32} M195-N207 peptides. Peptide mass spectra are shown for samples incubated in water and in D_2O buffer in the absence and presence of DnaK. The pepsin cleavage site is indicated with an arrow. In the left panel we show the spectra of full-length peptides while in the right panel the spectra of the cleavage peptide (MAPVL).

DnaK protects at least two amide hydrogens in the DnaK binding site of σ^{32}

The approach we followed for the HX experiments of σ^{32} in complex with DnaK was the following: immobilized DnaK was packed onto a column. Then, σ^{32} was injected into it and incubated with DnaK. The unbound σ^{32} was washed away and the column was incubated with D_2O buffer for different time points. The reaction was quenched and σ^{32} was eluted from the column by reducing the pH and temperature. In order to test the number of amide hydrogens protected when a substrate is bound to DnaK, we performed the HX experiments with the immobilized DnaK and two peptide substrates derived from σ^{32} , namely σ^{32} -Q132-Q144 and σ^{32} -M195-N207. The σ^{32} -M195-N207 peptide contains the DnaK binding site in the folded σ^{32} protein. The peptides were incubated with immobilized DnaK for 30 minutes in a column containing either immobilized DnaK or an anion exchange material for control. As shown in Figure 4.2, when DnaK is bound 4 amide hydrogens are protected in the σ^{32} -M195-N207 peptide. The same result was obtained with the σ^{32} -Q132-Q144 peptide. This is in agreement with the crystal structure

of the substrate-binding domain of DnaK in complex with a substrate peptide, where 3 hydrogen bonds are formed between DnaK and amide hydrogens of the co-crystallized peptide. A fourth amide hydrogen of the bound peptide was shielded from surrounding water. The experiment was repeated with σ^{32} . We found that 3 peptides exchange less in the presence of DnaK. Two peptides are located in the previously identified DnaK binding site: peptides 183-199 and 200-208 (Figures 5.3 and 5.4). Unfortunately, pepsin cleaves in the middle of the binding site, explaining the fact that we did not observe 4 protected hydrogens in that region. The same result was obtained when the σ^{32} -M195-N207 peptide was digested with pepsin (Figure 5.4, right panel). This result is consistent with the previously identified binding site of DnaK in σ^{32} . The difference in deuterium incorporation in these peptides decreased with longer incubation times, indicating a dynamic nature of the hydrogen bonds between the DnaK substrate-binding domain and σ^{32} (Figure 5.5). In addition, dissociation of the DnaK- σ^{32} complex in the course of the HX reaction contributes to an increase in deuterium incorporation at longer incubation times.

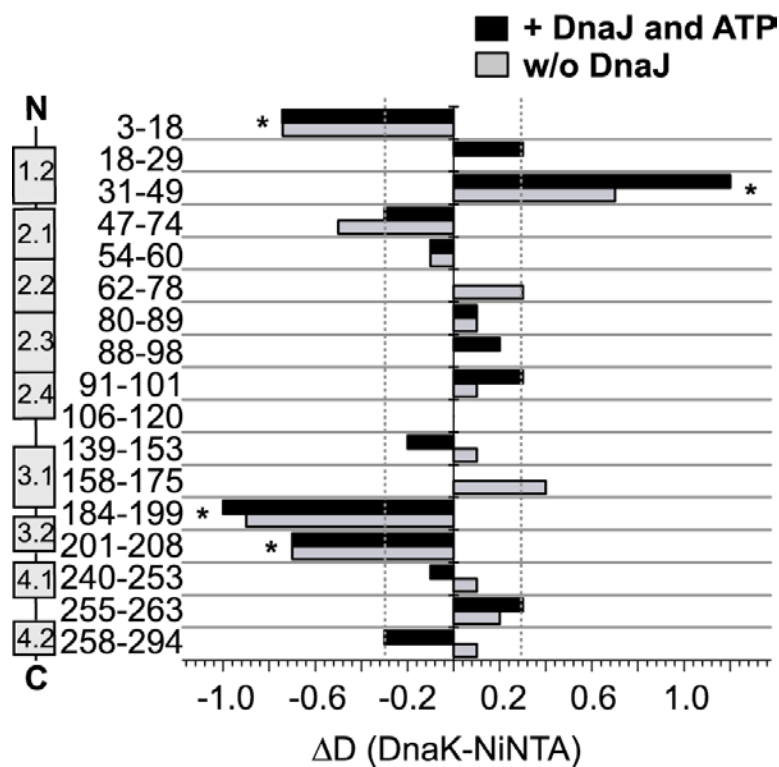


Figure 5.3. Difference of deuterium incorporation into σ^{32} bound to poros DnaK or NiNTA. Negative values indicate peptides that are protected when DnaK is bound, while positive values indicate peptides that are de-protected when DnaK is bound. Significant results ($P < 0.05$) are indicated with an asterisk.

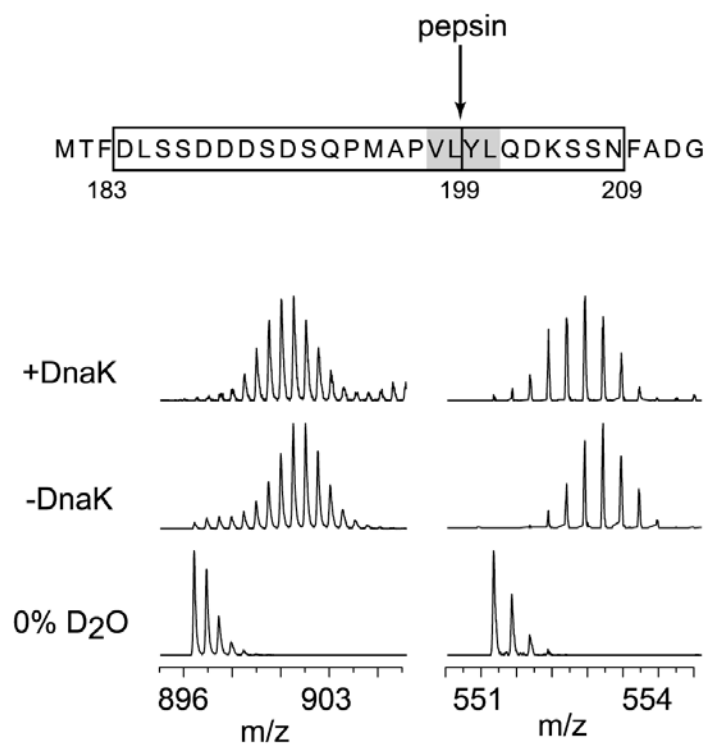


Figure 5.4. HX foot-printing of σ^{32} peptides. Peptide mass spectra are shown for samples incubated in water and in D_2O buffer in the absence and presence of DnaK. In the upper part we indicate the two peptides where protection was observed. The pepsin cleavage site is indicated with an arrow. In the left panel we show the peptide 183-199, and in the right panel the peptide 200-209.

Another peptide that showed protection when DnaK was bound to σ^{32} is a peptide in the N-terminus of σ^{32} . There are two alternative explanations for this observation. First, the N-terminal peptide constitutes a second binding site for DnaK that was missed in the protease protection assay. Second, DnaK-binding to σ^{32} could induce a conformational change leading to a protection of the N-terminal segment. The first possibility was excluded because a variant protein with amino acid replacement in this region (σ^{32} -L8E, L10E) has the same K_D for DnaK as σ^{32} wt. These results indicate that DnaK binds to σ^{32} in the region 200 and that at least 2 amide hydrogens are protected by DnaK binding.

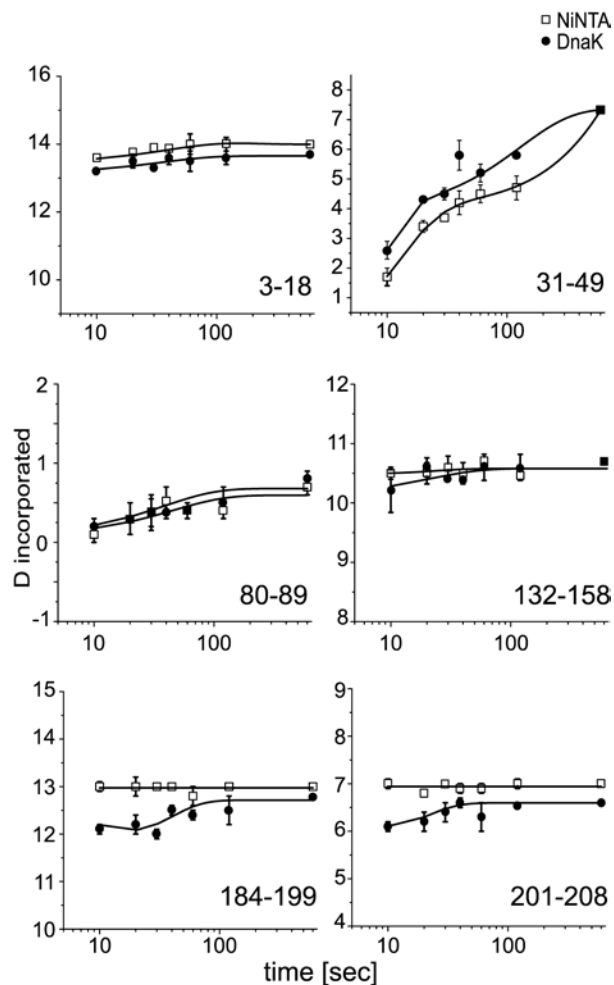


Figure 5.5. Kinetics of D₂O incorporation into different segments of σ^{32} . The amount of incorporated deuterium is plotted versus exchange time.

DnaK destabilizes the N-terminus of σ^{32}

One of the objectives of HX experiments of σ^{32} in complex with DnaK was to investigate whether DnaK can induce conformational changes in σ^{32} . In these experiments we observed that segment 31-49 exchanged more amide protons for deuterons when σ^{32} was bound to DnaK as compared to σ^{32} in the absence of DnaK, suggesting that there is a destabilization of this region upon binding of DnaK (Figure 5.6). This was observed throughout the time course of exchange (Figure 5.5). The same effect was observed when σ^{32} was incubated with DnaJ and ATP together with immobilized DnaK. This result indicates that DnaK induces a conformational change in σ^{32} thereby destabilizing the N-terminal region of σ^{32} .

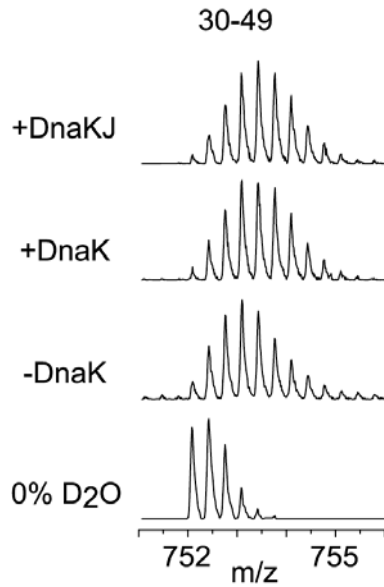


Figure 5.6. Unfolding of the N-terminal region of DnaK. The mass spectrum of a peptic fragment of σ^{32} is shown in water and after incubation in D_2O buffer in the absence and presence of DnaK, and also DnaK and DnaJ.

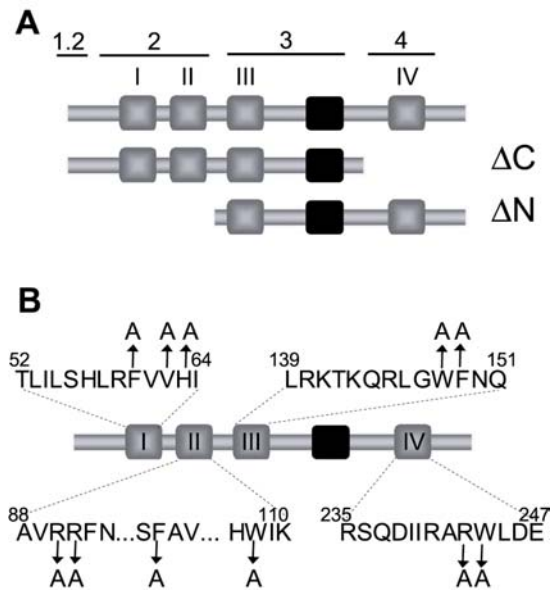


Figure 5.7. σ^{32} mutants. (A) σ^{32} deletion mutants. In ΔC one of the DnaJ potential binding sites was removed. In ΔN , two DnaJ potential binding sites were removed. (B) σ^{32} point mutants. The DnaK binding site is indicated in black.

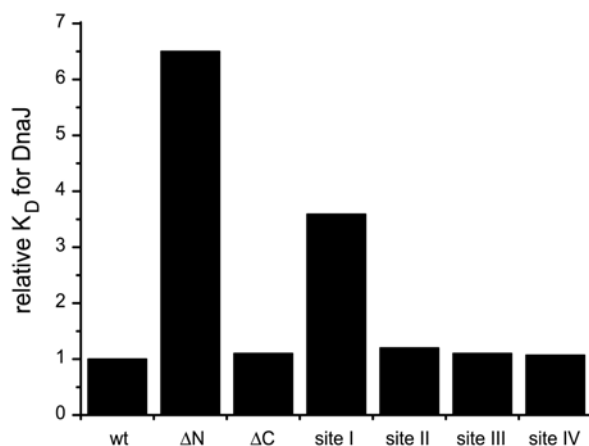


Figure 5.8. Comparison of the K_D for DnaJ of the different σ^{32} variant proteins. The K_D were determined using surface plasmon resonance spectroscopy. The relative K_D was calculated dividing the K_D of each σ^{32} variant by the K_D of σ^{32} wild-type.

DnaJ binds in the N-terminus of σ^{32}

The peptide library scans indicated at least four possible DnaJ binding sites in σ^{32} . These correspond to residues 52-64, 88-110, 139-151, and 235-247. The σ^{32} -derived peptide libraries are composed of 13mers that overlap with adjacent peptides on 10 residues. Therefore, all DnaJ potential binding sites at the primary sequence level are present. However, the DnaJ binding site in native σ^{32} does not need to be unstructured and contiguous since DnaJ only distinguishes side-chain hydrophobicity (Rüdiger *et al.*, 2001). The solvent accessibility of side-chain was analyzed in the σ^{32} model based on the crystal structures of *Thermus thermophilus* σ^A in complex with RNA polymerase. To map the binding site of DnaJ in native σ^{32} we made two deletion mutants (Figure 5.7): (i) in σ^{32} - ΔN two of the potential binding sites (I and II) were removed, and (ii) in σ^{32} - ΔC the C-terminal potential binding site (IV) was removed. The K_D for DnaJ of these two deletion mutants was determined using surface plasmon resonance spectroscopy. The K_D of the σ^{32} - ΔC mutant was similar to the K_D of σ^{32} wild-type. In the case of σ^{32} - ΔN , the K_D for DnaJ was 6.5-fold higher than for σ^{32} wild-type. It is known that σ^{32} and DnaJ each individually stimulate the ATP hydrolysis rate of DnaK, and that if they are incubated together with DnaK they stimulate synergistically the ATP hydrolysis rate of DnaK. A σ^{32} mutant that cannot bind DnaJ as efficiently as σ^{32} wild-type would be expected to fail in the DnaJ-mediated synergistic stimulation but not in the substrate

stimulation of the ATPase activity of DnaK. Single turn-over experiments were performed with σ^{32} wild-type and the two deletion mutants. Both deletion mutants stimulated the ATPase rate of DnaK like wild-type σ^{32} when they were incubated with DnaK in the absence of DnaJ. In the presence of DnaJ the σ^{32} - ΔC deletion mutant stimulated synergistically the ATP hydrolysis of DnaK like σ^{32} wild-type. However, for the ΔN deletion mutant such a synergistic stimulation of the ATP hydrolysis rate of DnaK could not be observed (Figure 5.9). To determine which of the two potential binding sites in the N-terminal domain was the binding site of DnaJ, in the folded protein we created point mutants of these sites and of two other potential DnaJ binding sites as a control (Figure 5.7). We determined the K_D of these four point mutants to DnaJ using surface plasmon resonance spectroscopy experiments. Site II, III and IV mutants bound to DnaJ like σ^{32} wild type. Only the site I mutant showed a different behavior (Figure 5.8). The single turn-over experiments were repeated with the four point mutants. Although all four mutants stimulated the ATP hydrolysis of DnaK like σ^{32} wild-type in the absence of DnaJ, only the mutant in site I showed a 3-fold decrease in the DnaJ-mediated synergistic stimulation of the ATPase rate of DnaK. Taken together, these results indicate that DnaJ binds to a single specific site in the N-terminal region of σ^{32} .

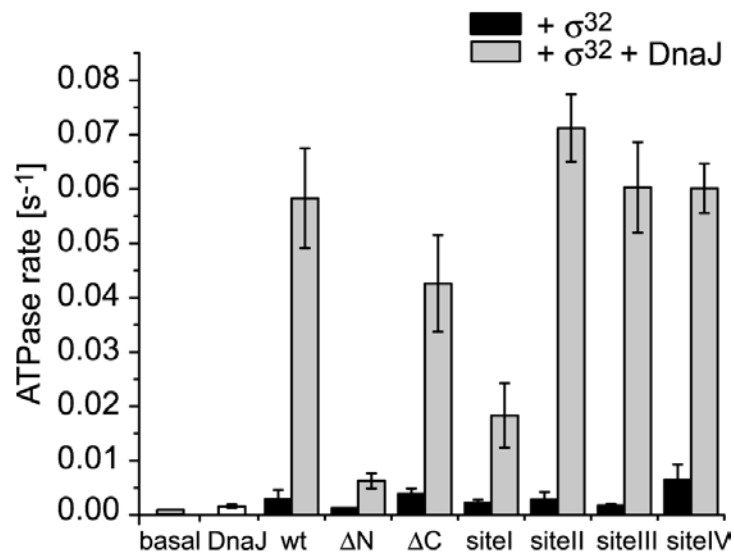


Figure 5.9. Single turn-over of DnaK and different σ^{32} mutant proteins with and without DnaJ.

σ^{32} - ΔN and σ^{32} - ΔC bind DnaK like σ^{32} wild-type

To test whether σ^{32} - ΔN and σ^{32} - ΔC mutants still bind DnaK like σ^{32} wt, gel filtration experiments were performed. σ^{32} and the deletion variants were labeled with tritium and radioactivity was measured in the different fractions. 5 μ M of σ^{32} wt and the deletion mutants were alternatively incubated for two hours at 30°C with 10 μ M of DnaK wt. The reaction mixture was injected onto a Superdex 75 analytical column, and the fraction of bound σ^{32} wt or the deletion mutants to DnaK was determined. As shown in Both deletion mutants bound DnaK to the same extent as σ^{32} wt (K_D for DnaK in σ^{32} wt and both deletion variants was 1 μ M). This is in agreement with the previously identified DnaK binding site since both mutants still contain the region where DnaK binds.

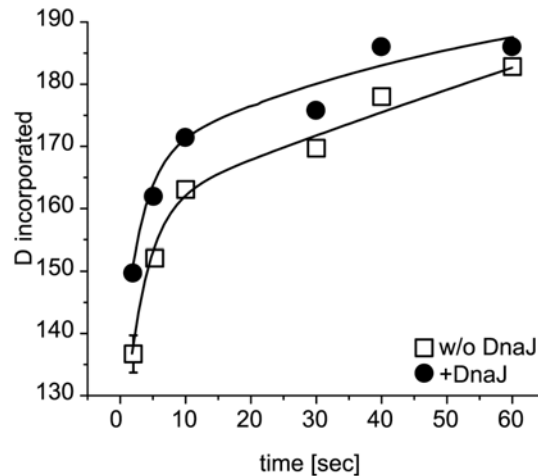


Figure 5.10. Kinetics of deuterium incorporation into σ^{32} free and in complex with DnaJ, which destabilizes σ^{32} upon binding.

DnaJ-bound σ^{32} is destabilized

To investigate whether DnaJ binding affects conformation of σ^{32} , we used HX-MS experiments with σ^{32} alone and σ^{32} in complex with DnaJ. In this case the experiments with σ^{32} and σ^{32} in complex with DnaJ were performed in solution. Under the conditions used DnaJ was not extensively digested by pepsin and therefore we could observe the majority of σ^{32} peptides even in the presence of DnaJ. Since the K_D of the σ^{32} -DnaJ

complex is about 20 nM, under the experimental conditions of 0.6 μM σ^{32} and 1 μM DnaJ 98% of σ^{32} was in complex with DnaJ at equilibrium.

To determine the overall amide hydrogen accessibility of DnaJ-bound σ^{32} we performed the HX-MS experiments first without online peptic digestion after the exchange reaction. The DnaJ- σ^{32} complex was incubated for 2 to 60 s in D_2O and subsequently analyzed in our HPLC-MS setup using gradient elution to separate the two full-length proteins. As shown in Figure 5.10, σ^{32} exchanges more amide hydrogens in the presence of DnaJ than in its absence. The data were fitted using a biexponential rate equation. The fitting results revealed that in the absence of DnaJ 150 amide hydrogens exchange at a rate of 1.13 s^{-1} and 41 at a rate of 0.026 s^{-1} . In the presence of DnaJ 159 amide hydrogens exchanged at a rate of 1.32 s^{-1} and 31 at a rate of 0.037 s^{-1} . Since the HX reaction occurred according to the so-called EX2 exchange mechanism the difference in stability of σ^{32} in the presence and absence of DnaJ ($\Delta\Delta\text{G}$) can be estimated from these values. In the presence of DnaJ 9 amide hydrogens more than in the absence of DnaJ exchanged with the fast rate of 1.3 s^{-1} . We can assume that these 9 amide hydrogens exchanged in the absence of DnaJ with the lower rate of 0.026 s^{-1} . This assumption is based on the fact that the number of amide hydrogens, which exchanged in the presence of DnaJ with the lower rate, was 10 smaller than in the absence of DnaJ. An acceleration of the exchange rate from 0.026 s^{-1} to 1.3 s^{-1} for 9 amide hydrogens results in a difference in stability of $86 \text{ kJ}\cdot\text{mol}^{-1}$. This result suggests that DnaJ-binding destabilizes σ^{32} .

DnaJ opens σ^{32} next to the DnaK binding site

To map the region where DnaJ destabilizes σ^{32} the HX experiments were repeated including a pepsin column in the HPLC setup. We found that the overall exchange kinetics of σ^{32} in the presence of DnaJ is composed of opposing effects on different regions of σ^{32} . An N-terminal segment of σ^{32} exchanges less amide hydrogens when DnaJ is bound to σ^{32} . This region is close to the identified DnaJ binding site. Thus, upon DnaJ binding to σ^{32} , DnaJ stabilized secondary structure in the N-terminal domain of σ^{32} . We did not find a protection in the actual DnaJ binding site. Since we only observe the exchange of backbone amide hydrogens in HX experiments these observations are consistent with DnaJ binding exclusively to amino acid side chains as suggested by

library scanning experiments (Rüdiger *et al.*, 2001). We also observed that two segments (residues 90-101 and 157-175) exchanged more amide hydrogens when σ^{32} was bound to DnaJ (Figure 5.11) than in the absence of DnaJ. The segment 157-175 is located close in sequence to the DnaK binding site and segment 90-101 is located in spatial vicinity of the dnaK binding site in our σ^{32} homology model onto the *T. thermophilus* σ^A structure (Figure 5.12). Therefore, DnaJ seems to make the DnaK binding site more accessible explaining the efficient delivery of σ^{32} to DnaK by DnaJ. Such a mechanism would also explain why DnaJ and σ^{32} stimulate the ATP hydrolysis rate of DnaK synergistically. Our result shows that DnaJ can also affect the conformation of σ^{32} .

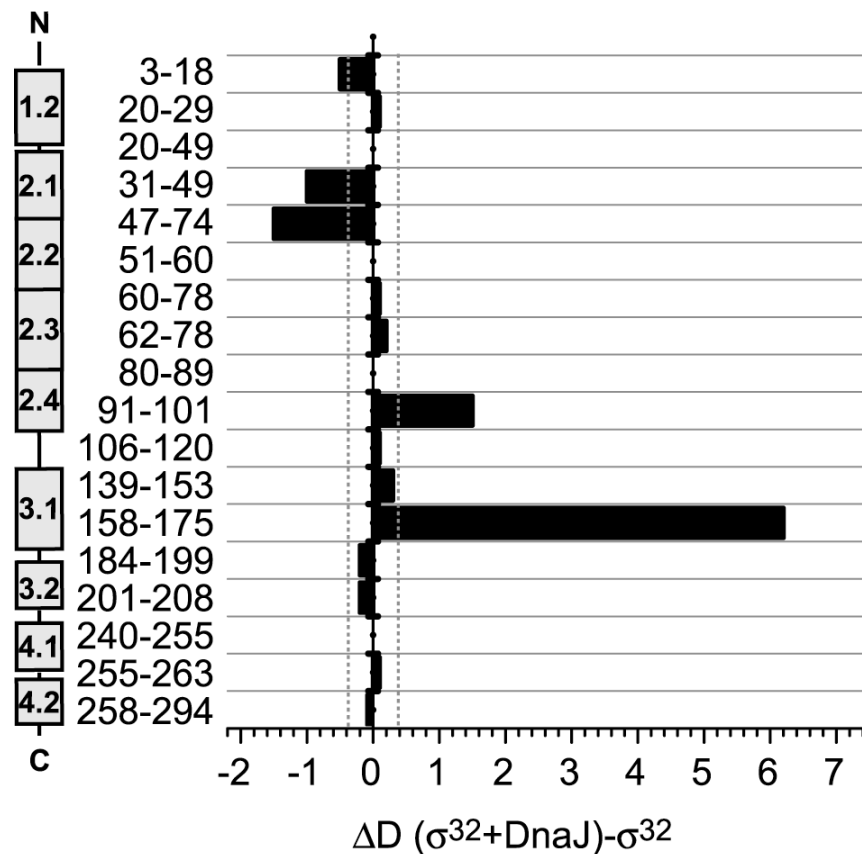


Figure 5.11. Difference of deuterium incorporation into σ^{32} free and bound to DnaJ. Negative values indicate peptides that are protected when DnaJ is bound, while positive ones indicate peptides that are de-protected when DnaJ is bound.

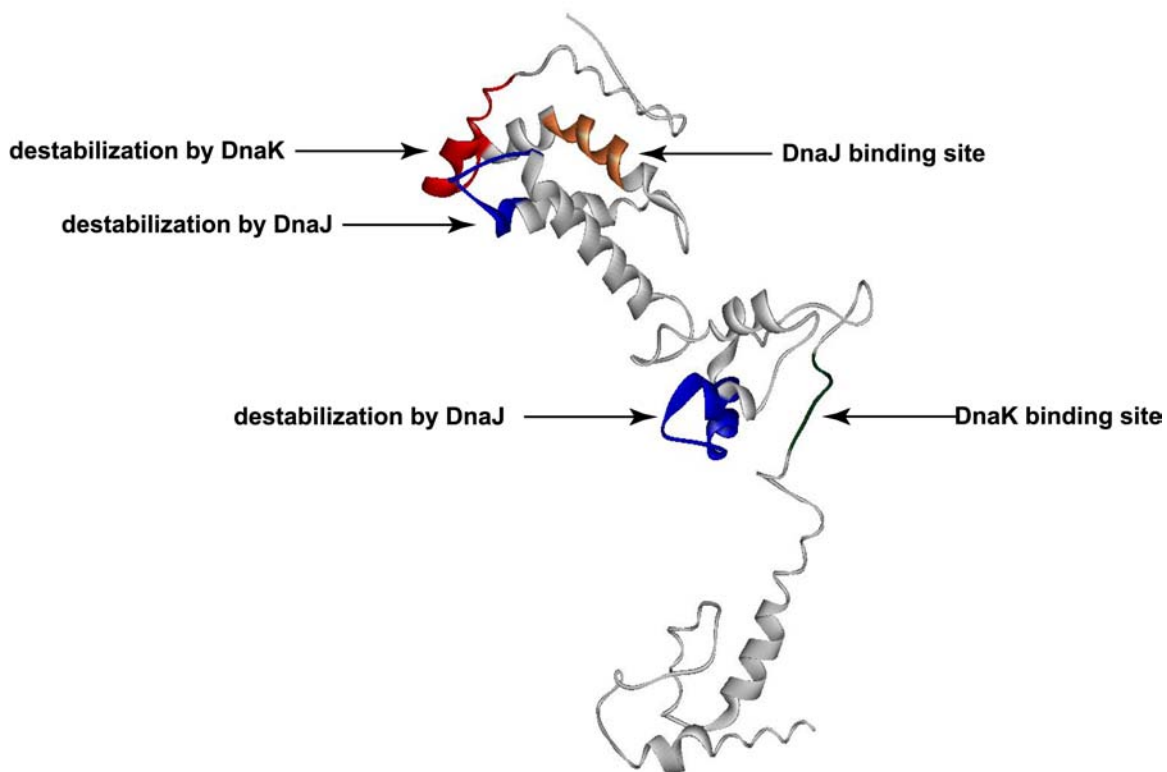


Figure 5.12. Molecular model of DnaK and DnaJ binding to σ^{32} . Secondary structure representation of homology model of σ^{32} onto *T. thermophilus* σ^{70} (PDB 1IW7, (Vassilyev et al., 2002)). The DnaK binding site is colored in green, and DnaJ binding sites is colored in orange. The sites destabilized by DnaK and DnaJ are shown in red and blue.

Conclusions

In this chapter we have characterized the interaction of the folded substrate σ^{32} with the DnaK-DnaJ chaperone system. DnaK binds in a surface-exposed hydrophobic stretch of residues located at positions 198 to 201 of the σ^{32} polypeptide chain. This binding site was confirmed using HD footprinting. In analogy to protease footprinting, HD footprinting can give information about binding interfaces in protein complexes. Amide hydrogen exchange was performed with σ^{32} alone and in complex with DnaK. Two peptides, residues 183-199 and 200-208, show protection when bound to DnaK. σ^{32} M195-N207, a σ^{32} -derived peptide containing the identified DnaK binding site, shows a

similar behavior. Furthermore, amide hydrogen exchange reveals a region (residues 31-49) that incorporated more deuterium in the presence of DnaK than in its absence. This suggests a small structural rearrangement within σ^{32} upon binding to DnaK resulting in a less compact structure. *In vivo* σ^{32} is degraded mainly by the AAA protease FtsH. Degradation of σ^{32} proceeds from the N-terminus to the C-terminus (Okuno *et al.*, 2004). In addition, FtsH lacks robust unfoldase activity and only degrades substrates efficiently when they have low intrinsic thermodynamic stability (Herman *et al.*, 2003). This suggests that a chaperone-induced unfolding of a secondary structure element may facilitate degradation of σ^{32} *in vivo*. Recently, *in vivo* more stable σ^{32} mutants were reported (Horikoshi *et al.*, 2004; Obrist and Narberhaus, 2005). Interestingly, they are located in the region where the destabilization by DnaK occurs. Thus, this is a crucial region of the regulation of σ^{32} . The DnaK system cannot stimulate the FtsH proteolysis of σ^{32} *in vitro*. It has been speculated that an X factor is missing. We cannot exclude that this destabilization exposes a binding site for an adaptor protein. For example, the SspB adaptor binds in the N-terminus of the substrate and targets its degradation by ClpX from the N-terminus (Levchenko *et al.*, 2003; Song *et al.*, 2003; Park *et al.*, 2007).

In this chapter we have also identified the region of σ^{32} where DnaJ binds, which is a hydrophobic stretch rich in aromatic residues. Mutational alterations of this site decreased the affinity of σ^{32} for DnaJ. HD footprinting does not show protection of this site when DnaJ is bound to σ^{32} . This is not surprising since DnaJ association with peptide substrate relies on side-chain contacts not detected with this method. Amide HD experiments reveal two conformational changes induced by DnaJ: a stabilization of the N-terminus close to the DnaJ binding site and a destabilization of the region close to the DnaK binding site.

It was proposed that DnaJ binds to substrates and hands them over to DnaK in a process that is coupled to ATP hydrolysis by DnaK (Laufen *et al.*, 1999). One possible mode of substrate transfer is that the peptide segment that is bound to DnaJ is directly handed over to DnaK's binding cleft (Rüdiger *et al.*, 2001). Another possibility is that DnaK and DnaJ bind in different regions. The fact that DnaK and DnaJ bind σ^{32} in different regions demonstrates that a direct transfer mechanism of the DnaJ bound site into the substrate binding cavity of DnaK is not operative in the case of σ^{32} . Since a

truncation and mutagenesis study on the native DnaK substrate RepA also suggests different binding sites for DnaK and DnaJ (Kim, 2002) this mode of cooperation between DnaJ and DnaK might be more general.

What are the effects of DnaJ on σ^{32} ? We observed that DnaJ induces a destabilization of σ^{32} close to the DnaK binding site. This suggests that DnaJ promotes an open conformation of σ^{32} thereby facilitating DnaK binding. These data explain the synergism of DnaJ and σ^{32} in stimulating DnaK's ATPase activity and of DnaJ's high efficiency in loading σ^{32} onto DnaK.

Chapter 6

Study of σ^{32} stable mutants

As we have described before, σ^{32} is an unstable protein with a half-life of approximately one minute. Upon heat-shock, the levels of σ^{32} increase transiently due to increased synthesis and stabilization. The DnaK chaperone system is required for rapid degradation of σ^{32} since it is stabilized in Δ dnaK, Δ dnaJ and Δ grpE mutants (Straus *et al.*, 1987, Tilly *et al.*, 1989). σ^{32} is degraded by membrane protease FtsH, a member of the AAA protein family. Even though the regulation of σ^{32} by DnaK, DnaJ and GrpE has been extensively investigated, its molecular mechanism remains obscure. Recently, a number of σ^{32} mutants that are stabilized *in vivo* were isolated (Horikoshi *et al.*, 2004; Obrist and Narberhaus, 2005; Gross, personal communication). Many of these mutants have amino acid substitutions in the N-terminal part of σ^{32} (residues 47-55). This region is close to the region where we observed the destabilization induced by DnaK. Stabilization can result from various factors. For example, enhanced affinity for the RNA polymerase would reduce the percentage of σ^{32} that is degraded. Some of these mutants

were tested for their affinity for core RNA polymerase and it was shown that the stabilization is not due to an increase in the latter. Another possibility is that the affinity for chaperones is changed, decreasing the amount of σ^{32} targeted for degradation. This last hypothesis has not been tested and further studies are required to understand why these σ^{32} mutants are more stable.

To evaluate the reason why these mutants are more stable, we analyzed two of them using HX experiments. We tested the mutants σ^{32} L47Q-L55Q isolated by Horikoshi *et al.* and σ^{32} I54N isolated by the Gross Group.

Comparison of σ^{32} I54N and σ^{32} wt

The protein σ^{32} with a replacement of isoleucine 54 for asparagine (σ^{32} I54N) is more stable *in vivo*. The Gross group has determined the K_D for GroEL, DnaK and RNA polymerase. The calculated K_D were similar to wt for all proteins. To characterize the σ^{32} I54N we performed HX experiments with full-length protein and compared them with σ^{32} wt. These proteins were incubated with deuterium buffer for different time intervals (from 5 seconds to 1 minute) and analyzed by mass spectrometry. As shown in Figure 6.1, for the full-length proteins there is not difference in deuterium incorporation. We then repeated the HX experiments in the presence of a pepsin column to evaluate both proteins at a peptide level (Figure 6.2). We found that the N-terminus of σ^{32} I54N incorporated more deuterium as compared to σ^{32} wt. This is the region where the mutation was introduced. We next located the residue I54 in our σ^{32} model (Figure 6.3). This residue faces the inside part of the protein and, therefore, it is not surprising that a replacement of a hydrophobic residue for a polar residue destabilizes this region of σ^{32} . We have also found two segments of σ^{32} I54N that exchange less than the segments of σ^{32} . These segments are 158-175 and 258-294. Interestingly, it was on segment 158-175 that we observed destabilization by DnaJ.

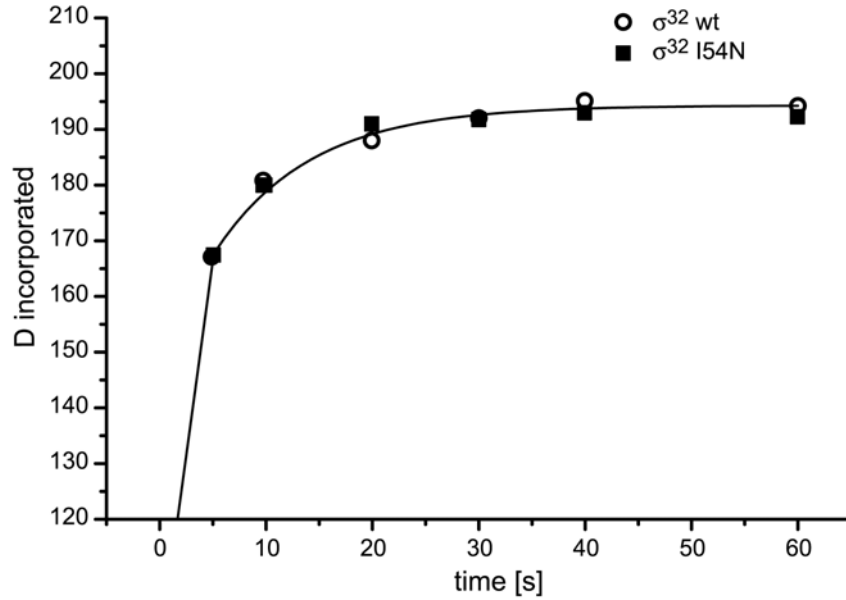


Figure 6.1. Deuterium incorporation into full-length σ^{32} wt and σ^{32} I54N. Both proteins incorporated the same amount of deuterium.

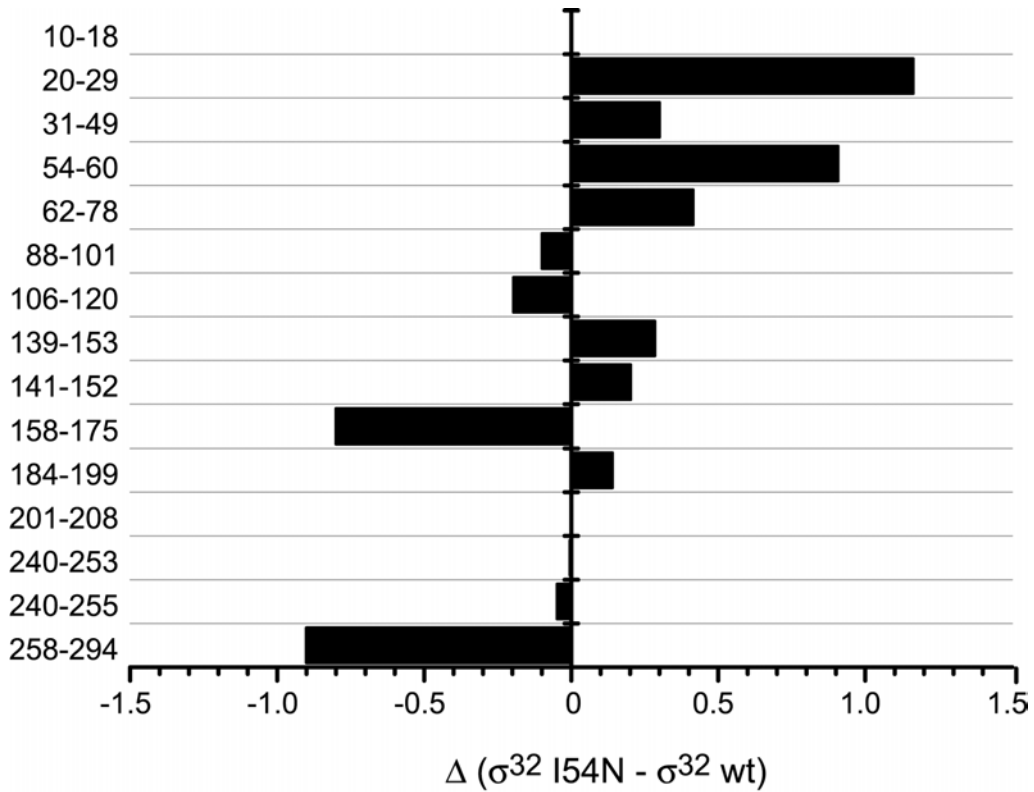


Figure 6.2. Difference of deuterium incorporation into σ^{32} I54N and σ^{32} wt. Positive values indicate peptides that exchange more in σ^{32} I54N than in σ^{32} wt, while negative values indicate peptides that exchange more in σ^{32} wt as compared to σ^{32} I54N.

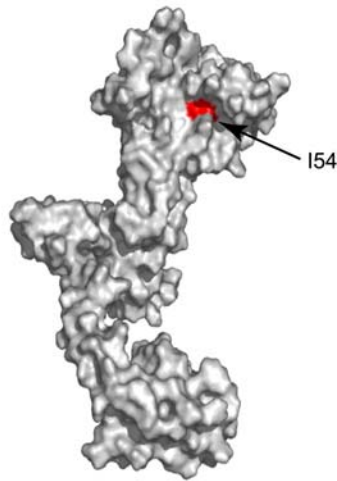


Figure 6.3. Localization of residue I54 in σ^{32} . Space-filling representation of homology models of σ^{32} onto *T. thermophilus* σ^{70} (PDB 1IW7, Vassylyev *et al.*, 2002). The residue I54 is colored in red.

σ^{32} L47Q-L55Q is more stable than σ^{32} wt in vitro

Horikoshi *et al.* had isolated several σ^{32} mutants that are more stable *in vivo*. All of them have altered residues in the N-terminus of σ^{32} . One of them, σ^{32} L47Q-L55Q, has a half-life more than 10-fold longer than wild-type. To characterize the σ^{32} L47Q-L55Q variant protein we performed HX experiments with full-length protein and compared it with σ^{32} wt. The proteins were incubated with deuterium buffer for different time intervals (from 5 seconds to 1 minute) and analyzed by mass spectrometry. As shown in Figure 6.4, from 5 to 20 sec σ^{32} L47Q-L55Q incorporated less deuterium than σ^{32} wt. For example, σ^{32} L47Q-L55Q incorporated 172 atoms of deuterium after 10 seconds whereas σ^{32} wt incorporated 180. We then repeated the HX experiments in the presence of a pepsin column to map the region that is more stable. In the case of σ^{32} L47Q-L55Q, we found a small deprotection in the N-terminus where the residues were replaced. In contrast, the C-terminus domain of σ^{32} L47Q-L55Q exchanged less than the C-terminus domain of σ^{32} wt. There is also a small stabilization in the segment 88-101 of σ^{32} L47Q-L55Q. We have found in Chapter 5 that this region is destabilized upon binding of σ^{32} to DnaJ.

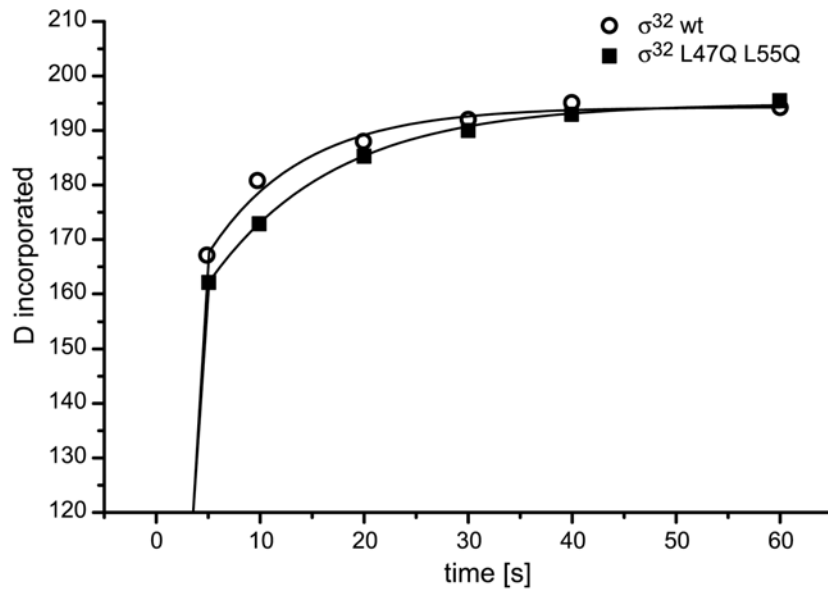


Figure 6.4. Deuteron incorporation into full-length σ^{32} wt and σ^{32} L47Q L55Q.

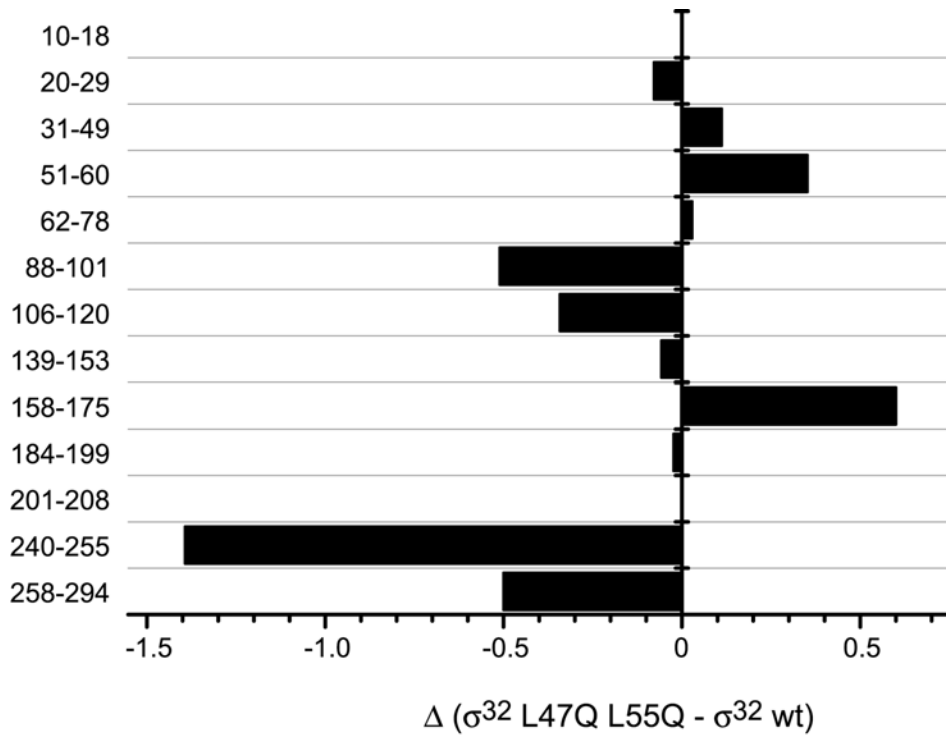


Figure 6.5. Difference of deuterium incorporation into σ^{32} L47Q L55Q and σ^{32} wt. Positive values indicate peptides that exchange more in σ^{32} L47Q L55Q than in σ^{32} wt, while negative values indicate peptides that exchange more in σ^{32} wt as compared to σ^{32} L47Q L55Q.

DnaJ destabilizes σ^{32} I54N and σ^{32} L47Q-L55Q

As mentioned above, the segments 158-175 of σ^{32} I54N and 88-101 of σ^{32} L47Q-L55Q are more stable than the same segments of σ^{32} wt. These two segments are destabilized in σ^{32} upon DnaJ binding. In order to evaluate whether these mutants are more stable because they are defective in the regulation by DnaJ, we performed HX experiments of the mutants in complex with DnaJ. DnaJ destabilized the same segments of σ^{32} I54N and σ^{32} L47Q-L55Q as it does in σ^{32} wt (data not shown). Therefore, these two proteins are destabilized by DnaJ.

DnaJ affinity for σ^{32} I54N and σ^{32} L47Q-L55Q is reduced

σ^{32} I54N and σ^{32} L47Q-L55Q could also be more stable in vivo because the affinity for DnaJ is reduced. To evaluate this possibility, we determined the K_D of these two σ^{32} protein variants using surface plasmon resonance. The K_D of DnaJ for σ^{32} I54N is 3-fold higher than for σ^{32} wt (Table 6.1). This K_D is in agreement with the one obtained by the Gross group. The K_D of DnaJ for σ^{32} L47Q-L55Q is 2-fold higher than for σ^{32} wt (Table 6.1). Next we indirectly determined the affinity of a protein for DnaJ using single turnover experiments (Figure 6.6). We performed them with DnaK, and with DnaK and DnaJ. σ^{32} I54N and σ^{32} L47Q-L55Q stimulated the ATP hydrolysis of DnaK like σ^{32} wt. However, σ^{32} I54N stimulated 2-fold less and σ^{32} L47Q-L55Q stimulated 1.8-fold less when they were incubated together with DnaJ. Taken together, these results indicate that the affinity of DnaJ for σ^{32} I54N and σ^{32} L47Q-L55Q is reduced.

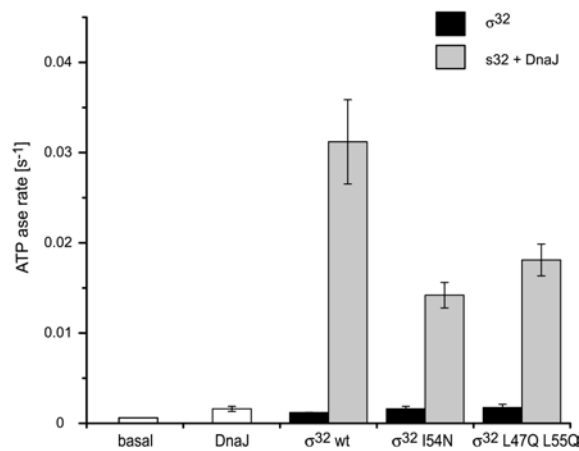


Figure 6.6. Single turn-over of DnaK and different σ^{32} with and without DnaJ.

Table 6.1. K_D of DnaJ for σ^{32} wt, σ^{32} I54N and σ^{32} L47Q-L55Q

	K_D (nM)
σ^{32} wt	21 ± 4
σ^{32} I54N	100 ± 1
σ^{32} L47Q-L55Q	48 ± 1

The K_D were determined by surface plasmon resonance. Between 300 and 400 response units of σ^{32} wt, σ^{32} I54N or σ^{32} L47Q-L55Q were immobilized onto a CM5 chip and then increasing concentrations of DnaJ were injected.

Conclusions

In this chapter we have analyzed two σ^{32} variant proteins, namely σ^{32} I54N and σ^{32} L47Q-L55Q, that are more stable *in vivo* than σ^{32} wt. Using HX experiments we evaluated these two proteins and found that in the case of σ^{32} I54N the segment 158-175 is more protected than in σ^{32} wt, and in the case of σ^{32} L47Q-L55Q the segment 88-101 is more protected than in σ^{32} wt. These two segments are destabilized in σ^{32} wt upon DnaJ binding.

In addition, we found that the affinity of DnaJ for these two proteins is smaller than the affinity of DnaJ for σ^{32} wt. This reduced affinity for DnaJ could explain why these proteins are more stable *in vivo*. DnaK and DnaJ target σ^{32} for degradation by FtsH. If the affinity for DnaJ is reduced for σ^{32} I54N and σ^{32} L47Q-L55Q then the half-life of both proteins should increase.

Chapter 7

The replication initiator protein RepE

As already described, the aim of the studies reported in this thesis is to obtain a deeper understanding of the mechanism of DnaK-substrate interactions. In Chapters 4, 5 and 6 we have studied the heat-shock transcription factor σ^{32} as a model substrate for DnaK and DnaJ. We have shown that DnaK and DnaJ destabilize σ^{32} . Another substrate of DnaK is RepE. RepE has a double function depending on its oligomeric state: as a dimer it represses its own synthesis, and as a monomer it works as a replication initiation protein. Under physiological conditions RepE predominantly exists as a dimer, and its conversion into monomers requires the concurrent action of DnaK, DnaJ and GrpE. The monomerization process is poorly understood due to a lack of structural information. Even though the structures of monomeric RepE54 (a variant of the RepE protein with arginine 118 substituted by proline) have been solved, there is no available structure for the dimer RepE. The details of the interaction of RepE wild-type with operator DNA are also unknown. The purpose of the studies reported in this chapter is to characterize the

RepE monomer and dimer using HX experiments. RepE was also used as a model substrate of DnaK and the DnaK-RepE interaction was studied.

Monomeric RepE54 is more stable than dimeric RepE

To determine the total amount of deuterium incorporated into dimeric RepE wild-type and monomeric RepE54 we performed HX experiments with full-length protein. We expected that the RepE dimer would exchange less than the monomer since the amino acids involved in the dimer interface should be less solvent-exposed. In previous work from this laboratory it was shown that the dimer incorporated more deuterons than the monomer. These experiments were performed for time points between 10 sec and 1 hour. We considered these time points to be too long to observe protection in the dimer interface. For this reason, we decided to repeat the experiments with the quenched-flow setup system. The HX experiments were performed with the quenched-flow setup system at time points between 200 msec and 1 sec. As shown in Figure 7.1, monomeric RepE54 exchanged less than dimeric RepE at all tested time points. This result indicates that monomeric RepE54 is more compactly folded than dimeric RepE and, even though the region where the dimer interface is located is expected to exchange less than in the monomer, there must be other regions in the dimer that are less folded than in the monomer. Another way of determining the stability of a protein is by using partial proteolysis. A more stable protein will be degraded slower or at higher concentrations of protease than a less stable one. To confirm that monomeric RepE54 is more stable than dimeric one we performed partial tryptic proteolysis followed by SDS-PAGE analysis with both proteins. Dimeric RepE was rapidly degraded even at the lowest trypsin concentrations whereas monomeric RepE54 was not (data not shown). Taken together, these results indicate that the monomeric RepE54 variant protein is more stable than the dimeric wild-type protein.

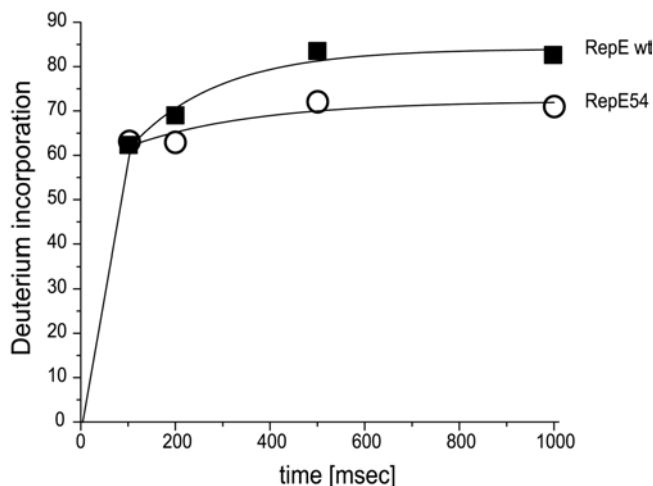


Figure 7.1. Amide hydrogen kinetics of full-length RepE wild-type (dimer) and RepE54 (monomer).

The dimer interface locates in region 97-128

To map the region where the molecules of RepE enter in contact with each other to form a dimer, we performed HX experiments with different incubation times in combination with peptic digestion and compared the deuterium incorporated into the dimeric wild-type protein and the monomeric variant protein. Figure 7.2 depicts a diagram of the difference between the amounts of deuterium incorporated into the monomer minus the dimer. Negative values of this difference indicate segments of the protein that incorporate less deuterium in the monomer as compared to the dimer, while positive values indicate segments of the protein that incorporate less deuterium in the dimer as compared to the monomer. When there is no difference between monomer and dimer, the value of the computed magnitude is zero. We observed three kinds of protein segments: (i) the segments that showed no difference, which are the majority of the peptides, (ii) the segments that incorporated more deuterium into the dimeric wild-type protein than into the monomeric variant, which are located in the N- and C-terminal regions of the protein, and (iii) the segments that incorporated more deuterons in the monomeric variant protein than into the dimeric protein. The latter are candidates to be involved in the formation of the dimer interface. These segments of RepE are poorly resolved in the crystal structure of monomeric RepE54, indicating a high flexibility. However, in a dimeric assembly they would prolong a β -sheet across the dimer interface

(Figure 7.3). Additional evidence for the hypothesis that these regions are involved in dimerization comes from mutation analysis. Variant proteins that are constitutively monomeric have amino acid substitutions in this region (Matsunaga *et al.*, 1995). These data are also consistent with the crystal structure of the N-terminal domain of RepA, which is related to RepE in structure but not in sequence and which crystallized as a dimer (Giraldo *et al.*, 2003). In RepA the dimerization interface comprises two β strands from different protomers, forming a central five-stranded antiparallel-pleated β -sheet. These two β -stands interact through hydrogen bonds. The region we found to be protected in the dimer corresponds to the dimer interface of RepA. Thus, we conclude that region 97-128 comprises the dimer interface.

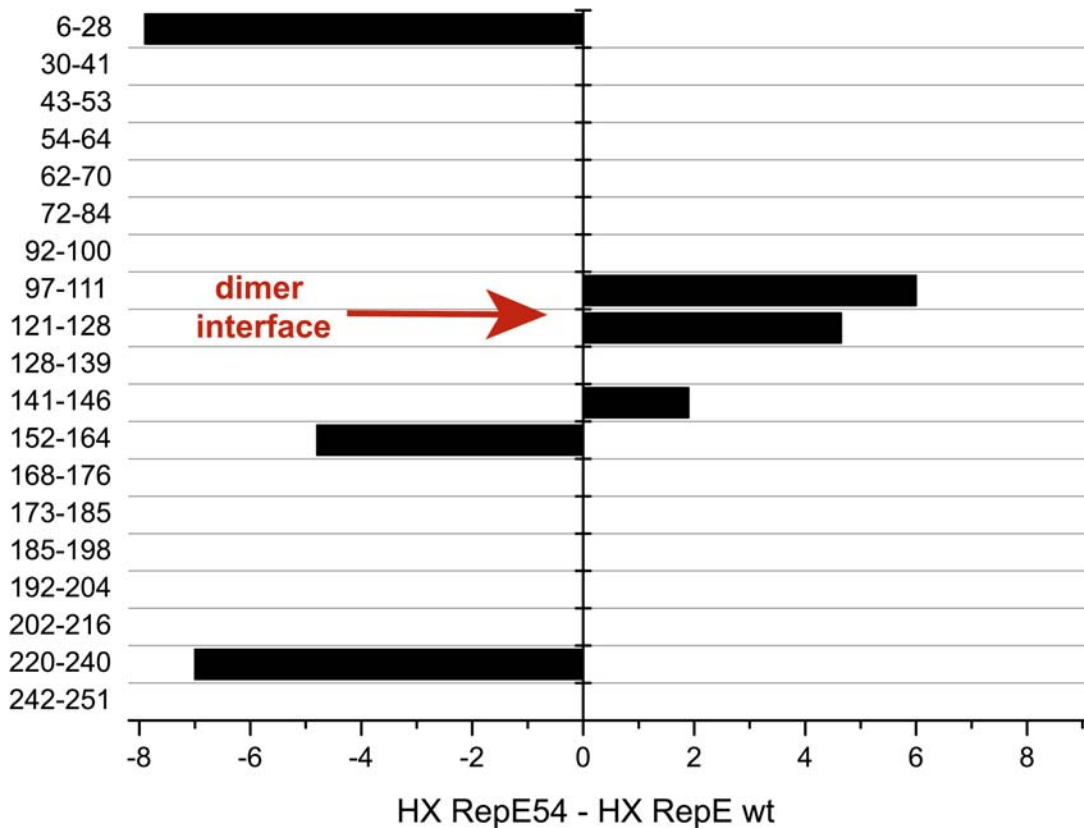


Figure 7.2. Differences of deuterium incorporation into RepE54 (monomer) and RepE wt (dimer). Negative values indicate segments of the protein that exchange less in the monomer, whereas positive values indicates segments of the protein that exchange more in the monomer.

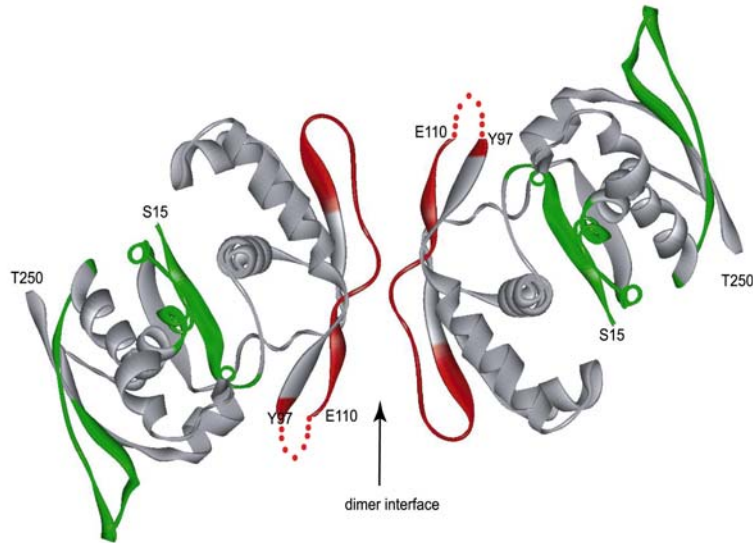


Figure 7.3. Structure of monomeric RepE. In green we show the regions of RepE that exchange more in the dimer. In red we show the regions that exchange more in the monomer, where the proposed dimer interface is located. With dots we indicate the amino acids that are not resolved in the crystal structure.

Monomerization of RepE requires marked conformational changes

Figure 7.5 shows the structure of monomeric RepE54 in complex with a 19-base pair iteron DNA (Komori *et al.*, 1999). N- and C-terminal domains of monomeric RepE54 are topologically similar and related one to each other by an internal two-fold symmetry. Both domains of RepE54 bind to the two major grooves of iteron DNA. Two helix-turn-helix motifs in RepE54, namely $\alpha 3$ -turn- $\alpha 4$ (residues 64-92) and $\alpha 3'$ -turn- $\alpha 4'$ (residues 168-242), are critical for directed repeat *ori2* binding. The $\alpha 3'$ -turn- $\alpha 4'$ motif is also a critical region for dimeric RepE binding to inverted repeat operator (Matsunaga *et al.*, 1995). In HX experiments, the segments from this region showed no differences between dimeric RepE wild-type and monomeric RepE54, indicating that this region does not change its conformation upon monomerization. Therefore, binding to DNA must be similar for both proteins. This is in agreement with the fact that the directed repeats sequence from *ori2* where monomeric RepE binds and the inverted repeats sequence from the operator where dimeric RepE binds contain 8 bp in common (Ishiai *et al.*, 1994).

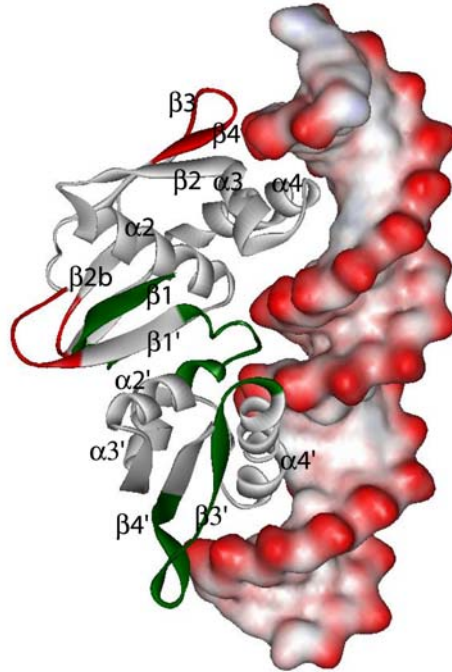


Figure 7.4. Structure of monomeric RepE in complex with DNA (1REP). In green we show the regions of RepE that exchange more in the dimer. In red we show the regions that exchange more in the monomer.

Komori *et al.* have modeled two RepE monomers on the inverted repeats of the operator (Komori *et al.*, 1999). A large steric hindrance occurred in the major part of the N-terminal domain of RepE and both helices $\alpha 4$ competed with each other for the major groove in the DNA. Bending the operator DNA did not compensate this steric hindrance between the RepE proteins. In HX experiments, the segments in regions 6-28, 152-164 and 220-240 exchange more in the dimer than in the monomer, indicating that dimeric RepE is more flexible in these regions (Figures 7.2 and 7.4). Segment 6-28 includes the $\beta 1$ that in monomeric RepE54 forms a small β -sheet with $\beta 1'$ (residues 147-150). In the structure of the N-terminal domain of RepA this β -sheet is disrupted and $\beta 1'$ forms an extension of $\alpha 5$ (Giraldo *et al.*, 2003). Our results are in agreement with the N-terminal structure of RepA since the lack of hydrogen-bonds between those two strands would result in higher deuterium incorporation in this region. These results indicate that monomerization of RepE requires marked conformational changes and that these

conformational changes are needed for accommodating dimeric RepE on the inverted repeat of the operator.

Monomeric and dimeric RepE bind to DnaK

One of the open questions about the Rep proteins is how they are regulated by the DnaK-DnaJ system. In $\Delta dnaK$ and $\Delta dnaJ$ strains it has been shown that the mini-F plasmid cannot replicate, and that replication is reestablished when RepE is mutated to proteins that are constitutively monomers. It has been speculated that the DnaKJ system is involved in the monomerization of RepE. However, this is not the only existing hypothesis. It has also been suggested that DNA facilitates the monomerization and that the DnaK-DnaJ chaperone system prevents the aggregation of the monomer since there are some hydrophobic regions that are exposed upon monomerization. This latter hypothesis is inconsistent with our data and the crystal structure. To elucidate what is the role of the DnaKJ system we tested the ability of DnaK to bind monomeric and dimeric RepE. We first evaluated the binding of DnaK to RepE using specific cross-linking. The DnaK Q424C variant protein was used, which has glutamine 424 located close to the binding pocket of DnaK replaced by a cysteine. It has been previously shown that this variant protein is fully functional in all assays including luciferase refolding (Laufen *et al.*, 1999). DnaK Q424C was labeled with a cysteine-specific UV-activable heterobifunctional crosslinker (BPJA). As shown in Figure 7.5, when RepE monomer and dimer were incubated with DnaK and irradiated with UV light, specific bands of the size expected for the DnaK-RepE complex appeared in both cases. These were bands 1 and 2, which were then cut and analyzed by mass spectrometry. We found that they contained DnaK and RepE. The DnaK-RepE complex was also formed when DnaJ and ATP was added to the reaction mix. We therefore conclude that both monomeric and dimeric RepE bind to DnaK.

DnaK binds in the C-terminus of RepE

In a previous work of our laboratory it was shown, using peptide libraries, that there are four potential DnaK binding sites in RepE (Figure 7.6). Two possible binding sites are located in the N-terminus of RepE, and the other two in the C-terminus.

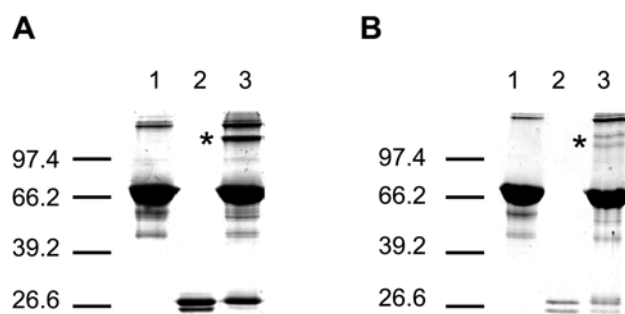


Figure 7.5. Site-specific crosslinking of BPIA-labeled DnaK with RepE54 (A) and RepE wild-type (B). After UV irradiation, proteins were separated by SDS-PAGE and stained with Coomassie. Lane 1 corresponds to DnaK alone, lane 2 corresponds to RepE alone and lane 3 corresponds to the complex. The crosslinking products between DnaK and RepE are indicated with asterisks.

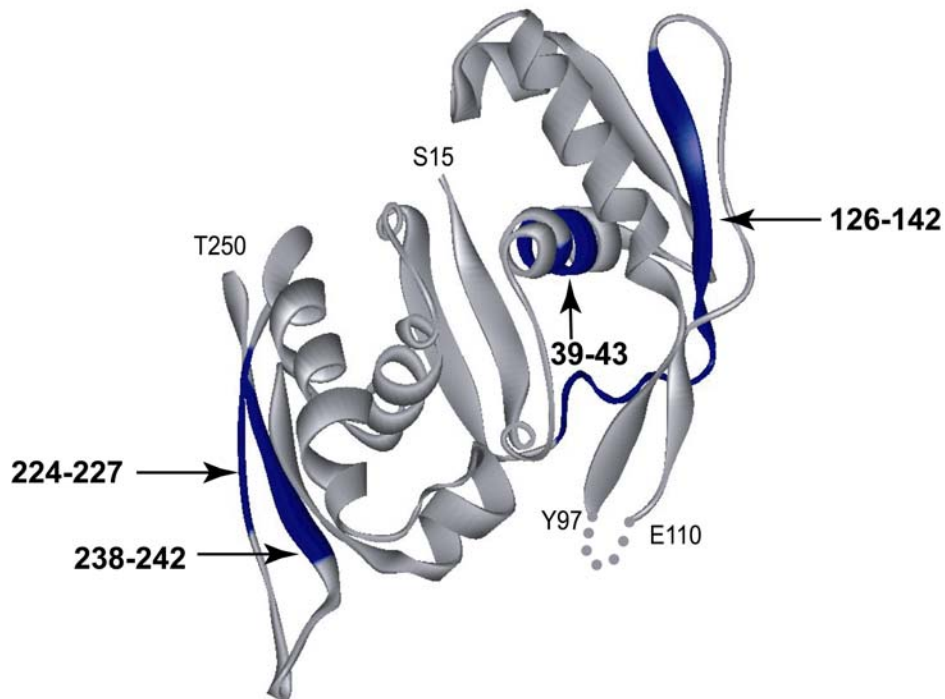


Figure 7.6. DnaK potential binding sites. In blue we indicate the DnaK potential binding sites obtained from peptide library scanning.

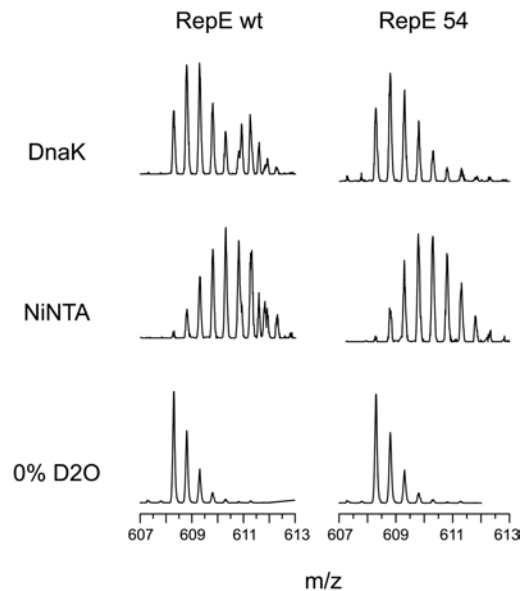


Figure 7.7. HX foot-printing of RepE wt and RepE54 peptides. Peptide mass spectra are shown for samples incubated in water and in D₂O buffer in the absence and presence of DnaK. The only peptide where a difference was observed was the peptide 240-251.

To map the DnaK binding site in native proteins, HX experiments were performed. We used immobilized DnaK as already described before for σ^{32} . We only found one peptide that showed protection when DnaK was bound. This is a peptide from region 240-251 (Figure 7.7), which is a region where there is a potential binding site for DnaK.

In order to confirm that DnaK binds in the C-terminus of RepE, we performed partial proteolysis experiments. RepE wt or RepE54 free or in complex with DnaK were digested with different concentrations of trypsin and the products were analyzed by mass spectrometry. We found two fragments that were produced after trypsin cleavage of RepE wt but not after the cleavage of DnaK-RepE wt complex. These fragments were 1-242 and 1-245. In the case of RepE54, the fragments 2-247, 8-245 and 5-244 were present for free RepE54 but not for the DnaK-Rep54 complex. This indicates that the C-terminus is protected by DnaK from proteolysis. Taken together, these results indicate that DnaK binds in the C-terminus of RepE in the region 240-251.

Conclusions

In this chapter we have characterized the structure of RepE dimer and RepE54, which is a constitutive monomer. Using HX experiments of full-length proteins we have shown that the monomer is more stable than the dimer. When we repeated our experiments introducing a pepsin column to map these differences we found that the peptides have three different exchange behaviors. Most of the peptides exchanged to the same extent in both proteins. Some peptides exchanged more in the monomer —these are the peptides that are involved in the formation of the dimer interface. Finally, we found peptides that exchanged more in the dimer (segments: 6-28, 1521-164, 220-240). These regions are more flexible in the dimer protein. This fact probably has a functional implication. The dimer-monomer transition requires structural rearrangements including the formation of additional secondary structure elements. This higher flexibility may be necessary for binding to the inverted-repeat operator.

Using the same approach as in Chapter 4 we were able to map the DnaK binding site in RepE: the former binds in a C-terminal hydrophobic site of the latter. We have shown that HX experiments in combination with a column containing immobilized DnaK are a powerful tool to map binding sites in its substrates.

DnaK induces monomerization of RepE. Interestingly, DnaK binding site (residues 240-250) is not close to the dimer interface (residues 97-128). Therefore, DnaK induces conformational changes in RepE in a region that is distant from its binding site. This situation is similar to the one we observed for σ^{32} : DnaK binds in the region 198-202 of σ^{32} but induces destabilization in the N-terminus (residues 31-49). We have observed a similar effect with DnaJ and σ^{32} .

Discussion

As stated in the Overview, the purpose of this Thesis is to characterize the interaction of DnaK with native substrates. To this end we have employed two different native substrates of DnaK: σ^{32} and RepE. The interaction of DnaK with σ^{32} and RepE was studied using HX experiments combined with mass spectrometry, which is a powerful tool to investigate protein conformational properties. In this section we make a summary of the obtained results and discuss the possible mechanism of action of DnaK.

In Chapter 3 we presented a quenched-flow setup system that allows HX experiments with as short as 100 ms exchange times. We have first evaluated the performance of the system: using apo-myoglobin as a model protein, we have demonstrated that the quenched-flow setup is accurate and reproducible with a low level of back-exchange. We have then investigated the conformational properties of *E. coli* heat-shock transcription factor σ^{32} free in solution. Using the quenched-flow setup we have detected at least 30 amide protons in the C-terminal region of σ^{32} that are protected

after 1 sec, and at least 25 after 5 sec. We have found that the C-terminus of σ^{32} is structured but yet very flexible. These structural properties can only be detected with very short exchange times given that after 10 seconds the C-terminus of σ^{32} has exchanged almost completely. The quenched-flow setup was also used in Chapter 7 to investigate the conformational differences between dimeric RepE wild-type and the monomeric RepE54 variant. In this case we were able to show that, even at very short exchange times, the monomer is more stable than the dimer. Summing up, in this thesis we have shown that the quenched-flow setup is suitable for mapping short-term conformational changes.

Our first approach to characterize the interaction of DnaK with σ^{32} was a crystallization attempt described in Chapter 4. We were able to purify DnaK- σ^{32} and DnaK-DnaJ- σ^{32} complexes in the high amounts that are needed for crystal screenings. Even though we have not yet been successful in obtaining crystals, this project is a still ongoing collaboration. We are currently trying to purify the different complexes formed *in vivo*. With this purpose we have created new plasmids and are still searching for the right conditions for this purification.

Since we could not obtain the crystal structure of the DnaK- σ^{32} and DnaK-DnaJ- σ^{32} complexes, we investigated the interaction of DnaK and DnaJ with σ^{32} using HX experiments in Chapter 5. We have confirmed that the previously identified DnaK binding site in σ^{32} is the actual binding site in the native protein. The identified DnaK binding site is located at position 198 to 201 in the σ^{32} polypeptide chain. This DnaK binding site consists of a hydrophobic core of 4 amino acids flanked by many hydrophilic and negatively charged residues. While these flanking segments do not promote DnaK binding, they may promote the surface exposure of the hydrophobic core residues including their peptide backbone, thereby facilitating the enclosure of this site through binding into DnaK's substrate binding cavity. In addition, the negative charges in the flanking segments may help to prevent aggregation of σ^{32} by electrostatic repulsion.

We have also localized the DnaJ binding site to the N-terminal domain of σ^{32} . Our conclusion resides on five lines of evidence. (1) The identified site is a high affinity site at the primary sequence as evidenced by peptide library scanning (Rüdiger *et al.*, 2001). (2) DnaJ binding to σ^{32} leads to a protection from HX of regions in close vicinity of the

identified site (Figure 5.12). (3) Truncations and point mutations decrease the affinity of DnaJ for σ^{32} . (4) The truncation and point mutants fail to stimulate the ATPase activity of DnaK in a synergistic fashion in the presence of DnaJ, while they stimulate the ATPase activity of DnaK in the absence of DnaJ like wild type σ^{32} (Figure 5.8). (5) The truncation mutant is not loaded onto DnaK in a DnaJ- and ATP-dependent way (Figure 5.8).

The DnaJ binding site in σ^{32} does not need to be unstructured since DnaJ only distinguishes side chain hydrophobicity and, unlike DnaK, does not depend on backbone contacts (Rüdiger *et al.*, 2001). This site is different from the DnaK binding site. The fact that DnaK and DnaJ bind to σ^{32} in different regions demonstrates that a direct transfer mechanism of the DnaJ-bound site into the substrate-binding cavity of DnaK is not operative in the case of σ^{32} . Since a truncation and mutagenesis study on the native DnaK substrate RepA also suggests different binding sites for DnaK and DnaJ (Kim *et al.*, 2002) this mode of cooperation between DnaJ and DnaK might be more general.

What are the effects of the DnaK and DnaJ chaperones on σ^{32} ? In the presence of DnaJ, σ^{32} exchanged amide hydrogens with an overall higher rate corresponding to a destabilization of 86 kJ·mol⁻¹. The localization of the destabilized regions revealed that one of them is in close vicinity to the DnaK binding site in the primary structure. This suggests that DnaJ promotes an open conformation of σ^{32} thereby facilitating DnaK binding. These data explain the synergism of DnaJ and σ^{32} in stimulating DnaK's ATPase activity and of DnaJ's high efficiency in loading σ^{32} onto DnaK.

DnaK also affects the conformation of σ^{32} . A segment in the N-terminal domain of σ^{32} , residues 31-49, shows in HX experiments more exchange in the presence of DnaK as compared to free σ^{32} . This region of σ^{32} is therefore less compact when σ^{32} is bound to DnaK, though the magnitude of this destabilization appears to be small (two amide hydrogens). In the HX experiments with full-length σ^{32} we did not observe any change in overall exchange rates. However, we observed hydrogen protection at the DnaK-binding site and at the very N-terminus (residues 3-18) in the HX experiments with pepsin digestion. In the binding site we could only measure a protection of 2 amide hydrogens due to the subsequent cleavage of the binding site during the peptic digestion. A model

peptide comprising this region shows a protection of 4 amide hydrogens in the absence of peptic digestion and of 2 amide hydrogens in its presence, indicating that in the full-length protein also 4 amide hydrogens within the DnaK binding site should be protected by binding to DnaK. Together with the single amide hydrogen that exchanges more slowly in the N-terminal segment, a total of at least 5 amide hydrogens in σ^{32} should be protected upon binding to DnaK. Since none were observed in the experiments with the full-length protein, an equal number of amide hydrogens are expected to be deprotected. The reason for the lower number of observed deprotected amide hydrogens is probably peptic digestion, which leads to a loss of information at every cleavage site. Therefore, the observed degree of destabilization in the N-terminal domain is most likely an underestimation of the total effect of DnaK on σ^{32} .

How could DnaK and DnaJ affect the conformation of σ^{32} ? There are principally two alternative ways. Chaperone binding could actively induce the conformational alteration in σ^{32} . Alternatively, σ^{32} could exist in at least two conformational states, a closed and an open state, which are in equilibrium with each other. Chaperone binding could shift this equilibrium to the open state by binding to it. However, irrespective of the way by which the chaperones affect the deprotection of amide hydrogens in σ^{32} , the result is the same: σ^{32} is destabilized in defined regions. In Figure D.1 we show a model of the regulation of σ^{32} by DnaK-DnaJ.

Recently, σ^{32} variant proteins with a longer half-life *in vivo* were reported (Horikoshi *et al.* 2004; Obrist and Narberhaus 2005; Gross personal communication). Interestingly, the amino acid substitutions in these σ^{32} variants are located in the region where the destabilization by DnaK occurs. This is thus a crucial region of the regulation of σ^{32} . In Chapter 6 we have investigated two of these σ^{32} variants (σ^{32} I54N and σ^{32} L47Q-L55Q) by HX experiments. We found that in the case of σ^{32} I54N the segment 157-175 is more protected than in σ^{32} wt, and in the case of σ^{32} L47Q-L55Q the segment 87-101 is more protected than in σ^{32} wt. These two segments are destabilized in σ^{32} wt upon DnaJ binding. In addition, we found that the affinity of DnaJ for these two proteins is lower than the affinity of DnaJ for σ^{32} wt. These two variant proteins are also impaired in the DnaJ- σ^{32} synergistic stimulation of the DnaK ATP hydrolysis. The reason for these

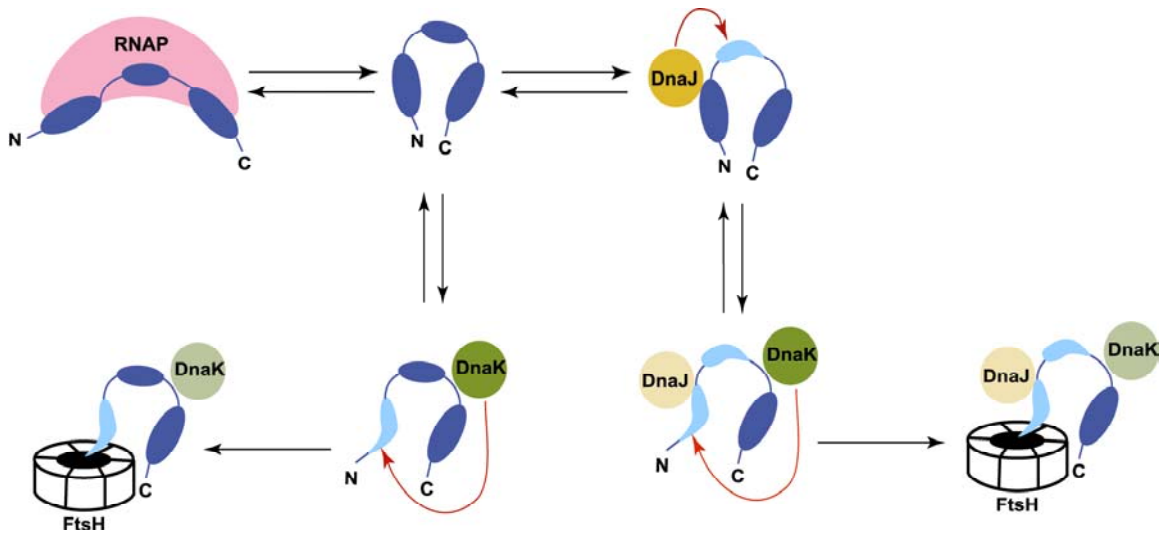


Figure D.1. Model of the regulation of σ^{32} by DnaK-DnaJ. DnaK and DnaJ bind in different regions of σ^{32} . DnaK binds in the C-terminal region of σ^{32} (aa 198-201) while DnaJ binds in the N-terminus region (aa 59-64). Both chaperones destabilize σ^{32} in regions distant to their binding sites. DnaK destabilizes the segment 31-49 of σ^{32} while DnaJ destabilizes two segments, one of them close to the DnaK binding site in the primary structure (aa 158-175). This suggests that DnaJ promotes an open conformation of σ^{32} thereby facilitating DnaK binding. The destabilizations induced by DnaK-DnaJ are indicated with red arrows and shown in light blue in the structure. The chaperone-induced unfolding of a secondary structure element may facilitate degradation of σ^{32} *in vivo* by the FtsH protease. DnaK and DnaJ could be bound to or released from σ^{32} during degradation (indicated with light green and light yellow). DnaK binding to σ^{32} prevents the binding to the RNA polymerase (RNAP).

two σ^{32} variants to be more stable *in vivo* could be that the DnaJ targeting to DnaK is impaired for these proteins.

What are the consequences of the interaction of the chaperones with σ^{32} *in vivo*? *In vivo*, σ^{32} is degraded mainly by the AAA⁺ protease FtsH. Degradation of σ^{32} proceeds from the N- to the C-terminus (Okuno *et al.*, 2004). In addition, FtsH lacks robust unfoldase activity and only degrades substrates efficiently when they have a low intrinsic thermodynamic stability (Herman *et al.*, 2003). This indicates that a chaperone-induced unfolding of a secondary structure element may facilitate degradation of σ^{32} *in vivo*. The DnaK system cannot stimulate the proteolysis of σ^{32} by full-length FtsH *in vitro*. It has been speculated that an unknown factor is missing. We cannot exclude that this destabilization exposes a binding site for an adaptor protein. For example, the SspB adaptor protein binds in the N-terminus of substrates and targets them to ClpX for

degradation, which starts from the N-terminus (Levchenko *et al.*, 2003; Song *et al.*, 2003; Park *et al.*, 2007).

How could the DnaK-DnaJ system regulate the activity of σ^{32} ? Our data indicate that the DnaK binding site is in close vicinity of, or is identical with, a site involved in RNAP binding. This conclusion resides on previous results from our laboratory. In these studies σ^{32} could be cross-linked to RNAP through an UV-activated cross-linker located in the close neighborhood of the DnaK binding site, and mutational alterations within the DnaK binding site reduced the affinity of RNAP to σ^{32} . These results are consistent with the reduced affinity of RNAP for the σ^{32} mutant protein encoded by the *rpoH113* allele that carries a deletion of residues 178 to 201 (Calendar *et al.*, 1988; Zhou *et al.*, 1992). These data are also consistent with the crystal structure of *T. thermophilus* RNAP holoenzyme, which shows that the σ^{70} region homologous to the DnaK binding site is enclosed between the β and β' subunit of RNAP (Vassylyev *et al.*, 2002). Consequently, DnaK and RNAP binding to this site are mutually exclusive, in consistence with earlier observations (Gamer *et al.*, 1996; Liberek *et al.*, 1992). This way of regulation of the activity of σ -factors seems to be a more general scheme as suggested by three recent crystal structures between σ -factors and their specific anti- σ -factors (Campbell *et al.*, 2003; Campbell *et al.*, 2002; Sorenson *et al.*, 2004). Although the individual σ -factor—anti- σ -factor pairs bind to each other in different ways, the effect is similar: at least one binding determinant for RNAP becomes inaccessible. However, under equilibrium conditions DnaK can not out-compete RNAP, neither in the ADP nor in the ATP bound state, since the dissociation equilibrium constant for the DnaK- σ^{32} interaction is 1.4 μM in the ADP state and at least ten-fold higher in the ATP state, while the K_D for RNAP is with 12 nM 100-fold lower, most likely due to the much larger interaction surface. The efficient competitive binding of DnaK to σ^{32} relies on the high association rate in the ATP-bound state and subsequent ATP hydrolysis, coordinated by DnaJ, to take advantage of the low dissociation rate of the ADP-bound state. Thus, the calculated non-equilibrium K_D is in the low nM range. The effect of DnaJ on the interaction of DnaK with σ^{32} is therefore twofold. First, the DnaK binding site within σ^{32} becomes more accessible, increasing the association rate between DnaK and σ^{32} . Second, synergistic

stimulation of the ATP hydrolysis leads to an efficient trapping of σ^{32} . It will be important to determine whether this mode of action of the DnaK-DnaJ team is generally applicable for other substrates and for Hsp70 homologues.

In Chapter 7 we studied the interaction between DnaK and another of its native substrates RepE. RepE can initiate replication or repress its own synthesis depending on its oligomeric state (monomer or dimer). DnaK, DnaJ and GrpE regulate RepE monomerization. The purpose of this Chapter was to characterize the mechanism of monomerization induced by the DnaK system. First, we investigated the conformation of dimeric RepE wild-type and the monomeric variant RepE54. Using HX experiments, we mapped the dimer interface in RepE. It is located in the region 96 to 128. Our result is supported by different data: (1) variant proteins that are constitutively monomeric have amino acid substitutions in this region (Matsunaga *et al.*, 1995), (2) these segments of RepE are poorly resolved in the crystal structure of monomeric RepE54, indicating a high flexibility. However, in a dimeric assembly they would prolong a β -sheet across the dimer interface (Figure 7.3), (3) the dimerization interface in RepA which is related to RepE in structure but not in sequence comprises two β strands from different protomers, forming a central five-stranded antiparallel-pleated β -sheet (Giraldo *et al.*, 2003). These two β -strands interact through hydrogen bonds. The region we found to be protected in the dimer corresponds to the dimer interface of RepA.

Is binding to DNA similar in monomeric RepE wild-type and dimeric RepE54? N- and C-terminal domains of monomeric RepE54 are topologically similar and related to each other by an internal two-fold symmetry (Komori *et al.*, 1999). Both domains of RepE54 bind to the two major grooves of iteron DNA. Two helix-turn-helix motifs in RepE54, namely $\alpha 3$ -turn- $\alpha 4$ (residues 64-92) and $\alpha 3'$ -turn- $\alpha 4'$ (residues 168-242), are critical for directed repeat *ori2* binding. In HX experiments, the segments from this region showed no differences between dimeric RepE wild-type and monomeric RepE54, indicating that this region does not change its conformation upon monomerization. Therefore, binding to DNA must be similar for both proteins. This is in agreement with the fact that the directed repeats sequence from *ori2* where monomeric RepE binds and the inverted repeats sequence from the operator where dimeric RepE binds contain 8 bp

in common (Ishiai *et al.*, 1994). In addition, the $\alpha 3'$ -turn- $\alpha 4'$ motif is also a critical region for dimeric RepE binding to inverted repeat operator (Matsunaga *et al.*, 1995).

How is the mechanism of monomerization? In HX experiments, the segments in regions 5-28, 151-164 and 219-240 exchange more in the dimer than in the monomer, indicating that dimeric RepE is more flexible in these regions. Segment 5-28 includes the $\beta 1$ that in monomeric RepE54 forms a small β -sheet with $\beta 1'$ (residues 147-150). In the structure of the N-terminal domain of RepA this β -sheet is disrupted and $\beta 1'$ forms an extension of $\alpha 5$ (Giraldo *et al.*, 2003). Our results are in agreement with the N-terminal structure of RepA since the lack of hydrogen-bonds between those two strands would result in higher deuterium incorporation in this region. Our results indicate that monomerization of RepE requires marked conformational changes. The higher flexibility in RepE dimer may be needed for accommodating it on the inverted repeat of the operator.

With crosslinking experiments we showed that DnaK binds to both RepE wild-type and RepE54. Using the same approach as in Chapter 5, we were able to map the DnaK binding site in RepE: DnaK binds in a C-terminal hydrophobic site of RepE (segment 240-250). The binding site for both RepE proteins was the same. This result was confirmed with trypsin partial proteolysis experiments. We found that C-terminal fragments were protected from trypsin cleavage in DnaK-RepE wt complex but not in free RepE wt. We obtained the same result with Rep54.

How could DnaK induce the monomerization of RepE? We showed that there are marked conformational changes in the monomerization of RepE. Monomeric RepE54 is more stable than the dimeric RepE wild-type even though the dimer interface is more stable in RepE wild-type. RepE is in equilibrium between dimer and monomer. The dimerization K_D has been estimated to be approximately 0.3 nM (Ishiai *et al.*, 1994). Thus, under physiological conditions RepE will be majority as a dimer and require the action of DnaK system to monomerize and bind to *ori2*. We propose that DnaK system induces the monomerization of RepE and remains bound to monomeric RepE to avoid reformation of the dimer. This hypothesis is supported by the fact that the DnaK also binds to monomeric RepE.

What is the function of DnaJ? There are 5 potential binding sites for DnaJ in RepE (data no shown). The DnaJ binding site in native RepE remains to be elucidated. One way to find this site is to create point mutants and evaluate the affinity for DnaJ like we did for σ^{32} . It also would be interestingly to study whether DnaJ induces conformational changes in RepE. We speculate that DnaJ also destabilizes RepE and makes the DnaK binding site more accessible. This hypothesis is based in the fact that RepE cannot initiate mini-F replication in *ΔdnaJ* strains and that DnaJ together with RepE stimulate synergistically the ATP hydrolysis of DnaK in single turn-over experiments (data no shown). This DnaJ effect on RepE requires further investigation.

DnaK regulates the activity of different native proteins in the cell. It can inhibit the activity of some proteins like in the case of σ^{32} and it can activate the activity of other proteins like in the case of RepE. We propose that inactivation is a consequence of structural destabilization whereas activation stems from structural stabilization.

In conclusion, in this Thesis we have characterized the interaction of two native substrates with the DnaK system. Our data explain how the chaperone system regulates the activity of σ^{32} . We also elucidated the molecular mechanism of RepE monomerization and contributed to the understanding of the regulation of RepE by the DnaK system.

Materials and methods

Computer software

Acrobat 5.0	Adobe
Analyst QS (with BioAnalyst)	Applied Biosystems/MDS SCIEX
EndNote 4.0	ISI ResearchSoft
GPMAW	Lighthouse Data
Graphit 5.0	Erithacus Software Ltd.
HXPep	Z. Zhang
Illustrator 9.0	Adobe
MagTrans	Z. Zhang
Office 2000	Microsoft Corp.
PepSea 2.2	MDS Proteomics
Photoshop 6.0	Adobe
Weblab Viewer 5.0	Molecular Simulations Inc.

Equipment

Mass spectrometers

QSTAR Pulsar i Hybrid MS/MS System	Applied Biosystems/MDS SCIEX
UltraFlex MALDI-TOF/TOF	Bruker Daltonics

HPLC pumps

1100 Series Capillary Pump	Agilent
1100 Series Binary HPLC Pump	Agilent
LC-10ADVP HPLC	Shimadzu
Rheos 2000 Micro HPLC	Flux Instruments
Ultimate HPLC with Switchos and Famos	LC Packings

Other equipment

Speed-Vac	Bachofer
UV lamp B-100AP	Ultraviolet Products
French Press	SLM-Amin.co
ÄKTA FPLC and columns	Amersham Pharmacia
RoboCycler	Stratagen
Spektrometer UV-1601	Shimadzu
Scintillation counter	Beckman
Fuji FLA 2000 fluorimager	

Chemicals

If not otherwise stated all chemicals were analytical grade and obtained from Roth, Sigma or Merck. For mass spectrometry only high purity solvents (HPLC grade) were used.

Kits

QIAGEN[®] Plasmid Prep Kit.
QIAGEN[®] PCR DNA and Gel Band Purification Kits.

Proteins and Enzymes

BSA	Sigma-Aldrich
DNase A	Sigma
Lysozyme	Roth
Gel filtration standard	Biorad
Myoglobin	Sigma
Poroszyme Immobilized Pepsin	Applied Biosystems
Restriction enzymes	New England Biolabs, Roche
T4-DNA ligase	New England Biolabs, Roche
Trypsin (sequencing grade)	Promega

DNA and Protein Size Standards

GeneRuler [™] 1kb DNA Ladder	Fermentas
Prestained Protein Ladder (SM0671)	Fermentas
Prestained Protein Ladder (SM0441)	Fermentas

Protein Ladder (SM0431)

Fermentas

Peptides

Pep44 (σ^{32} -Q132-Q144)

J. Schneider-Mergener, Charité Berlin

Pep65 (σ^{32} -M195-N207)

J. Schneider-Mergener, Charité Berlin

Antibiotic stock solutions (1000x)

Ampicillin 100 mg/ml in H₂O (stored at -20°C)

Chloramphenicol 20 mg/ml in 70% (v/v) ethanol (stored at -20°C)

Kanamycin 50 mg/ml in H₂O (stored at -20°C)

Tetracycline 10 mg/ml in 70% (v/v) ethanol (stored -20°C)

Strains

MC4100 lab collection (Casadaban, 1976)

F⁻ araD139 Δ (argF-lac)U169 rpsL150 relA1 deoC1 ptsF25 rpsR flbB5301

BB1553 lab collection (Bukau & Walker, 1990)

MC4100 *Δ dnaK52::Cm^r sidB1*

BB1994 lab collection

BB1553, pDMI.1

DH5 α lab collection

supE44 Δ lacU169 deoR (f80lacZAM15)hsdR17 recA1 endA1 gyrA96 thi-1 relA1

DH5 α Z1 lab collection (Lutz & Bujard, 1997)

DH5 α *lacI^f tetR Spec^r*

WKG191 lab collection (Kelley & Georgopoulos, 1997)

MC4100 *araD139 Δ ara714 Δ dnaK52::Cm^r sidB1*

CJ236 lab collection (Kunkel *et al.*, 1987)

dut1, ung1, thi-1, relA1/pCJ105(F' cam^r)

BL21 lab collection

hsdSgal (λ cIts857 ind1 Sam7 nin5 lacUV5-T7 gene1)

BB7142 lab collection

BL21 Δ ftsH

Plasmids

pUHE21-2fd Δ 12 lab collection (Lanzer, 1988)
(*colE1* Amp^r Lac 03/04 promotor/operator)

pMPM-A4 lab collection (Mayer, 1995)
(*colE1* Amp^r *araC*, pBAD promotor)

pBluescript II KS+ = pBSKS+ Stratagene (Alting-Mees & Short, 1989)
phagemid vector, ampicillin resistant

pWR01 lab collection
pBSKS+(*repE*)

pWR02 lab collection
pBSKS+(*repE54*)

Primers

10His-EcoRI	aattcATGCATCACCATCACCATCATCACCATCACGGCGGTTTC
10His-NcoI-rev	catgGAACCGCCGTGATGGTGTGATGGTGTGATGGTGTGATGGTGTGATGCATG
3'HindIII 145-251	cgataagcttgatatcgc
3'HindIII 1-144	cgtaagcttagTTCTGTAAACCCGATAAAGAA
3'HindIII RepE 10His	cgaagcttCTAgtgatggtgatggtgatggtgatggtgatgTCCTGTGTCGTCATGGAAG
3'RepE 224AAAA	GCCTTTCTTTTTCTCagcagcagcagcGCGCATTGGAGTTC
3'repE delta220	cgaagcttTCAAGTTCTGCTGTTGATC
5'NcoI 145-251	ccggCcATGGCGTTTACGCAGTTTCGGC
5'RepE	ggatggagtgaaggagg
5'RepE 244AAAA	GAACTCCAATGCGCgctgctgctgctGAGAAAAAGAAAGGC
5'RepE EcoRI w/oNhis	gggaattcATGGCGGAAACAGCGG
5'RepE KpnI	cggggtaccGCGGAAACAGCGGTTATC
5'RepE KpnI 144-251	cggggtaccCGGTTTACGCAGTTTCGG
3's32EcoRI	ggtggtgaattcTTAgtgatggtgatggtg
3'SUMO KpnI BamHI	cgggatccgtaccACCAATCTGTTCTCTGTGAGCC
3'HindIII rpoH	ggaagcTTACGCTTCAATGGCAGC
3'SBD HindIII	caggagtccaagcTTAGGC
5'NdeI Sumo	GGAGATATACATATGGG
5'rpoH EcoRI	cggaattcATGACTGACAAAATGCAAAG
5'rpoH KpnI	cggggtaccGACAAAATGCAAAGTTTAGC
5'SBD 389 NdeI	gcgcatatggtactgctgctggacgttaccCG
3'rpoH 122Cter SpeI	CCGactagtTTAgtgatggtgatggtgatg
3'rpoH 122 SpeI	CGGactagttaACGCCAGTTACGCAGAAC
5'rpoH 122Cter EcoRI	ccgGAATTCATGCGTATCGTCAAAGTTGCG
3'rpoH 210 SpeI	CGGGactagttaGTCCGCAAAGTTAGATGATTTATC
3'rpoH 218 SpeI	CGGactagttaTTCCCAGTTATCATCTTCAATG
3'rpoH 224 SpeI	CGGactagttaACGGTTTGCCGCTGCTC
3'rpoH 235 SpeI	CGGactagttaGCGTTTCGTCCAGACCCTG
5'rpoH-liz NdeI	CCATGGGCAGCAGCCATC

rpoH L47Q	TGCTTCctgATCGCC
rpoH L55Q	GTGAGActgGATCAG
rpoH I54N	AGACAGGtTCAGCGT
rpoH N94C	cttccgggcagaaacggc

Media

LB broth	10 g/l tryptone 5 g/l yeast extract 5 g/l NaCl 15 g/l agar (only for culture plates)
----------	---

2x YT	16 g/l tryptone 5 g/l NaCl
-------	-----------------------------------

Buffers

KII buffer	25 mM Hepes KOH pH 7.6 50 mM KCl 5 mM MgCl ₂
------------	---

HKNM buffer	25 mM Hepes KOH pH 7.6 50 mM KCl 150 mM NaCl 5 mM MgCl ₂ 7 mM β-mercaptoethanol
-------------	--

T-Buffer	20 mM Tris/HCl, pH 7.8 200 mM KCl 10 mM MgCl ₂ 2 mM DTT 5% glycerol 0.05% Tween-20
----------	--

Others

nick-column (sephadex G50)	Amersham Pharmacia
ultracentrifugation spin column	Vivaspin
TLC plates: PEI celluloseF	Merck 1.05579
[α ³² P] ATP: 10 μCi/ul	Amersham Biosciences
D ₂ O (99.9%)	Cambridge Isotope Laboratories
Poros R1	Applied Biosystems
Poros R2	Applied Biosystems

by centrifugation at 4000 rpm for 10 minutes. The medium was decanted and the tube was stood in an inverted position on a pad of paper towels for 1 minute to drain away the last traces of media. The pellet was resuspended in 2 ml of storage solution, dispensed into aliquots, frozen in liquid nitrogen and stored at -80°C .

Transformation

DNA was added to 50 μl of the competent cells. The tube was incubated on ice for 30 minutes on ice. Then the tube was incubated 90 seconds at 42°C (40°C for Δ dnaK strains) and 2 minutes on ice. 500 μl of LB media was added to the tube and it was inoculated 45 minutes at 37°C (or 30°C) to allow bacteria to recover and express the antibiotic resistance marker encoded by the plasmid. 100 μl of transformed cells were plated onto agar LB medium containing the appropriate antibiotic.

Purification of plasmid DNA

Plasmid DNA isolation was performed using either the small-scale QIAGEN[®] Quick Spin method or the large-scale QIAGEN[®] Plasmid Midi Kit according to the protocol provided by the manufacturer.

Cloning 10His-RepE and 10His-RepE R118P

The plasmids pWR07 and pWR08 were cut with NcoI and EcoRI. The resulting fragment was purified with QIAGEN[®] gel extraction kit according to the manufacture instruction. Then the purified fragment was ligated to the 10His-EcoRI and 10His-NcoI-rev previously annealed.

PCR Cloning of σ^{32} deletion mutants

The rpoH gene was amplified by PCR (polymerase chain reaction) from the pMPM-4A-rpoH-liz plasmid. The primers were designed such that they were complementary to the beginning and to the base that wanted to be deleted of the rpoH gene and contained EcoRI and SpeI sites, respectively. rpoH PCR product was cut with EcoRI and SpeI and inserted into pMPM-4A, which was also cut with EcoRI and SpeI. The resulting plasmid

was transformed into the *E. coli* strains DH5 α Z1 and BB7142. All plasmids were sequenced.

Site directed mutagenesis

Buffers

Annealing buffer	20 mM tris/HCl pH 7.5 2 mM MgCl ₂ 50 mM NaCl
10x Polmix	200 mM Tris/HCl pH 7.5 20 mM DTT 100 mM MgCl ₂ 5 mM dNTP 4 mM ATP 0.5 mg/ml BSA

Method

Mutant genes of rpoH (rpoH N94C, rpoH L47Q-L55Q, rpoH I54N) were created by *in vitro* mutagenesis according to Kunkel (Kunkel *et al.*, 1991). Single-stranded DNA (ssDNA) of pMPM-4A-rpoH was prepared using the *E. coli* host strain CJ236 and helper phage M13KO7. CJ236 is *dut*⁻ and *ung*⁻, and therefore deficient for the enzymes dUTPase (Dut) and uracil-N glycosylase (Ung). The mutagenic oligonucleotide was annealed to the deoxyuridine-containing ssDNA, and was extended and ligated using T7 DNA polymerase and T4 DNA ligase, respectively. The DNA was transformed into *E. coli* DH5 α Z1, which is *ung*⁺, thereby degrading the original uridine-containing strand. The newly synthesized strand that contained the mutated bases was replicated to produce intact mutated plasmid, which was confirmed by sequencing.

Annealing:

1 μ L phosphorylated primer, 1 μ l ssDNA (1 μ g), 1 μ l 10x annealing buffer, and 7 μ l H₂O were heated to 95°C for 2 min, slowly cooled to 30°C, and then placed on ice.

Elongation/Ligation:

To the annealed template-primer 10 μ l of 10x polmix buffer and 79 μ l H₂O were added, incubated on ice for 5 min, at room temperature for 5 min, and at 37°C for 2 h. Then, 5 μ l were used for transformation into DH5 α Z1.

Cloning of σ^{32} and DnaK (crystallization approach)

The original idea was to co-express σ^{32} and DnaK (without the C-terminal tail), in order to purify *in vivo* pre-assembled complexes. σ^{32} and DnaK (up to 607) were cloned into a pUHE-based vector and the proteins were over-expressed in a delta dnaK52-host strain (BB1994). The expression level of the complex was too low. *In vivo*, σ^{32} is degraded by the AAA+ protein FtsH (a membrane-anchored ATP dependent metal protease, Tomoyasu *et al.*, 1998, Tatsuta *et al.*, 2000). It has been shown in the past that σ^{32} is better expressed in delta ftsH strains. The vector expressing the complex was cloned into a delta dnaK, delta ftsH strain. This strain grown very slowly and was not suitable for the expression of the complex. An alternative protocol was made: σ^{32} was purified using Ni²⁺-affinity chromatography, and then DnaK was added to σ^{32} bound to the Ni²⁺-column. The complex was formed in the Ni²⁺-column and the unbound DnaK could be washed away. After elution and cleavage, a gel filtration column was run to separate free σ^{32} from the complex. In the same way the DnaK/DnaJ/ σ^{32} complex and the DnaJ/ σ^{32} complex were purified.

σ^{32} was cloned into a plasmid with a L-arabinose inducible promoter (pMPM-A4). We placed at the N-terminus of σ^{32} a hexahistidine-tag (His₆-tag) followed by a Ppx cleavage site.

DnaK without the C-terminal tail (up to aa 607) was cloned in a pUHE-based vector. Over-expression was performed in a delta dnaK52-host strain (BB1994). The substrate-binding domain (SBD) of DnaK without the C-terminal tail (aa 389-607) was also cloned in a pUHE-based vector and over-expressed in a delta dnaK52-host strain.

Biochemical Methods

SDS Gel Electrophoresis

Buffers

4x SDS stacking gel buffer	0.5 M Tris/HCl, pH 6.8 0.4% SDS
4x SDS separation gel buffer	1.5 M Tris/HCl, pH 8.8 0.4% SDS
4x gel loading buffer	500 mM Tris/HCl, pH 6.8 8% (w/v) SDS 40% (v/v) glycerol 20% (v/v) β -mercaptoethanol 0.6% (w/v) bromophenol blue
1x SDS gel running buffer	25 mM Tris, pH 8.0 200 mM glycine 0.1% (w/v) SDS
Coomassie staining solution	0.2% (w/v) Coomassie Brilliant Blue R250 50% (v/v) methanol 5% (v/v) acetic acid
Coomassie destaining solution	50% (v/v) methanol 5% (v/v) acetic acid

SDS-PAGE gels were prepared according to Laemmli (Laemmli, 1970) and protein bands were visualized by Coomassie staining.

Protein Quantification

The protein concentration was determined using the Bradford method (Bradford, 1976). The Bradford reagent (Biorad) was diluted 1:5 with water and 1 ml was mixed with 1–5 μ l of the protein solution. After 5 minutes of incubation the absorption was measured at 595 nm in a spectrophotometer. For calibration were used different amounts of BSA (0, 1, 2, 4, 5 and 10 mg/ml BSA).

Purification of $_{10}$ His-RepE

Buffers

Lysis buffer A	40 mM Na ₂ HPO ₄ /NaH ₂ PO ₄ , pH 7.9 450 mM NaCl 0.1 mM EDTA 1 mM PMSF 10% glycerol
Buffer A	40 mM Na ₂ HPO ₄ /NaH ₂ PO ₄ , pH 7.9 100 mM NaCl 20 mM imidazole 10% glycerol
Buffer B	40 mM Na ₂ HPO ₄ /NaH ₂ PO ₄ , pH 7.9 100 mM NaCl 20 mM imidazole 10% glycerol
Buffer C	40 mM Na ₂ HPO ₄ /NaH ₂ PO ₄ , pH 7.9 50 mM NaCl 500 mM imidazole 10% glycerol
Buffer D	40 mM Na ₂ HPO ₄ /NaH ₂ PO ₄ , pH 7.9 10% glycerol
Buffer E	40 mM Na ₂ HPO ₄ /NaH ₂ PO ₄ , pH 6.6 100 mM NaCl 0.1 mM EDTA 7 mM β-mercaptoethanol 10% glycerol
Buffer F	40 mM Na ₂ HPO ₄ /NaH ₂ PO ₄ , pH 6.6 100 mM NaCl 0.2 mM EDTA 7 mM β-mercaptoethanol 10% glycerol

Overproduction and cell lysis:

Over-expression of ₁₀His-RepE or ₁₀His-RepE mutants was performed in a WKG191-host strain. 3L of 2xYT complemented with 100 µg/l ampicilin were inoculated with an overnight culture of the corresponding strain. The culture was grown at 30°C until an OD₆₀₀ of 0.6. Cells were induced with L-arabinose (0,2% final concentration). After 4 hours, cells were harvested by centrifugation at 4°C and stored at -80°C.

All further steps were carried out on ice or at 4 °C. Cells were re-suspended in 120 ml of lysis buffer and lysed with a French press. Cell debris was removed by centrifugation for 30 min at 18,000 rpm.

NiNTA

The supernatant was added to NiNTA (QIAGEN[®]) that was equilibrated with buffer A and incubated at 4°C shaken end-over-end for 1 hour. The NiNTA was packed in a disposable column and washed with 20 volume column buffer A, 20 volume column buffer B and again with 20 volume column buffer A. The protein was eluted with buffer C and diluted 5 times in buffer D.

Cation exchange chromatography (SP-sepharose)

The protein solution was loaded onto a 5 ml SP-sepharose column that was equilibrated on buffer E. The column was washed with 100 ml buffer A and eluted with 100 ml gradient of 0 to 50% buffer F into 1 ml fractions. The RepE containing fractions were pooled and stored at -80C.

Purification of DnaK-His₆

Buffers

Lyses buffer	20 mM Tris-HCL pH 7.9 100 mM KCl 20 mM imidazole 1 mM PMSF
Buffer A	20 mM Tris-HCL pH 7.9 100 mM KCl 20 mM imidazole
Buffer B	20 mM Tris-HCL pH 7.9 1 M KCl 20 mM imidazole
ATP buffer	40 mM Tris-HCl 100mM KCl 5 mM MgCl ₂ 5 mM ATP 20 mM imidazole

Buffer C	20 mM Tris-HCL pH 7.9 100 mM KCl 500 mM imidazole
Buffer D	40 mM Tris-HCl
Buffer E	40 mM Hepes-KOH pH 7.6 50 mM KCl 5 mM MgCl ₂
Buffer F	40 mM Hepes-KOH pH 7.6 1 M KCl 5 mM MgCl ₂

Overproduction and cell lysis

Over-expression of DnaK-His₆ was performed in a BL21-host strain. 10L of 2xYT complemented with 100 µg/l ampicilin were inoculated with an overnight culture of the corresponding strain. The culture was grown at 30°C until an OD₆₀₀ of 0.8. Cells were induced with IPTG (1 mM final concentration) over-night. Cells were harvested by centrifugation at 4°C and stored at -80°C.

All further steps were carried out on ice or at 4 °C. Cells were re-suspended in 200 ml of lyses buffer and lysed with a French press. Cell debris was removed by centrifugation for 30 min at 18,000 rpm (repeated two times).

NiNTA

The supernatant was mixed with 8 ml of NiNTA agarose previously equilibrated with buffer A and incubated at 4°C for 30 minutes. The sample slurry was poured onto a disposable column. The column was washed with 20 column volume buffer A, 20 column volume of buffer B, 10 volume column ATP buffer and again with 20 volume column buffer A. The protein was eluted with buffer C and diluted in buffer D.

Anion exchange chromatography (resource Q)

The protein sample was loaded onto a 6 ml resource Q column that was equilibrated with buffer E. The column was washed with 100 ml buffer A and eluted with 100 ml gradient of 0 to 50% buffer F into 0.75 ml fractions. The DnaK containing fractions were pooled and stored at -80C.

Purification of σ^{32} -His₆

Buffers

Lysis buffer	20 mM Tris-HCl pH 7.9 100 mM NaCl 0.05% Na-desoxycholate 1 mM PMSF
Buffer A	20 mM Tris-HCl pH 7.9 450 mM NaCl 20 mM imidazole
Buffer B	20 mM Tris-HCl pH 7.9 1 M NaCl 20 mM imidazole
ATP buffer	40 mM Tris-HCl 100mM KCl 5 mM MgCl ₂ 5 mM ATP 20 mM imidazole
Buffer C	20 mM Tris-HCL pH 7.9 100 mM KCl 500 mM imidazole
Gel filtration buffer	40 mM Hepes-KOH pH 7.9 200 mM KCl 10 % glycerol

Overproduction and cell lysis:

Over-expression of σ^{32} -His₆ wt and σ^{32} -His₆ mutants was performed in a BB7142-host strain carrying the rpoH-containing vector. 3L of 2xYT complemented with 100 μ g/l ampicilin were inoculated with an overnight culture of the corresponding strain. The culture was grown at 30°C until an OD₆₀₀ of 0.8. Cells were induced with L-arabinose (0,2% final concentration). After 4 hours, cells were harvested by centrifugation at 4°C and stored at -80°C.

All further steps were carried out on ice or at 4 °C. Cells were re-suspended in 75 ml of lyses buffer and lysed with a French press. Cell debris was removed by centrifugation for 60 min at 40,000 rpm.

NiNTA

The supernatant was mixed with 3 ml of NiNTA agarose previously equilibrated with buffer A and incubated at 4°C for 60 minutes. The sample slurry was poured onto a disposable column. The column was washed with 20 column volume buffer A, 20 column volume of buffer B, 10 volume column ATP buffer and again with 20 volume column buffer A. The protein was eluted with buffer C. The eluent was concentrated using a 20ml vivaspin ultracentrifugation spin column (10KDa MWCO).

Gel filtration (Superdex 75 16/60)

3 ml of the concentrated protein solution were loaded onto a Superdex 75 gel filtration column equilibrated with gel filtration buffer. 1ml fractions were collected. The σ^{32} -His₆ containing fractions were pooled, divided in suitable aliquots, frozen in liquid nitrogen and stored at -80°C.

Purification of DnaJ

Buffers

Lyses buffer	50 mM tris-HCl, pH 8 10 mM DTT 0.6% (w/v) Brij 58 1mM PMSF 0.8 mg/ml Lysosyme
Buffer A	50 mM sodium phosphat buffer pH 7 5 mM DTT 1 mM EDTA 0.1% (w/v) Brij 58
Buffer B	50 mM sodium phosphat buffer pH 7 5 mM DTT 1 mM EDTA 0.1% (w/v) Brij 58 2 M Urea
Buffer C	50 mM Tris-HCl, pH 7.5 5 mM DTT 0.1% (w/v) Brij 58 2 M Urea 50 mM KCl

Buffer D 50 mM Tris-HCl, pH 7.5
 5 mM DTT
 0.1% (w/v) Brij 58
 2 M Urea
 50 mM KCl
 600 mM KH₂PO₄

Buffer E 25 mM HEPES-KOH, pH 7.0
 100 mM KCl

Overproduction and cell lysis

The strain BB2583 was grown in 10L of 2xYT complemented with ampicillin (100 µg/l) and kanamycin (50 µg/l) at 30°C to OD₆₀₀=0.3-0.4. Expression of DnaJ was induced by addition of IPTG to a final concentration of 1 mM. After 5 hours, cells were harvested by centrifugation at 4°C and stored at -80°C.

All further steps were carried out on ice or at 4 °C. Cells were re-suspended in 200 ml of lyses buffer and lysed with a French press. Cell debris was removed by centrifugation for 60 min at 40,000 rpm.

Ammonium sulfate precipitation

1 volume of buffer A was added to the supernatant and DnaJ was precipitated by addition of (NH₄)₂SO₄ to a final concentration of 65% (w/v; 398g/l). The sample was stir at 4°C for 30 minutes and then, centrifugated at 15000 rpm during 10 min.

Cation exchange chromatography (SP-sepharose)

The ammonium sulfate pellet was dissolved in 220 ml buffer B and dialyzed against 5L buffer B. DnaJ (30 ml aliquots) was loaded onto a 30 ml SP-sepharose column (equilibrated with buffer B), washed with buffer B (5 column volumes) and eluted with a linear gradient of 0 to 1 M KCl (7 column volumes) and 1 column volume 100% 1 M KCl into 3 ml fractions. DnaJ containing fractions were pooled and precipitated with ammonium sulfate (80%; 516 g/L). The ammonium sulfate pellet was dissolved in 50 ml buffer C and dialyzed against 5L buffer C.

Hydroxyapatit

The sample was loaded onto a 60 ml hydroxyapatit column equilibrated in buffer C and washed with 40 mL buffer C, further washed with 60 mL buffer C + 1 M KCl. Finally washed again with 80 mL buffer C. DnaJ is eluted with a linear gradient of 60 ml 0 to 50% buffer D and 80 mL 50% buffer D. The DnaJ containing fractions are pooled and dialyzed against 2L buffer E.

Cation exchange chromatography (Poros SP20)

The sample is loaded onto a 2 ml Poros SP20 column (equilibrated with buffer B), washed with buffer B and eluted with a linear gradient of 0 to 1 M KCl (15 column volumes). The DnaJ containing fractions were pooled and dialyzed against 2L buffer E. The pool was divided in suitable aliquots, frozen in liquid nitrogen and stored at -80°C .

Purification of DnaK

Buffers

BufferA	25 mM Hepes-KOH pH 7.6 50 mM KCl 5 mM MgCl ₂ 10 mM β -mercaptoethanol 1 mM EDTA
BufferB	25 mM Hepes-KOH pH 7.6 1 M KCl 5 mM MgCl ₂ 10 mM β -mercaptoethanol 1 mM EDTA
BufferC	50 mM Tris-HCl pH 7.6 10% Sucrose 0.1 M (NH ₄) ₂ SO ₄ 5 mM EDTA 5 mM DTT (freshly added)
ATP-buffer	25 mM Hepes-KOH pH 7.6 50 mM KCl 5 mM MgCl ₂ 10 mM β -mercaptoethanol 10 mM ATP

10 mM MgCl₂

Overproduction and cell lysis

The strain BB4279 was grown in 5L of 2xYT complemented with ampicillin (100 µg/l) and kanamycin (50 µg/l) at 30°C to OD₆₀₀=0.3-0.4. For induction IPTG was added to a final concentration of 1 mM and the culture were further incubated over night at 30 °C.

All steps were carried out at 4 °C and on ice, respectively. Cell paste (47 g) was resuspended in 200 ml buffer C and 1 mM (final) PMSF. The cells were lysed using a micro-fluidizer (P=10000-15000). Cell debris was removed by centrifugation for 10 min at 18,000 rpm and then for 2 hours at 40,000rpm.

Ammonium sulfate precipitation

DnaK was precipitated by addition of 280g/l of (NH₄)₂SO₄. The sample was stir at 4°C for 30 minutes and then, centrifugated at 10,000 rpm during 10 min. The pellet was resuspended in 40 ml bufferA and dialyzed against 3 l bufferA over night.

Anion exchange chromatography (DEAE-Cellulose)

The dialyzed protein solution is cleared from particles by centrifugation at 18,000 rpm for 10 minutes and subsequent filtrated through a 0.45 µm filter. It was loaded onto a 250 ml DEAE-cellulose column that was equilibrated to bufferA. The column was washed with 300 ml bufferA and eluted with a 700 ml gradient of 0 to 50 % bufferB. The column was washed with 300 ml 100% bufferB. 10 ml fraction were collected 280 ml after the start of the gradient and until the end of the gradient. The DnaK containing fractions were pooled and directly applied to affinity chromatography on ATP-agarose.

Affinity chromatography (ATP-agarose)

0.27 g of ATP-agarose were swollen for at least 2 h in bufferA and washed with 10 ml bufferB and re-equilibrated with 10 ml bufferA (batch procedure). The pooled fractions from DEAE-chromatography were added to the equilibrated ATP-agarose and incubated at 4 °C in a 50 ml falcon tube shaking end-over-end for 30 min. The agarose was packed into a disposable column and washed with 10 ml bufferA and 10 ml bufferB. DnaK was eluted with ATP-buffer in the following way. The washed ATP agarose was resuspended

in the column in an equal volume of ATP-buffer and incubated for 45 min at 4 °C. After this time the agarose was repacked and the eluate collected in one fraction. An additional 10 ml of ATP-buffer were added onto the column and the eluate collected in fractions of 1 ml size.

Anion exchange chromatography (Resource Q)

The DnaK-containing fractions of the sephacryl column were loaded onto a resource Q strong anion-exchanger. The column was washed with 40 ml buffer A and DnaK eluted with a 100 ml gradient of 0 to 50 % buffer B. Fractions of 1.3 ml size are collected. The DnaK containing fractions were pool, aliquots were frozen in liquid nitrogen and stored at -80 °C.

Purification of the DnaK/ σ^{32} , DnaK/DnaJ/ σ^{32} and DnaJ/ σ^{32} complexes

Buffers

Buffer A	20 mM Tris-HCl pH 7.9 200 mM NaCl 20 mM imidazole
Buffer B	20 mM Tris-HCl pH 7.9 1M NaCl 20 mM imidazole
ATP-buffer	40mM Tris-HCl pH 7.9 100 mM KCl 5mM MgCl ₂ 10 mM ATP 20 mM imidazole
Incubation buffer	20 mM Hepes-KOH pH 7.6 50 mM KCl 5 mM MgCl ₂ 20 mM imidazole 10% glycerol
Buffer C	20 mM Hepes-KOH pH 7.6 50 mM KCl 5 mM MgCl ₂ 10% glycerol

Overproduction of σ^{32} and cell lysis

6L of 2xYT complemented with 100ug/L ampicillin were inoculated with an overnight culture of the Δ ftsH strain carrying the rpoH-containing vector. The culture was grown at 30°C to an OD₆₀₀ of 0.8. For induction, L-arabinose was added to a final concentration of 0.2% and the culture was incubated for 3 hours at 30°C. Cells were harvested by centrifugation for 10 min at 5000g, and the pellets were resuspended in 300 ml of lysis buffer. All steps were carried out at 4°C or on ice. Cells were lysed using French press at a pressure of 1,000 psi. Cell debris were separated from lysates by centrifugation for 30 min at 20,000 g (twice).

NiNTA agarose

The supernatant containing σ^{32} was mixed with Ni-NTA agarose (5 ml bed volume) equilibrated with buffer A and mixed end-over-end at 4°C during one hour. The Ni²⁺-agarose was transferred to a 50 ml falcon tube and washed 4 times with 45 ml buffer B, 4 times with 45 ml buffer A and 2 times with 45 ml ATP-buffer. The ATP wash was intended to remove wt DnaK. The Ni²⁺-agarose was incubated 30 min with ATP-buffer and then washed again with incubation buffer to remove the ATP. DnaK (1-607) was added to the Ni²⁺-column (DnaK does not contain His-tag) and incubated 1 hour at 4°C. The column was washed with incubation buffer. Then, the Ppx protease was added and incubated with the Ni²⁺-agarose for 4 hours. The eluted protein was loaded onto a Superdex 200 gel filtration column, equilibrated with buffer C. The fractions containing the complex were pooled and concentrated. The glycerol was removed during the concentration step. For the complex DnaK/DnaJ/ σ^{32} the same procedure was followed, except for one difference: DnaJ was added first, and only after 20 minutes DnaK. For the DnaJ/ σ^{32} complex, instead of adding DnaK, DnaJ was added, with an incubation time of 20 min.

Overproduction of DnaK (1-607)

4L of 2xYT complemented with 100 μ g/L ampicillin and 50 μ g/L kanamycin were inoculated with an overnight culture of the BB1994 strain carrying the dnaK (1-607) containing vector. The culture was grown at 30°C to an OD₆₀₀ of 0.3-0.5. For induction, IPTG was added to a final concentration of 1 mM and the culture was incubated for at

least 5 hours at 30°C. Cells were harvested by centrifugation for 10 min at 5000g, and the pellets were resuspended in 80 ml of lysis buffer (same as lysis buffer purification of DnaK). All steps were carried out at 4°C or on ice. Cells were lysed using a French press at a pressure of 1,000 psi. Cell debris were separated from lysates by centrifugation for 30 min at 20,000 g (twice). The DnaK protein was precipitated with 0.28 mg/ml (NH₄)₂SO₄ on ice and centrifugated for 15 min at 10,000 rpm. The protein pellet was resuspended in 40 ml incubation buffer and dialyzed against 3 L incubation buffer over night.

Overproduction of DnaJ

4L of 2xYT complemented with 100µg/L ampicillin and 50 µg/L kanamycin were inoculated with an overnight culture of the BB2583 strain with contains the pUHE-dnaJ plasmid. The culture was grown at 30°C to an OD₆₀₀ of 0.4. For induction, IPTG was added to a final concentration of 1 mM and the culture was incubated for 4-5 hours at 30°C. Cells were harvested by centrifugation for 10 min at 5000g, and the pellets were resuspended in 100 ml of lysis buffer. All steps were carried out at 4°C or on ice. Cells were lysed using a French press at a pressure of 1,000 psi. Cell debris were separated from lysates by centrifugation for 30 min at 20,000 g (twice). The DnaK protein was precipitated with 0.398 mg/ml (NH₄)₂SO₄ on ice and centrifugated for 15 min at 10,000 rpm. The protein pellet was resuspended in 100 ml buffer C and dialyzed against buffer C for 3 hours. The protein was loaded on a SP-sepharose column and eluted with a gradient 0-666 mM KCl. The DnaJ-containing fractions were pooled and dialyzed against incubation buffer.

Labeling with ³H-N-succinimidyl-propionate (NSP)

Buffers

NSP buffer	50 mM K ₂ HPO ₄ /KH ₂ PO ₄ , pH 7.6
	200 mM KCl
	10 % glycerin

Proteins were dialysed overnight in NSP buffer. 1500 pmol of the dialysed proteins were added to 1500 pmol of ³H-NSP previously dried under nitrogen. The mixture was

incubated for 2 hours at room temperature and dialysed again overnight in NSP buffer to remove unbound $^3\text{H-NSP}$.

Interaction of σ^{32} and DnaK

Analytical gel filtration

$^3\text{H-}\sigma^{32}/\sigma^{32}$ (5 μM) was incubated with different concentrations of DnaK (5-30 μM) in a total volume of 20 μl of HKNM buffer at 30°C for 2 hours. The sample was spun at 13000 rpm for 10 min and 90 μl of ice cold HKNM buffer was added. The sample was loaded onto a Superdex 75 HL 10/30 previously equilibrated with KII buffer to separate DnaK-bound and free $^3\text{H-SH3}/\text{SH3}$. Gel filtration experiments were performed at 4°C. Fractions of 0.5 ml were collected and 4 ml of Optima Gold scintillation cocktail was added to each fraction. The amount of radioactivity was determined using a scintillation counter. The same procedure was repeated using HKNM buffer plus 0.4 M Na_2SO_4 .

For the interaction of $^3\text{H-}\sigma^{32}/\sigma^{32}$ with DnaK and DnaJ, $^3\text{H-}\sigma^{32}/\sigma^{32}$ (5 μM) was incubated with DnaK (10 μM), DnaJ (1 μM) and ATP (1mM) in a final volume of 20 μl of HII buffer at 30°C for 10 min. Then the sample was treated as described before.

The dissociation constant was calculated from the Scatchard plot analysis of the data using a single binding site model (one DnaK molecule binds to one σ^{32} molecule).

ATPase single turn-over experiments

Isolation of the DnaK-ATP complex

A nick-column (sephadex G50) was equilibrated with KII buffer. 1 ml of BSA (1mg/ml) was loaded onto the column and eluted with 3 column volumes of KII buffer. DnaK (30 μM) was incubated with ATP (800 μM) and [$\alpha^{32}\text{P}$] ATP (12 μCi) in a final volume of 50 μl of KII buffer on ice for 2 min. The nick-column was connected to a fraction collector. The reaction mixture was loaded onto the column and 1ml KII buffer was added to the column. Two drops fractions were collected and the peak was detected with a Geiger counter. The first peak appeared between fraction 8 and 12. The first peak and the following 3 fractions were pooled and divided in 6.5 μl fractions (ca. 30 aliquots). The fractions were frozen in liquid nitrogen and stored at -80°C.

Preparation of the TLC-plates

Each TLC plate was divided in 3. In each plate, vertical lines were drawn with pencil every 1 cm. At 1 cm from the bottom one horizontal line was drawn. On each start position 2 μ l of ADP/ATP (5 μ M each) solution was spotted.

Single turn-over assay

DnaK-ATP complex was thawed at 30°C. 0.5 μ l was diluted on 3.5 μ l of KII buffer and 2 μ l of it were spotted on position one of the TLC plates. 6 μ l of the DnaK-ATP complex were added to 44 μ l of a premix solution containing the co-factors to be tested. Aliquots of 2 μ l were spotted onto the TLC-plate. For fast kinetics (DnaK + DnaJ + substrate), the time points were: 6", 12", 18", 30", 1', 2', 5' and 10'. For slow kinetics (DnaK + DnaJ or DnaK + substrate), the time points were: 30", 1', 2', 3', 5', 10', 15' and 20'. For very slow kinetics (DnaK basal rate), the time points were 5', 10', 15', 25' 40' 60', 90' and 120'. Plates were developed in 3.6% Hac/400 mM LiCl, dried and exposed to bleached FI-screens overnight. The screens were analysed with Fuji FLA 2000 fluorimager.

Attachment of Crosslinker to Proteins

Benzophenone-4-iodoacetamide (BPIA, 10 Å spacer) was used for the crosslinking of DnaK and substrate. BPIA is a heterobifunctional cross-linker, which reacts with thiol groups of cysteine side chains, and reacts unspecifically with close binding partners after UV activation. DnaK with specific cysteine mutation (Q424C) was labeled with the cross-linker. Potential intermolecular disulphide bridges were reduced with 5 mM TCEP before the protein solution was dialyzed against KII buffer. When handling photoreactive crosslinkers, direct light was avoided. However, it was not necessary to work in a dark room since activation only occurs at $\lambda < 400$ nm (UV light).

Labeling with BPIA

Labeling was performed in the presence of 1 mM TCEP. BPIA stock solution was added to a final concentration of 1 mM and the protein concentration was 50-100 μ M. Since BPIA can side react with primary amines, over-labeling may occur. The reaction was

followed by ESI-MS and stopped by addition of β ME once it is complete. After dialysis against K11 buffer, the protein concentration was determined, aliquots frozen in liquid nitrogen and stored at -80°C .

Crosslinking Reaction

The reaction was performed in 20 μl K11 buffer containing 6 μM DnaK-Cys with the crosslinker attached, 6 μM ATP, and 6 μM protein substrate (RepE). Crosslinking mixtures were incubated for 60 min at 30°C and subsequently irradiated on ice with UV light (365 nm, 100W) at a distance of 3 cm for 30 min. Crosslinking products were analyzed by SDS-PAGE with subsequent Coomassie blue staining and mass spectrometry.

In-gel Digest

The gel was washed with water before precisely cutting out the band of interest. The band was chopped into smaller cubes (1x1x1 mm) and put into a reaction tube. The gel pieces were washed with 100 μl of 100 mM NH_4HCO_3 plus 100 μl ACN until the blue color had disappeared. The liquid was removed, 100 μl ACN were added and left for 5-10 min until the gel pieces have shrunk. The supernatant was removed and the gel pieces were dried in vacuum centrifuge. Afterwards, the gel pieces were swollen on ice for 45 min with 50 mM NH_4HCO_3 containing 12.5 ng/ μl trypsin (Promega, sequencing grade). After excess trypsin was removed 5 μl of 50 mM NH_4HCO_3 were added to prevent the gel pieces from drying. The digest was performed at 37°C over night and stopped by acidification with 2 μl of 10% TFA. After 30 min, the supernatant containing the peptides was transferred into a new reaction tube. For a second elution step, 10 μl of 0.1% TFA were added to the gel pieces and left for another 30-60 min. Both supernatants were pooled.

Immobilization of DnaK

On Poros Al

DnaK was immobilized into Poros Al material. Aldehyde groups on the surface of the support react selectively with primary amines of the protein to form a Schiff's base, which are then converted into a stable secondary amine linkage by reduction with

NaCNBH₃. The immobilization was performed according to the protocol provided by the manufacturer.

20 mg NaCNBH₃ was dissolved in 2 ml of 25 mM HEPES/KOH, pH 7.0 100 mM KCl containing approx. 10 mg/ml DnaK. Then, 0.1 g of POROS 20 AL powder was added to form a homogeneous suspension. After slowly adding 2 ml of 2 M Na₂SO₄, the reaction continued at 4°C ON. Throughout this time, the tube was turned end-over-end to ensure gentle mixing.

To quench the reaction, 5 µl ethanolamine was added and incubated for 2 more hours. The support material was washed with K11 buffer, K11 supplemented with ATP and again with K11 to remove free DnaK. Immobilized DnaK was stored at 4°C in K11 buffer containing 0.05% NaN₃.

Trap column

A slurry of POROS 50 R1 or 50 R2 bulk material (Applied Biosystems) were packed into 2 x 20 mm column.

Analytical column

ZORBAX 300SB-C₈ (300 Å pore size and 3.5 µm particles) bulk material was obtained from Agilent. The slurry was packed into 0.75 mm ID Peek tubing (Upchurch) via a pressure bomb because the backpressure was too high for packing with a syringe. After packing and washing with 5% ACN, the tubing was cut to get the appropriate column length (usually 5-8 cm) and both ends were secured with 2 µm stainless steel screens and male nuts with standard external threads.

In-line Peptic Digestion/Rapid-Desalting HPLC Setup

The setup consisted of two HPLC pumps (Agilent 1100 Series), a Rheodyne injection valve (Model 7725i) with a 200 µl stainless steel sample loop, and a 2-position/10-port valve with microelectric actuator (Valco C2-1000EP6). A schematic drawing of the setup is shown in *Figure 3.3*. Pump A delivered the solvent for desalting (300 µl/min, 0.05% TFA) and pump B for elution (20 µl/min, 70% ACN, 0.05% TFA). Quenched samples were loaded via the injection valve and pushed through the pepsin column (2 x 20 mm)

by pump A. The resulting peptic fragments were immediately trapped on a self-packed reversed-phase column (POROS 50 R1) for desalting and concentration. After 2 min the 10-port valve was switched to elute the peptides with organic solvent (pump B) directly into the electrospray ion source of the quadrupole time-of-flight mass spectrometer. At the same time the pepsin column was back flushed by pump A. The digestion, desalting and elution required less than 3 min. The whole setup was immersed in an ice bath to minimize back-exchange. For kinetic measurements of the full-length protein the pepsin column was omitted.

The timing and sequence of operation of the valves were controlled by the Agilent 1100 Series Capillary Pump. Each run was started by sample injection. The switch of the Rheodyne 7725i valve provided an electrical start signal for the Agilent Pump, which in turn provided the actuator of the 2-position/10-port valve an electrical signal to switch from 'load' to 'elute' position after the programmed time.

On-line Quenched-Flow Amide Hydrogen Exchange Setup

The setup employed to measure amide hydrogen exchange in a millisecond time scale consisted of five HPLC pumps (one Agilent 1100 Series Capillary pump (A), one Agilent 1100 Series Binary pump (B), one Rheos 2000 Micro pump (1), and two Shimadzu LC-10ADVP pumps (2 & 3)), a Rheodyne injection valve (Model 8125) with a 5 μ l stainless steel sample loop, and two Valco 2-position/10-port valves with microelectric actuators (Model C2-1000EP6). A schematic drawing of the setup is shown in Figure M.M.1 Protein samples (100-200 pmol in <5 μ l) were injected and pushed by pump 1 with a flow rate of 6 μ l/min towards a mixing tee, which was also connected with pump 2 delivering D₂O-buffer (25 mM HEPES, pD 7.6, 50 mM KCl, and 5 mM MgCl₂) with a flow rate of 150 μ l/min. Hence, the injected samples were diluted 1:25 in D₂O-buffer and pushed through the delay line where amide hydrogen exchange occurred. The exchange time was adjusted by the volume of the delay line (e.g. 2.6 μ l \equiv 1 s). The exchange reaction was quenched in a second mixing tee by 1:1 dilution of the sample with quench buffer (0.5 M KH₂PO₄/H₃PO₄, pH 2.2) delivered by pump 3 with a flow rate of 150 μ l/min. The quenched sample was then pushed through the pepsin column and immediately trapped on a reversed-phase column (0.8 x 3 mm, POROS 10 R1).

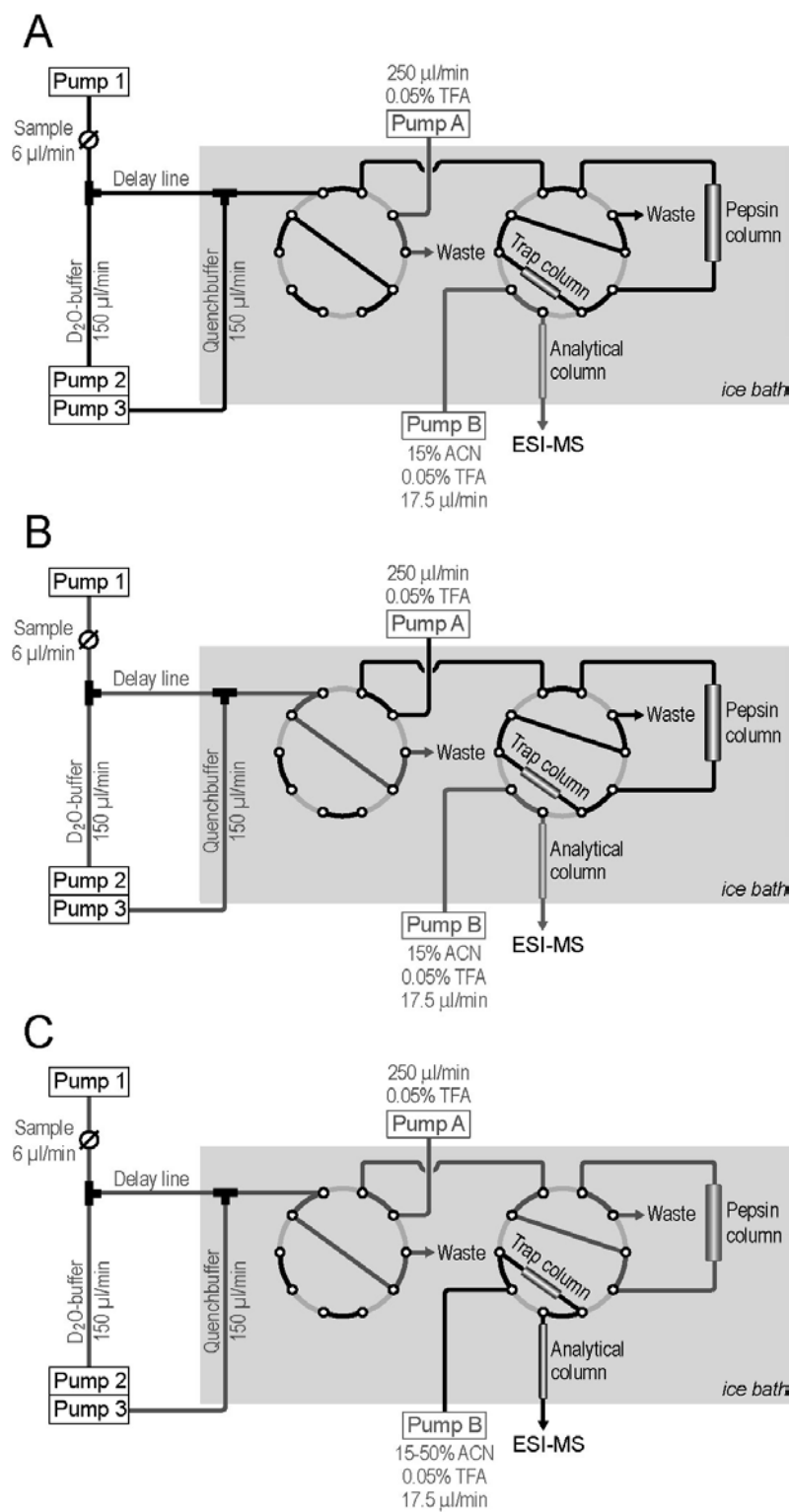


Figure MM.1. Schematic representation of the HPLC-MS quenched setup (A) HX position, (B) desalting position and (C) MS analysis position.

For the desalting of trapped peptic peptides, the left 2-position/10-port valve was switched, and 0.05% TFA was delivered by pump A (250 μ l/min). After 1 min, the right 2-position/10-port valve was switched to elute the desalted peptic peptides from the trap column over a 0.75 mm ID x 6 cm analytical reversed-phase column packed with ZORBAX 300SB-C8 (3.5 μ m particles) directly into the electrospray source. The solvent for elution was delivered by pump B with a flow rate of 17.5 μ l/min using the following short gradient: buffer A (0.05% TFA) to buffer B (90% ACN, 0.05% TFA), having the profile: %B: 15 \rightarrow 55 (0 \rightarrow 10 min), %B: 55 \rightarrow 100 (10 \rightarrow 11 min), %B: 100 \rightarrow 15 (11 \rightarrow 12 min). The last eluted peptide was detected 12 minutes after sample injection. All lines delivering quench buffer or quenched sample were immersed in an ice bath to minimize back-exchange. For kinetic measurements of the full-length proteins the pepsin column was omitted.

Off-line Amide Hydrogen Exchange Experiments

Amide hydrogen exchange was initiated by a 20-fold dilution of 100 pmol protein into D₂O containing 25 mM HEPES, pD 7.6, 50 mM KCl, and 5 mM MgCl₂ at room temperature. After different elapsed times (from 1 to 30 sec), the exchange reaction was quenched by decreasing the temperature to 0°C and the pH to 2.2 with 500 mM K_xH_yPO₄. Quenched samples were loaded via the injection valve and pushed through the pepsin column by pump A. Hereafter, the experimental setup was as described above.

Data Analysis of Amide Hydrogen Exchange Experiments

Peptic peptides were identified separately either by static nanoESI-MS/MS (see 3.2.6) or by on-line nanoLC/MS/MS (see 3.2.7) on the basis of their fragment ion spectra. After internal recalibration, the mass error was below 10 ppm and hence more peptides could be identified on the basis of their exact mass.

The deuterium content of the peptides was calculated by using the average mass difference between the isotopic envelopes of the deuterated and the undeuterated peptides. The average masses were determined with the MagTran software (Zhang & Marshall, 1998). Overlapping peptides sequences were used to improve the resolution of amide hydrogen exchange measurements (Zhang & Smith, 1993; Yang & Smith, 1997).

Only peptides that differ in length at their C-termini have been used. The deuterium occupancy for the non-overlapping C-terminal sequence extension was easily calculated by subtraction of the deuterium levels of the peptides. In order to avoid erroneous interpretations, peptides that differ in length at their N-termini have been neglected. The main problem is that deuterons incorporated at N-terminal amide groups are readily lost during desalting and it is thus not possible to determine whether this amide group was deuterated or protiated before being quenched (at acidic pH the positive charge on the N-terminus increases the exchange rate at the adjacent amide hydrogen by a factor of ~10). Adjustments were made for deuterium losses due to back-exchange during analysis based on appropriate controls, a 0% deuterium control (i.e. protein that has never been exposed to D₂O) and a 100% deuterium control (i.e. protein in which all exchangeable hydrogens have been replaced with deuterium) according to following formula (Zhang & Smith, 1993)

$$D = \frac{\langle m \rangle - \langle m_{0\%} \rangle}{\langle m_{100\%} \rangle - \langle m_{0\%} \rangle} \cdot N$$

where D is the number of deuterons present in a particular peptic peptide after incubation of the protein in D₂O, N is the total number of amide hydrogens in that peptide, and $\langle m \rangle$ is the experimentally observed average mass. $\langle m_{0\%} \rangle$ and $\langle m_{100\%} \rangle$ are the average molecular masses of the same peptide obtained by analysis of the non-deuterated and the fully deuterated controls, respectively. Fully deuterated controls were obtained by denaturing the protein in 4 M Gdn/HCl followed by lyophilization. D₂O was added to the initial volume and left at 60°C to dissolve the precipitated protein and buffer salts before the next lyophilization. Lyophilization and dissolving in D₂O was repeated 5 times. All exchangeable hydrogens in the unfolded protein and the buffer salts were thereby replaced by deuterium. Then, the protein was dissolved in a appropriate volume of D₂O to obtain a concentration of 2 M Gdn/DCl and refolded by rapid 1:100 dilution into D₂O-buffer at 0°C. After 15 h incubation at 4°C, the refolded mixture was centrifuged at 13,000 rpm to remove any aggregated protein.

Biacore

Biacore is a quantitative method that allows the study of macromolecular interactions in real time with low amount of protein. Using Biacore it is possible to obtain the kinetic data for an interaction between macromolecules. Biacore technology relies on the phenomenon of surface plasmon resonance (SPR). SPR is phenomenon that occurs in thin conducting films at an interface between media of different refractive index: the glass of a sensor surface (high refractive index) and a buffer (low refractive index). As molecules are immobilized on a sensor surface, the refractive index at the interface between the surface and a solution flowing over the surface changes, altering the angle at which reduced-intensity polarized light is reflected from a supporting glass plane. The change in angle, caused by binding or dissociation of molecules from the sensor surface, is proportional to the mass of bound material and is recorded in a sensorgram.

Measurements on Biacore are based on interaction of molecules in solution with a molecule attached to a sensor chip. The molecule immobilized on the sensor chip is the ligand and the molecule free in solution is the analyte. The response is measured in resonance units (RU). The response is directly proportional to the concentration of biomolecules on the surface.

The sensor chip

The sensor chip is a glass slide coated with a thin layer of gold. The standard chip is the CM5 that has a matrix of carboxymethylated dextran covalently attached to the gold surface.

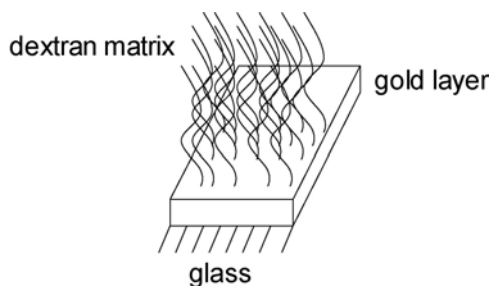


Figure MM.2. Schematic representation of a Biacore sensor chip.

The dextran matrix is activated with carboxymethyl groups with a mixture of N-hydroxysuccinimide (NHS) and N-ethyl-N'-(dimethyl-aminopropyl)-carbodiimidine (EDC). These active groups are able to reacting covalently with the ligand molecule. Each chip has four different flow cells. Generally two cells are used as blank surface and in the other two the ligand is attached.

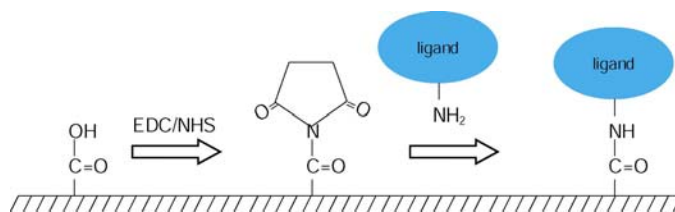


Figure MM.3. Schematic representation of the immobilization procedure onto CM5 sensor chip.

Immobilization of the σ^{32}

σ^{32} wt and mutants were immobilized on CM5 sensor chips via amine coupling. Amine coupling introduces N-hydroxysuccinimide esters into the surface matrix by modification of the carboxymethyl groups with a mixture of N-hydroxysuccinimide (NHS) and N-ethyl-N'-(dimethyl-aminopropyl)-carbodiimidine (EDC). These esters then react spontaneously with amines on the ligand to form covalent bonds. The CM5 sensor chip was activated with a 7 minutes pulse of 0.05 M NHS/0.2 M EDC at a flow rate of 5 μ l/min. σ^{32} wt and mutants were diluted in acetate buffer pH = 5 to a final concentration of 100 nM and injected at a flow rate of 5 μ l/min to achieve a total of 100-150 RU. The excess of reactive groups on the chip was deactivated with a 7 minutes pulse of 1 M ethanolamine hydrochloride pH 8.5 at a flow rate of 5 μ l/min.

Kinetic measurements

Different amounts of DnaJ (30-500 nM) were inject at a flow rate of 30 μ l/min during 2 minutes. The dissociation time was 7 minutes. After each injection the chip was regenerated with Tris buffer pH 8.5. In all experiments, DnaJ was injected through an

empty flow cell. For each DnaJ concentration the empty flow cell was subtracted from the flow cell where σ^{32} was immobilized to eliminate unspecific interactions.

Determination of k_{on} , k_{off} and K_D

Figure M.M.4 shows a typical sensogram obtained after injection of analyte. The sensogram can be divided into association phase and dissociation phase.

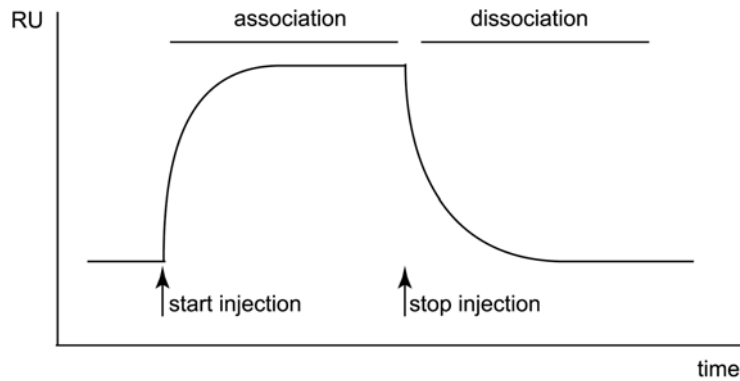


Figure MM.4. Schematic representation of a typical sensogram.

From the association phase, the association rate constant can be determined by fitting the exponential curve with the following double exponential equation. From the dissociation, the dissociation rate constant can be determined by fitting the exponential curve with the following double exponential equation. Then K_D can be calculated with,

$$K_D = k_{off} / k_{on}$$

K_D can also be determined from the equilibrium phase using the Michaelis and Menten equation,

$$v = V_{max} [S] / (K_D + [S])$$

Crystal Screenings

The protein solutions containing σ^{32} , DnaK/ σ^{32} , DnaK/DnaJ/ σ^{32} or DnaJ/ σ^{32} were concentrated to 10 mg/ml by centrifugal filtration. The buffer was exchange against

buffer C without glycerol. Initial conditions for crystal formation were screened by the hanging-drop method using a crystallization tool containing 24 well plates (Nextal) with drops containing 1 μ l of protein and 1 μ l of well solution. The screenings were performed at 4°C and 16°C. 96 different crystallization conditions were analyzed (Nextal Classics buffers).



Figure MM.5. Hanging-drop method using a crystallization tool containing 24 well plates. For each plate 6 different proteins samples can be analyzed.

Limited proteolysis with trypsin of σ^{32} and σ^{32} -DnaK complex

Buffer

Trypsin buffer	20 mM TRIS pH = 8
	200 mM NaCl
	5% (v/v) glycerol
	1 mM DTT
	10 mM MgCl ₂

50 pmol of σ^{32} and σ^{32} -DnaK complex were digested in a 10 μ l volume with different concentration of trypsin (1.5-0.03 pmol) for 30 minutes at 25°C. Reaction were terminated by addition of Laemmli loading buffer and boiling. Those samples analysed later by mass spectrometry were diluted in phosphate buffer (0.4 M, pH = 2.4). Reaction product were analysed on 16% SDS-gels followed by Coomassie staining. The molecular mass of the proteolyzed fragments was analysed by electrospray mass spectrometry as described above.

References

Alfano C, McMacken R. (1989). Heat shock protein-mediated disassembly of nucleoprotein structures is required for the initiation of bacteriophage lambda DNA replication. *J Biol Chem* 264: 10709-18.

Altting-Mees MA, Short JM. (1989). pBluescript II: gene mapping vectors. *Nucleic Acids Res* 17: 9494.

Anfinsen CB. (1973). Principles that govern the folding of protein chains. *Science* 181: 223-30.

Bai Y, Milne JS, Mayne L, Englander SW. (1993). Primary structure effects on peptide group hydrogen exchange. *Proteins* 17: 75-86.

Banecki B, Liberek K, Wall D, Wawrzynow A, Georgopoulos C, et al. (1996). Structure-function analysis of the zinc finger region of the DnaJ molecular chaperone. *J Biol Chem* 271: 14840-8.

Barouch W, Prasad K, Greene L, Eisenberg E. (1997). Auxilin-induced interaction of the molecular chaperone Hsc70 with clathrin baskets. *Biochemistry* 36: 4303-8.

Berjanskii MV, Riley MI, Xie A, Semenchko V, Folk WR, Van Doren SR. (2000). NMR structure of the N-terminal J domain of murine polyomavirus T antigens. Implications for DnaJ-like domains and for mutations of T antigens. *J Biol Chem* 275: 36094-103.

Blaszczak A, Georgopoulos C, Liberek K. (1999). On the mechanism of FtsH-dependent degradation of the sigma 32 transcriptional regulator of Escherichia coli and the role of the DnaK chaperone machine. *Mol Microbiol* 31: 157-66.

Buczynski G, Slepnev SV, Sehorn MG, Witt SN. (2001). Characterization of a lidless form of the molecular chaperone DnaK: deletion of the lid increases peptide on- and off-rate constants. *J Biol Chem* 276: 27231-6.

Bukau B. (1993). Regulation of the Escherichia coli heat-shock response. *Mol Microbiol* 9: 671-80.

Bukau B and Horwich AL. (1998). The Hsp70 and Hsp60 chaperone machines. *Cell* 92: 351-66.

Bukau B and Walker GC. (1990). Mutations altering heat shock specific subunit of RNA polymerase suppress major cellular defects of E. coli mutants lacking the DnaK chaperone. *Embo J* 9: 4027-36.

Calendar R, Erickson JW, Halling C, Nolte A. (1988). Deletion and insertion mutations in the rpoH gene of Escherichia coli that produce functional sigma 32. *J Bacteriol* 170: 3479-84.

Callaci S, Heyduk E, Heyduk T. (1999). Core RNA polymerase from E. coli induces a major change in the domain arrangement of the sigma 70 subunit. *Mol Cell* 3: 229-38.

Campbell EA, Korzheva N, Mustaev A, Murakami K, Nair S, et al. (2001). Structural mechanism for rifampicin inhibition of bacterial rna polymerase. *Cell* 104: 901-12.

Campbell EA, Masuda S, Sun JL, Muzzin O, Olson CA, et al. (2002). Crystal structure of the Bacillus stearothermophilus anti-sigma factor SpoIIAB with the sporulation sigma factor sigmaF. *Cell* 108: 795-807.

Campbell EA, Muzzin O, Chlenov M, Sun JL, Olson CA, et al. (2002). Structure of the bacterial RNA polymerase promoter specificity sigma subunit. *Mol Cell* 9: 527-39.

Campbell EA, Tupy JL, Gruber TM, Wang S, Sharp MM, et al. (2003). Crystal structure of Escherichia coli sigmaE with the cytoplasmic domain of its anti-sigma RseA. *Mol Cell* 11: 1067-78.

Casadaban MJ. (1976). Transposition and fusion of the lac genes to selected promoters in Escherichia coli using bacteriophage lambda and Mu. *J Mol Biol* 104: 541-55.

Connolly JP, Augustine JG, Francklyn C. (1999). Mutational analysis of the engrailed homeodomain recognition helix by phage display. *Nucleic Acids Res* 27: 1182-9.

Ellis RJ. (2001). Macromolecular crowding: obvious but underappreciated. *Trends Biochem Sci* 26: 597-604.

Engen JR and Smith DL. (2001). Investigating protein structure and dynamics by hydrogen exchange MS. *Anal Chem* 73: 256A-65A.

Feifel B, Schonfeld HJ, Christen P. (1998). D-peptide ligands for the co-chaperone DnaJ. *J Biol Chem* 273: 11999-2002.

Flaherty KM, DeLuca-Flaherty C, McKay DB. (1990). Three-dimensional structure of the ATPase fragment of a 70K heat-shock cognate protein. *Nature* 346: 623-8.

Flaherty KM, McKay DB, Kabsch W, Holmes KC. (1991). Similarity of the three-dimensional structures of actin and the ATPase fragment of a 70-kDa heat shock cognate protein. *Proc Natl Acad Sci U S A* 88: 5041-5.

Gamer J, Bujard H, Bukau B. (1992). Physical interaction between heat shock proteins DnaK, DnaJ, and GrpE and the bacterial heat shock transcription factor sigma 32. *Cell* 69: 833-42.

Gassler CS, Buchberger A, Laufen T, Mayer MP, Schroder H, et al. (1998). Mutations in the DnaK chaperone affecting interaction with the DnaJ cochaperone. *Proc Natl Acad Sci U S A* 95: 15229-34.

Giraldo R, Fernandez-Tornero C, Evans PR, Diaz-Orejas R, Romero A. (2003). A conformational switch between transcriptional repression and replication initiation in the RepA dimerization domain. *Nat Struct Biol* 10: 565-71.

Gisler SM, Pierpaoli EV, Christen P. (1998). Catapult mechanism renders the chaperone action of Hsp70 unidirectional. *J Mol Biol* 279: 833-40.

Gross CA, Chan C, Dombroski A, Gruber T, Sharp M, et al. (1998). The functional and regulatory roles of sigma factors in transcription. *Cold Spring Harb Symp Quant Biol* 63: 141-55.

Gross CA, Chan CL, Lonetto MA. (1996). A structure/function analysis of Escherichia coli RNA polymerase. *Philos Trans R Soc Lond B Biol Sci* 351: 475-82.

Gruber TM, Bryant DA. (1997). Molecular systematic studies of eubacteria, using sigma70-type sigma factors of group 1 and group 2. *J Bacteriol* 179: 1734-47.

Guisbert E, Herman C, Lu CZ, Gross CA. (2004). A chaperone network controls the heat shock response in *E. coli*. *Genes Dev* 18: 2812-21.

Haouz A, Glandieres JM, Zentz C, Pin S, Ramstein J, et al. (1998). Solvent effects on horse apomyoglobin dynamics. *Biochemistry* 37: 3013-9.

Hendrick JP, Langer T, Davis TA, Hartl FU, Wiedmann M. (1993). Control of folding and membrane translocation by binding of the chaperone DnaJ to nascent polypeptides. *Proc Natl Acad Sci U S A* 90: 10216-20.

Herman C, Prakash S, Lu CZ, Matouschek A, Gross CA. (2003). Lack of a robust unfoldase activity confers a unique level of substrate specificity to the universal AAA protease FtsH. *Mol Cell* 11: 659-69.

Herman C, Thevenet D, D'Ari R, Bouloc P. (1995). Degradation of sigma 32, the heat shock regulator in *Escherichia coli*, is governed by HflB. *Proc Natl Acad Sci U S A* 92: 3516-20.

Horikoshi M, Yura T, Tsuchimoto S, Fukumori Y, Kanemori M. (2004). Conserved region 2.1 of *Escherichia coli* heat shock transcription factor sigma32 is required for modulating both metabolic stability and transcriptional activity. *J Bacteriol* 186: 7474-80.

Ishiai M, Wada C, Kawasaki Y, Yura T. (1992). Mini-F plasmid mutants able to replicate in *Escherichia coli* deficient in the DnaJ heat shock protein. *J Bacteriol* 174: 5597-603.

Ishiai M, Wada C, Kawasaki Y, Yura T. (1994). Replication initiator protein RepE of mini-F plasmid: functional differentiation between monomers (initiator) and dimers (autogenous repressor). *Proc Natl Acad Sci U S A* 91: 3839-43.

Johnson RS and Walsh KA. (1994). Mass spectrometric measurement of protein amide hydrogen exchange rates of apo- and holo-myoglobin. *Protein Sci* 3: 2411-8.

Kanemori M, Nishihara K, Yanagi H, Yura T. (1997). Synergistic roles of HslVU and other ATP-dependent proteases in controlling in vivo turnover of sigma32 and abnormal proteins in *Escherichia coli*. *J Bacteriol* 179: 7219-25.

Kanemori M, Yanagi H, Yura T. (1999). Marked instability of the sigma(32) heat shock transcription factor at high temperature. Implications for heat shock regulation. *J Biol Chem* 274: 22002-7.

Karzai AW and McMacken R. (1996). A bipartite signaling mechanism involved in DnaJ-mediated activation of the *Escherichia coli* DnaK protein. *J Biol Chem* 271: 11236-46.

Kawasaki Y, Wada C, Yura T. (1990). Roles of *Escherichia coli* heat shock proteins DnaK, DnaJ and GrpE in mini-F plasmid replication. *Mol Gen Genet* 220: 277-82.

Kawasaki Y, Wada C, Yura T. (1991). Mini-F plasmid mutants able to replicate in the absence of sigma 32: mutations in the repE coding region producing hyperactive initiator protein. *J Bacteriol* 173: 1064-72.

Kawasaki Y, Wada C, Yura T. (1992). Binding of RepE initiator protein to mini-F DNA origin (ori2). Enhancing effects of repE mutations and DnaJ heat shock protein. *J Biol Chem* 267: 11520-4.

Kelley WL, Georgopoulos C. (1997). The T/t common exon of simian virus 40, JC, and BK polyomavirus T antigens can functionally replace the J-domain of the Escherichia coli DnaJ molecular chaperone. *Proc Natl Acad Sci U S A* 94: 3679-84.

Kim SY, Sharma S, Hoskins JR, Wickner S. (2002). Interaction of the DnaK and DnaJ chaperone system with a native substrate, P1 RepA. *J Biol Chem* 277: 44778-83.

Komori H, Matsunaga F, Higuchi Y, Ishiai M, Wada C, Miki K. (1999). Crystal structure of a prokaryotic replication initiator protein bound to DNA at 2.6 Å resolution. *Embo J* 18: 4597-607.

Kunkel TA, Roberts JD, Zakour RA. (1987). Rapid and efficient site-specific mutagenesis without phenotypic selection. *Methods Enzymol* 154: 367-82.

Laemmli UK. (1970). Cleavage of structural proteins during the assembly of the head of bacteriophage T4. *Nature (London)*, **227**, 680-685.

Langer T, Lu C, Echols H, Flanagan J, Hayer MK, Hartl FU. (1992). Successive action of DnaK, DnaJ and GroEL along the pathway of chaperone-mediated protein folding. *Nature* 356: 683-9.

Lanzer M and Bujard H. (1988). Promoters largely determine the efficiency of repressor action. *Proc Natl Acad Sci U S A* 85: 8973-7.

Laufen T, Mayer MP, Beisel C, Klostermeier D, Mogk A, et al. (1999). Mechanism of regulation of hsp70 chaperones by DnaJ cochaperones. *Proc Natl Acad Sci U S A* 96: 5452-7.

Levchenko I, Grant RA, Wah DA, Sauer RT, Baker TA. (2003). Structure of a delivery protein for an AAA+ protease in complex with a peptide degradation tag. *Mol Cell* 12: 365-72.

Li J, Qian X, Sha B. (2003). The crystal structure of the yeast Hsp40 Ydj1 complexed with its peptide substrate. *Structure* 11: 1475-83.

Li W, Stevenson CE, Burton N, Jakimowicz P, Paget MS, et al. (2002). Identification and structure of the anti-sigma factor-binding domain of the disulphide-stress regulated sigma factor sigma(R) from *Streptomyces coelicolor*. *J Mol Biol* 323: 225-36.

Liberek K, Galitski TP, Zylicz M, Georgopoulos C. (1992). The DnaK chaperone modulates the heat shock response of *Escherichia coli* by binding to the sigma 32 transcription factor. *Proc Natl Acad Sci U S A* 89: 3516-20.

Liberek K, Marszalek J, Ang D, Georgopoulos C, Zylicz M. (1991). *Escherichia coli* DnaJ and GrpE heat shock proteins jointly stimulate ATPase activity of DnaK. *Proc Natl Acad Sci U S A* 88: 2874-8.

Linderstrom-Lang, KU. (1958). In Symposium on Protein Structure. (A. Neuberger, ed.) Methuen London 23-34.

Linke K, Wolfram T, Bussemer J, Jakob U. (2003). The roles of the two zinc binding sites in DnaJ. *J Biol Chem* 278: 44457-66.

Lodish H, Berk A, Matsudaira P, Kaiser CA, Krieger M, Scott MP, Zipursky SL, Darnell J. (2003). *Molecular Cell Biology*. Ed. Freeman (Fifth edition).

Lovett MA and Helinski DR. (1976). Method for the isolation of the replication region of a bacterial replicon: construction of a mini-F'kn plasmid. *J Bacteriol* 127: 982-7.

Lutz R and Bujard H. (1997). Independent and tight regulation of transcriptional units in *Escherichia coli* via the LacR/O, the TetR/O and AraC/I1-I2 regulatory elements. *Nucleic Acids Res* 25: 1203-10.

Maki S, Miki T, Horiuchi T. (1984). DNA sequence of an amber replication mutant indicates that a 29 kd protein is the product of the F plasmid replication gene. *Mol Gen Genet* 194: 337-9.

Malhotra A, Severinova E, Darst SA. (1996). Crystal structure of a sigma 70 subunit fragment from *E. coli* RNA polymerase. *Cell* 87: 127-36.

Matsunaga F, Kawasaki Y, Ishiai M, Nishikawa K, Yura T, Wada C. (1995). DNA-binding domain of the RepE initiator protein of mini-F plasmid: involvement of the carboxyl-terminal region. *J Bacteriol* 177: 1994-2001.

Mayer MP. (1995). A new set of useful cloning and expression vectors derived from pBlueScript. *Gene* 163: 41-6.

Mayer MP and Bukau B. (1998). Hsp70 chaperone systems: diversity of cellular functions and mechanism of action. *Biol Chem* 379: 261-8.

Mayer MP, Schroder H, Rudiger S, Paal K, Laufen T, Bukau B. (2000a). Multistep mechanism of substrate binding determines chaperone activity of Hsp70. *Nat Struct Biol* 7: 586-93.

Mayer MP, Rudiger S, Bukau B. (2000b). Molecular basis for interactions of the DnaK chaperone with substrates. *Biol Chem* 381: 877-85.

McCarty JS, Buchberger A, Reinstein J, Bukau B. (1995). The role of ATP in the functional cycle of the DnaK chaperone system. *J Mol Biol* 249: 126-37.

McCarty JS, Rudiger S, Schonfeld HJ, Schneider-Mergener J, Nakahigashi K, et al. (1996). Regulatory region C of the E. coli heat shock transcription factor, sigma32, constitutes a DnaK binding site and is conserved among eubacteria. *J Mol Biol* 256: 829-37.

Misselwitz B, Staeck O, Rapoport TA. (1998). J proteins catalytically activate Hsp70 molecules to trap a wide range of peptide sequences. *Mol Cell* 2: 593-603.

Morimoto RI, Tissieres A and Georgopoulos C. (1990). The stress response, function of the proteins, and perspectives. In Morimoto, R., Tissieres, A. and Georgopoulos, C. (eds.), *Stress proteins in biology and medicine*. Cold Spring Harbor Press, Cold Spring Harbor, New York, pp. 1-36.

Morita M, Kanemori M, Yanagi H, Yura T. (1999). Heat-induced synthesis of sigma32 in Escherichia coli: structural and functional dissection of rpoH mRNA secondary structure. *J Bacteriol* 181: 401-10.

Morita MT, Tanaka Y, Kodama TS, Kyogoku Y, Yanagi H, Yura T. (1999). Translational induction of heat shock transcription factor sigma32: evidence for a built-in RNA thermosensor. *Genes Dev* 13: 655-65.

Murakami KS, Masuda S, Campbell EA, Muzzin O, Darst SA. (2002). Structural basis of transcription initiation: an RNA polymerase holoenzyme-DNA complex. *Science* 296: 1285-90.

Murakami KS, Masuda S, Darst SA. (2002). Structural basis of transcription initiation: RNA polymerase holoenzyme at 4 Å resolution. *Science* 296: 1280-4.

Obrist M and Narberhaus F. (2005). Identification of a turnover element in region 2.1 of Escherichia coli sigma32 by a bacterial one-hybrid approach. *J Bacteriol* 187: 3807-13.

Okuno T, Yamada-Inagawa T, Karata K, Yamanaka K, Ogura T. (2004). Spectrometric analysis of degradation of a physiological substrate sigma32 by Escherichia coli AAA protease FtsH. *J Struct Biol* 146: 148-54.

- Park EY, Lee BG, Hong SB, Kim HW, Jeon H, Song HK. (2007). Structural Basis of SspB-tail Recognition by the Zinc Binding Domain of ClpX. *J Mol Biol* 367: 514-26.
- Pellecchia M, Montgomery DL, Stevens SY, Vander Kooi CW, Feng HP, et al. (2000). Structural insights into substrate binding by the molecular chaperone DnaK. *Nat Struct Biol* 7: 298-303.
- Pellecchia M, Szyperski T, Wall D, Georgopoulos C, Wuthrich K. (1996). NMR structure of the J-domain and the Gly/Phe-rich region of the Escherichia coli DnaJ chaperone. *J Mol Biol* 260: 236-50.
- Qian YQ, Patel D, Hartl FU, McColl DJ. (1996). Nuclear magnetic resonance solution structure of the human Hsp40 (HDJ-1) J-domain. *J Mol Biol* 260: 224-35.
- Rist W, Graf C, Bukau B, Mayer MP. (2006). Amide hydrogen exchange reveals conformational changes in hsp70 chaperones important for allosteric regulation. *J Biol Chem* 281: 16493-501.
- Rist W, Jorgensen TJ, Roepstorff P, Bukau B, Mayer MP. (2003). Mapping temperature-induced conformational changes in the Escherichia coli heat shock transcription factor sigma 32 by amide hydrogen exchange. *J Biol Chem* 278: 51415-21.
- Rist W, Rodriguez F, Jorgensen TJ, Mayer MP. (2005). Analysis of subsecond protein dynamics by amide hydrogen exchange and mass spectrometry using a quenched-flow setup. *Protein Sci* 14: 626-32.
- Rudiger S, Germeroth L, Schneider-Mergener J, Bukau B. (1997). Substrate specificity of the DnaK chaperone determined by screening cellulose-bound peptide libraries. *Embo J* 16: 1501-7.
- Rudiger S, Schneider-Mergener J, Bukau B. (2001). Its substrate specificity characterizes the DnaJ co-chaperone as a scanning factor for the DnaK chaperone. *Embo J* 20: 1042-50.
- Russell R, Wali Karzai A, Mehl AF, McMacken R. (1999). DnaJ dramatically stimulates ATP hydrolysis by DnaK: insight into targeting of Hsp70 proteins to polypeptide substrates. *Biochemistry* 38: 4165-76.
- Saito H, Uchida H. (1977). Initiation of the DNA replication of bacteriophage lambda in Escherichia coli K12. *J Mol Biol* 113: 1-25.
- Schmid D, Baici A, Gehring H, Christen P. (1994). Kinetics of molecular chaperone action. *Science* 263: 971-3.
- Song HK, Eck MJ. (2003). Structural basis of degradation signal recognition by SspB, a specificity-enhancing factor for the ClpXP proteolytic machine. *Mol Cell* 12: 75-86.

Straus D, Walter W, Gross CA. (1990). DnaK, DnaJ, and GrpE heat shock proteins negatively regulate heat shock gene expression by controlling the synthesis and stability of sigma 32. *Genes Dev* 4: 2202-9.

Straus DB, Walter WA, Gross CA. (1987). The heat shock response of *E. coli* is regulated by changes in the concentration of sigma 32. *Nature* 329: 348-51.

Straus DB, Walter WA, Gross CA. (1989). The activity of sigma 32 is reduced under conditions of excess heat shock protein production in *Escherichia coli*. *Genes Dev* 3: 2003-10.

Szabo A, Korszun R, Hartl FU, Flanagan J. (1996). A zinc finger-like domain of the molecular chaperone DnaJ is involved in binding to denatured protein substrates. *Embo J* 15: 408-17.

Szabo A, Langer T, Schroder H, Flanagan J, Bukau B, Hartl FU. (1994). The ATP hydrolysis-dependent reaction cycle of the *Escherichia coli* Hsp70 system DnaK, DnaJ, and GrpE. *Proc Natl Acad Sci U S A* 91: 10345-9.

Szyperski T, Pellicchia M, Wall D, Georgopoulos C, Wuthrich K. (1994). NMR structure determination of the *Escherichia coli* DnaJ molecular chaperone: secondary structure and backbone fold of the N-terminal region (residues 2-108) containing the highly conserved J domain. *Proc Natl Acad Sci U S A* 91: 11343-7.

Tatsuta T, Joob DM, Calendar R, Akiyama Y, Ogura T. (2000). Evidence for an active role of the DnaK chaperone system in the degradation of sigma(32). *FEBS Lett* 478: 271-5.

Theysen H and Schuster HP, Packschies L, Bukau B, Reinstein J. (1996). The second step of ATP binding to DnaK induces peptide release. *J Mol Biol* 263: 657-70.

Tilly K and Yarmolinsky M. (1989). Participation of *Escherichia coli* heat shock proteins DnaJ, DnaK, and GrpE in P1 plasmid replication. *J Bacteriol* 171: 6025-9.

Tolun A and Helinski DR. (1982). Separation of the minimal replication region of the F plasmid into a replication origin segment and a trans-acting segment. *Mol Gen Genet* 186: 372-7.

Tomoyasu T, Gamer J, Bukau B, Kanemori M, Mori H, et al. (1995). *Escherichia coli* FtsH is a membrane-bound, ATP-dependent protease which degrades the heat-shock transcription factor sigma 32. *Embo J* 14: 2551-60.

Tomoyasu T, Ogura T, Tatsuta T, Bukau B. (1998). Levels of DnaK and DnaJ provide tight control of heat shock gene expression and protein repair in *Escherichia coli*. *Mol Microbiol* 30: 567-81.

Vassylyev DG, Sekine S, Laptenko O, Lee J, Vassylyeva MN, et al. (2002). Crystal structure of a bacterial RNA polymerase holoenzyme at 2.6 Å resolution. *Nature* 417: 712-9.

Wall D, Zylicz M, Georgopoulos C. (1994). The NH₂-terminal 108 amino acids of the Escherichia coli DnaJ protein stimulate the ATPase activity of DnaK and are sufficient for lambda replication. *J Biol Chem* 269: 5446-51.

Watson LA, Phua SH, Bergquist PL, Lane HE. (1982). An Mr 29000 protein is essential for mini-F maintenance in E. coli. *Gene* 19: 173-8.

Wawrzynow A, Banecki B, Wall D, Liberek K, Georgopoulos C, Zylicz M. (1995). ATP hydrolysis is required for the DnaJ-dependent activation of DnaK chaperone for binding to both native and denatured protein substrates. *J Biol Chem* 270: 19307-11.

Wawrzynow A and Zylicz M. (1995). Divergent effects of ATP on the binding of the DnaK and DnaJ chaperones to each other, or to their various native and denatured protein substrates. *J Biol Chem* 270: 19300-6.

Yang H and Smith DL. (1997). Kinetics of cytochrome c folding examined by hydrogen exchange and mass spectrometry. *Biochemistry* 36: 14992-9.

Yura T, Nakahigashi K. (1999). Regulation of the heat-shock response. *Curr Opin Microbiol* 2: 153-8.

Zhang Z and Smith DL. (1993). Determination of amide hydrogen exchange by mass spectrometry: a new tool for protein structure elucidation. *Protein Sci* 2: 522-31.

Zhou YN and Gross CA. (1992). How a mutation in the gene encoding sigma 70 suppresses the defective heat shock response caused by a mutation in the gene encoding sigma 32. *J Bacteriol* 174: 7128-37.

Zhou YN, Walter WA, Gross CA. (1992). A mutant sigma 32 with a small deletion in conserved region 3 of sigma has reduced affinity for core RNA polymerase. *J Bacteriol* 174: 5005-12.

Zhu X, Zhao X, Burkholder WF, Gragerov A, Ogata CM, et al. (1996). Structural analysis of substrate binding by the molecular chaperone DnaK. *Science* 272: 1606-14.

Zimmerman SB and Trach SO. (1991). Estimation of macromolecule concentrations and excluded volume effects for the cytoplasm of Escherichia coli. *J Mol Biol* 222: 599-620.

Publications

Rist W, Rodriguez F, Jorgensen TJ, Mayer MP. (2005) Analysis of subsecond protein dynamics by amide hydrogen exchange and mass spectrometry using a quenched-flow setup. *Protein Sci* 14: 626-32.

Raviol H, Sadlish H, Rodriguez F, Mayer MP, Bukau B. 2006. Chaperone network in the yeast cytosol: Hsp110 is revealed as an Hsp70 nucleotide exchange factor. *Embo J* 25: 2510-8.

Rodriguez F, Rist W, Arsene-Ploetze F, Rüdinger S, Mayer MP, Bukau B. Regulation of the transcription factor σ^{32} by the DnaK-DnaJ chaperone system (submitted).

Rodriguez F, Rist W, Mayer MP, Bukau B. Molecular mechanism of DnaK- mediated monomerization of the F-plasmid replicator protein RepE (manuscript in preparation).

Abbreviations

Å	Ångström
aa	amino acid(s)
ACN	acetonitrile
ADP	adenosine diphosphate
ATP	adenosine triphosphate
βME	2-mercaptoethanol
bp	base pairs
BPIA	benzophenone-4-iodacetamide
Da	Dalton (atomic mass unit)
DMSO	dimethyl sulfoxide
DNA	deoxyribonucleic acid
DnaJ	Hsp40 chaperone in <i>E. coli</i>
DnaK	Hsp70 chaperone in <i>E. coli</i>
DTT	1,4-dithiothreitol
<i>E. coli</i>	<i>Escherichia coli</i>
EDTA	ethylenediamine-N,N,N',N'-tetraacetic acid
ESI	electrospray ionization
GroEL	Hsp60 chaperone in <i>E. coli</i>
GroES	Hsp10 cochaperone in <i>E. coli</i>
GrpE	nucleotide exchange factor for DnaK
HEPES	4-(2-hydroxyethyl)piperazine-1-ethanesulfonic acid
HPLC	high-performance liquid chromatography

Hsc70	heat shock cognate 70 kDa protein
Hsp	heat shock protein
HX	amide hydrogen exchange
ID	inner diameter
IPTG	Isopropyl- β -D-thiogalactopyranoside
kDa	kilodalton
LC	liquid chromatography
μ M	micromolar
MALDI	matrix assisted laser desorption/ionization
MeOH	methanol
mRNA	messenger ribonucleic acid
MS	mass spectrometry
MS/MS	tandem mass spectrometry
<i>m/z</i>	mass-to-charge ratio
NMR	nuclear magnetic resonance
OD	optical density outer diameter
PAGE	polyacrylamide gel electrophoresis
PCR	polymerase chain reaction
PDB	protein data bank
PEEK	polyethyletherketone polymer
PMSF	phenylmethanesulfonyl fluoride
ppm	parts per million
PVDF	poly(vinylidene difluoride)
RNA	ribonucleic acid
RNAP	RNA polymerase
RP	reversed-phase
σ^{32}	Sigma32, heat shock transcription factor
SBD	substrate binding domain
SDS	sodium dodecyl sulphate
TCEP	tris(2-carboxyethyl) phosphine
TFA	trifluoroacetic acid
TOF	time-of-flight
Tris	2-Amino-2-(hydroxymethyl)-1,3-propanediol
z	number of charges on an ion

The 1-letter code for amino acids was used.

Acknowledgment

I would like to thank all those people who made this thesis possible.

First, I would like to express my sincere gratitude to my supervisor Prof. Bernd Bukau for his guidance, encouragement and advice throughout this study.

I would like to thank Prof. Felix Wieland for being my second supervisor.

My sincere thanks also to my co-supervisor PD Matthias Mayer for his continuous guidance and advice throughout the course of this thesis.

I would like to thank Rainer N., Holschi, Christoph, Heather, Markus, Wolfgang, Heike, Rainer S., Martha, Christian, Joselyne, Claus and Matthias for the nice working atmosphere in the lab and, especially to Wolfgang for introducing me into HX experiments and Christian and Joselyne for our mass spec discussions. I would like to thank Matthias, Damon, Joselyne, Claus, Rainer S. and Christian for their comments and suggestions for the editing of my thesis.

I would like to thank Prof. Seth Darst and Dr. Elizabeth Campbell for their hospitality and for introducing me into crystallization. The time in New York was a great experience.

Thanks Ana, Marina, Claudio and Rodrigo for being always there in the good and the bad moments.

I would like to thank my parents and my sister because they have always been close despite the distance.

Finally, I would like to thank Pablo for his unconditional love and because without his continuous support and encouragement this thesis wouldn't have been possible.